MASS TRANSFER CHARACTERISTICS IN AN AGITATED SLURRY REACTOR OPERATING UNDER FISCHER-TROPSCH CONDITIONS

by

Jean-philippe Soriano

B.S. in Chemical Engineering and Chemistry, CPE Lyon, France, 2003

Submitted to the Graduate Faculty of

the School of Engineering in partial fulfillment

of the requirements for the degree of

Master of Science in Chemical Engineering

University of Pittsburgh

2005

UNIVERSITY OF PITTSBURGH

SCHOOL OF ENGINEERING

This thesis was presented

by

Jean-philippe Soriano

It was defended on

February 11, 2005

and approved by

Robert Enick, Professor, Chemical and Petroleum Engineering Department

Badie I. Morsi, Professor, Chemical and Petroleum Engineering Department

Rachid Oukaci, Associate Professor, Chemical Engineering Department

Patrick Smolinski, Associate Professor, Mechanical Engineering Department

Thesis Director: Badie I. Morsi, Professor, Chemical and Petroleum Engineering Department

ABSTRACT

MASS TRANSFER CHARACTERISTICS IN AN AGITATED SLURRY REACTOR OPERATING UNDER FISCHER-TROPSCH CONDITIONS

Jean-philippe Soriano, M.S.

University of Pittsburgh, 2005

In this study, the equilibrium solubility, C^*, and the volumetric mass transfer coefficient, k_La, were measured for 4 different gases (He, CO, N_2 and H_2) in two different liquids (Poly-Alpha-Olefins, PAO-8 and C_{70} Sasol Wax) in a 1-liter agitated reactor operating in a Gas Inducing mode under the typical conditions of Fischer-Tropsch synthesis. The effect of operating variables, including pressure (0.7 – 3.5 MPa), temperature (423 – 523 K), mixing speed (13.3 – 20 Hz), and alumina powder (used as a support for cobalt catalyst) concentration (0 - 50 wt.%) on k_La and C^* values were statistically investigated using the Central Composite Statistical design and analysis technique. The data were measured within wide ranges of operating condition covering the industrial range of this Fischer-Tropsch synthesis. The transient physical gas absorption technique was used to determine k_La under the operating conditions used.

The C^* values for the four gases in the two liquids used appeared to increase linearly with increasing pressure at constant temperature, i.e., obey Henry's Law over the pressure ranges studied. The C^* values were found to decrease and then increase with increasing temperature and the effect of temperature on C^* was described by an Arrhenius-type equation, where the apparent

activation energy of absorption was a function of temperature. The solubility values for the four gases in the two liquids used followed the trend: $C^*_{CO} > C^*_{N2} > C^*_{H2} > C^*_{He}$ and the values in Sasol wax were slightly higher than obtained those in PAO-8.

The k_La values for the four gases in the two liquids were found to increase with increasing pressure, temperature and mixing speed. The k_La values, however, slightly decreased (20%) at solid concentrations less than 30 wt% and then dramatically decreased (80%) with increasing solid concentrations from 30 to 50 wt%. Under similar operating conditions, k_La values for the four gases were found to be higher in Sasol wax than in PAO-8. This behavior was related to the greater gas-liquid interfacial area created in the Sasol wax due to its lower surface tension and foamability when compared with those of the PAO-8.

Statistical correlations were developed to predict the k_La values for the four gases in the two liquids with a regression coefficient (R^2) greater than 97%. Also, an empirical correlation using dimensionless numbers was proposed to predict k_La values in gas induction slurry agitated reactors with a regression coefficient (R^2) greater than 94%.

DESCRIPTORS

Absorption

Agitated reactor

Central Composite Statistical Design

Fischer-Tropsch

Polyalphaolephins

Sasol Wax

Slurry

Solubility

Syngas

Volumetric liquid-side mass transfer coefficient

TABLE OF CONTENTS

LIST OF TABLES

LIST OF FIGURES

NOMENCLATURE

a	Gas-liquid interfacial area per unit liquid volume, m^{-1}
a_p	Solid-liquid interfacial area, m^{-1}
C^*	Solubility of the gas at equilibrium, kmol m^{-3}
C_L	Concentration of the gas in the liquid bulk, kmol m^{-3}
C_S	Average solid concentration in gas-free slurry, kg m^{-3}
C_V	Volumetric solid concentration, %
D_{AB}	Mutual diffusion coefficient of solute A in solvent B, $cm^2\ s^{-1}$
$d_{imp.}$	Impeller diameter, m
d_p	Particle diameter, m
d_s	Sauter mean particle diameter, m
d_T	Diameter of the reactor, m
g	Gravitational constant, $m^2\ s^{-1}$
H_{0a}	Pre-exponential constant in equation (6-2)
He	Henry's law constant, bar m^3 $kmol^{-1}$
H_L	Liquid height above the impeller, m
H_V	Molar heat of vaporization, $J.mol^{-1}$
k	Phase mass transfer coefficient, m s^{-1}
K_p	Reaction rate constant, m s^{-1}
m	Phase weight, kg

MW	Phase molecular weight, kg $kmol^{-1}$
N	Mixing speed, Hz or rpm
n	Carbon number, -
n_0	Coefficient in equations (4-13) and (4-14), -
N_{CRI}	Critical mixing speed for gas induction, Hz or rpm
P	Pressure, bar
P_c	Critical pressure, bar
P_i	Parachor contribution group of component *i*, -
P^S	Saturated vapor pressure of the liquid, bar
Q_G	Gas volumetric flow rate, m^3s^{-1}
r	Coefficient in equation (4-12), -
R	Universal gas constant, $kJ.kmol^{-1}.K^{-1}$
R_S	Overall rate of reaction, kmol m^{-3} s^{-1}
s	Dimensionless coefficient in equation (2-2)
T	Temperature, K
t	time, s
T_b	Boiling point, C
T_c	Critical temperature, K
TD	Tank diameter, cm
T_r	Reduced temperature, -
TV	Tank volume, Liter
v_A	Molar volume of solute A at its normal boiling point temperature, cm^3 mol^{-1}
V_c	Critical volume, m^3 kmol

V_G Volume of the gas phase, m^3

V_L Volume of the liquid phase, m^3

w_i Mass fraction of component *i*, -

x_i Mole fraction of component *i* in the liquid phase, -

X_i Value of the *i*th variable in equation (4-28), unit of the variable

x_j Coded variable, -

Y Physical property correlated in equation (4-13), -

$Y_{\infty,0}$ Coefficient in equations (4-13) and (4-14), -

y_i Mole fraction of component *i* in the gas phase, -

Z_c Critical compressibility, -

Greek symbols

ϕ_i Volume fraction of phase *I*, -

α_i Constant in equation (6-8)

β Correlating parameter in equations (4-13) and (4-14), -

β_i Constant in equation (6-8)

γ_i Constant in equation (6-8)

δ Film thickness, m

ΔE Apparent activation energy of absorption, kJ/kmol

δ_i Solubility parameter of phase *I*, $(J.m^{-3})^{0.5}$

ε Phase holdup, -

η Constant in equation (6-8)

λ	Solvent association factor, -
λ_i	Constant in equation (6-8)
μ	Phase viscosity, kg m^{-1} s^{-1}
ν	Kinematic viscosity, m^2/s
ν_{pre}	Phase molar volume, $m^3.kmol^{-1}$
ρ	Phase density, kg m^3
σ_L	Surface tension of the liquid, N m^{-1}
Ψ	Coefficient in equation (5-27)
ω	Accentric factor, -

Subscripts

A	Solute
avg.	Average
B	Solvent
C	Critical condition
cat.	Catalyst phase
eq.	Equilibrium
F	Final
G	Gas phase
I	Initial
L	Liquid phase
m	Mixture

pre	Preheater
r	Reactor
S	Solid phase
SL	Slurry phase
V	Vapor phase

Abbreviations and acronyms

bbl	barrel
CTL	Coal-to-Liquid
EIA	Energy Information Administration
F-T	Fischer-Tropsch
GIR	Gas Inducing Reactor
GSR	Gas Sparging Reactor
GTL	Gas-to-Liquid
NYMEX	New York Mercantile Exchange
OPEC	Organization of the Petroleum Exporting Countries
PAO	Polyalphaolefin
PR-EOS	Peng-Robinson Equation of State
SAR	Surface Aeration Reactor
SEM	Scanning Electron Microscope
tcm	Trillion cubic meter
TD	Tank diameter

TV	Tank volume
WGS	Water Gas Shift

Dimensionless numbers

Eu	Euler Number, $P/(N^2 d_{imp.}^2 \rho_L)$
Re	Reynolds Number, $(N \rho_L d_{imp.}^2)/ \mu_L$
Sc	Schmidt Number, $\mu_L/(\rho_L D_{AB})$
Sh	Sherwood Number, $(k_L a \, d_{imp.}^2)/D_{AB}$
We	Weber Number, $(N^2 d_{imp.}^3 \rho_L)/ \sigma_L$

ACKNOWLEDGMENTS

My sincere gratitude goes to my advisor Professor Badie I. Morsi for his expert guidance and support throughout this work and during my stay in his research group at the University of Pittsburgh. I'm also grateful to Professor Robert Enick, Dr. Rachid Oukaci and Professor Patrick Smolinski for serving at my committee.

I would like to extend my thanks for the technical support and cooperation of the Chemical and Petroleum Engineering faculty and staff, Mr. Rob Toplak, Mr. Bob Maniet and Mr. Ron Bartlett.

I am grateful to the my research group mates Dr. Arsam Behkish, Dr. Romain Lemoine, Mr. Yannick Heintz and Mr. Laurent Sehabiague for their constructive comments and contribution, and for their help and encouragement during my stay in Pittsburgh.

My deepest appreciation goes to my parents, brother, family and friends for their encouragement and support throughout my studies. I dedicate this thesis to my parents Monique and Michel Soriano.

1.0 INTRODUCTION

Crude oil had been considered an abundant and lasting cheap source of energy until 1949 when studies[(1)*] began to show that oil won't last as long as it was expected. In 1971, other studies[(2)] predicted that the world oil production would peak due to the progressive depletion of existing resources, decline of proven reserves, and tighter spare capacity of the oil producing countries. The peak production year, known as Hubbert peak, however, has not yet been accurately forecasted; and even though experts and government agencies generally agreed that peaking would occur in the coming decades, no consensus on the actual peaking year has been reached. For instance, peaking year has ranged from 2021 to 2112, with a most probable occurrence in the year 2037, using 12 different models and scenarios by the US Energy Information Administration[(3)] (EIA); and more recently studies[(4, 5)] have predicted that peaking would even occur sooner, with estimates ranging from the year 2010 to 2020.

This uncertainty of predicting oil production peaking and continued worldwide oil demand dramatically affects the oil prices as can be observed in Figure 1. It should be mentioned that in 2004, the crude oil price is around 45 $/bbl which is far from targeted price of 22-28 $/bbl set by the Organization of Petroleum Exporting Countries (OPEC); and is also twice as the price of 25$/bbl in early year 2002. In addition, the future oil prices are likely to follow an increasing trend due to the following factors:

* Parenthetical references placed superior to the line of text refer to the bibliography.

- Spare capacity is getting tighter[6] in all petroleum producing countries and reserve growth is declining;
- Recoverable oil reserves will require much higher capital investments in order to be exploited when compared to low capital cost reserves exploited today[6] (deeper reserves, more expensive areas to drill, poorer oil quality needing more treatment);
- Developing countries, and more specifically China and India with their increasing demand, are likely to worsen the problem. For example, since early 1990s, China's oil demand has risen faster than anywhere else in the world (around 6% annual growth[7]) and yet, Chinese oil consumption still remains low when compared to other developed or even developing countries leaving plenty of room for growth[6];
- Political unrest in the Middle-east; and
- Tougher environmental laws preventing oil companies from drilling in wild-life reserve regions.

Thus, from the current and future oil supply/demand and increasing prices, it is of prime importance to find alternative fuel sources in order to dampen the economical impact of energy crunch. To this end, synthetic fuels, mainly produced via Fischer-Tropsch (F-T) synthesis are exhibiting quite interesting features, which make them good candidates as alternative and/or complementary sources of fuel. Due to the large quality of raw materials (coal or natural gas) which could be used in the F-T process, the intrinsic properties of the produced liquids exhibits the following advantages when compared to traditional oil:

- The F-T products obtained are cleaner than traditional oil[8] and do not require any further treatment to remove undesirable impurities (sulfur compounds, acid gases removal, etc.)
- The F-T process equipment can be installed on-site in large remote natural gas reservoirs[9] which would have been uneconomical to exploit otherwise; and therefore the F-T process can solve expensive transportation costs of liquid natural gas (LNG).
- Natural gas or coal needed for the production of the synthesis gas (H_2 and CO) used for the F-T process are plentiful and available at a low cost. Reserves of natural gas are around 50% more abundant than that of oil, and coal reserves also exceed those of oil by about 20 times[10], as can be seen in Table 1.
- Natural gas, which otherwise would have been flared during oil production can be used as a valuable feedstock in a F-T process[9].

The interest in Gas-To-Liquid (GTL) or Coal-To-Liquid (CTL) technologies using the Fischer-Tropsch process will certainly increase in the coming years with more attractive costs when compared to that of crude oil. It is estimated that using F-T synthesis to produce fuels can become more competitive if the price of the crude oil exceeds 20-24$/bbl[9-11]. The existing commercial plants using the F-T technology, however, are still scarce (a table summarizing planned and existing GTL plants in the world is provided in Appendix A) and effort should be made to lower production costs to be competitive with oil. Thus, it is important to fully understand parameters influencing the overall performance of the industrial F-T process such as reaction kinetics, heat and mass transfer and hydrodynamics. Unfortunately, most of the available data in literature are rather inconsistent since they were obtained with systems that are

under conditions not necessarily representative of the actual F-T process (air/water, no solid particles, high temperature but atmospheric pressure experimental data), and accordingly the use of such data for the design, modeling and scale-up of F-T reactors can be misleading. Therefore, the main objective of this study is to determine the mass transfer parameters for different gases in representative F-T products in a 3-phase agitated reactor, operating under different pressures, temperatures, mixing speeds and solid loadings similar to those employed in F-T industrial process.

Figure 1: NYMEX Light Sweet Crude Price

Table 1: Carbon Sources World Reserves[12]

		Value	Units
Oil			
Undiscovered conventional		732	Billion bbl
Reserve growth		688	Billion bbl
Remaining reserves		891	Billion bbl
Cumulative production		710	Billion bbl
	Total	3021	Billion bbl
Natural Gas			
Undiscovered conventional		147.1	tcm
Reserve growth		103.6	tcm
Remaining reserve		135.7	tcm
Cumulative production		49.6	tcm
	Total	436.0	tcm
Coal			
Proven reserves		984.5	Billion tons

2.0 LITERATURE REVIEW AND BACKGROUND

The mass transfer characteristics in a slurry agitated reactor is of prime importance for a better understanding of industrial gas-liquid-solid processes, where it has been reported in literature[13] that, for F-T process at high catalyst loading (over 35 wt.%), the mass transfer can be the rate-limiting step of the overall process. In the following sections, a brief introduction on the typical F-T process reactions and 3-phase agitated reactors is given. Also, the impact of process main operating variables and physical properties of the gas-liquid-solid system on the mass transfer coefficients are presented.

2.1 THE FISCHER-TROPSCH PROCESS

In the early 1920s, Franz Fischer and Hans Tropsch discovered that liquid hydrocarbons could be produced from a reaction between a mixture of carbon monoxide and hydrogen (syngas) over a metal catalyst, under some specific operating conditions, which is known as the Fischer-Tropsch process. The F-T synthesis is rather old and its development had been more for strategic rather than economic reasons as in Germany during World War II or in South Africa during apartheid era. There is, however, a growing interest in F-T technologies since it might represent an alternative to oil in the coming decades. The F-T synthesis can yield to several main products with eventually some side reactions:

The main product reactions are:

Olefins: $2nH_2 + nCO \rightarrow C_nH_{2n} + nH_2O$ $(2<n<N)$

Paraffins: $(2n+1)H_2 + nCO \rightarrow C_nH_{2n+2} + nH_2O$ $(1<n<N)$

Alcohols: $2nH_2 + nCO \rightarrow C_nH_{2n+2}O + (n-1)H_2O$

In these reactions, *n* is the average carbon number of the hydrocarbon product, which is strongly dependent on the operating conditions used in the process, such as temperature, pressure, catalyst type, H_2/CO ratio, etc.

The possible side reaction:

Water Gas Shift (WGS): $H_2O + CO \rightarrow CO_2 + H_2$ (with iron oxide catalyst)

Also, during the F-T process, the following reactions, which could greatly affect both total conversion and selectivity should be considered and avoided:

- Hydrogenation of CO to CH_4.
- Decomposition of CO to carbon and CO_2 (catalyst coking).
- Oxidation of the iron oxide catalyst.

The main factors to be taken into account for the understanding of the Fischer-Tropsch process in slurry phase are:

1. The hydrodynamics (gas holdup, axial/radial catalyst distribution).

2. Heat and mass transfer (heat and mass transfer coefficients, gas-liquid interfacial area, liquid-solid interfacial area, pore diffusion coefficients, reactants absorption and adsorption coefficients).
3. Thermodynamics,
4. Process operating conditions (temperature, pressure, catalyst loadings, etc.).
5. Reaction kinetics and stoichiometry (orders with respect to reactants, products, rate constants, mechanism).

It should be mentioned, however, that the mass transfer should be thoroughly investigated since it could be the rate-limiting step in F-T processes operating with high catalyst loading[13], and accordingly the next sections focuses specifically on the mass transfer characteristics in 3-phase (gas-liquid-solid) agitated reactors.

2.2 3-PHASE AGITATED REACTORS

Due to their low initial cost, ease of operation and great flexibility of control, agitated reactors are widely used in industry. When considered as a Gas-Liquid-Solid contactor, different modes of operation to achieve the mixing of all 3 phases can be used. Depending on the process requirements, agitated reactors can be operated in the following 3 modes as depicted in Figure 2:

- Surface Aeration Reactor (SAR)
- Gas Inducing Reactor (GIR)
- Gas Sparging Reactor (GSR)

For the SAR, the contact between the slurry and the gas phase occurs mainly at the flat interface between these 2 phases and the mass transfer takes place by diffusion of the gas into the liquid. As the mixing speed increase, however, the reactor reach the point where the surface between the gas and the slurry can break up and bubbles can be entrained into the slurry.

The GIR is a cost-effective way to increase mass transfer by inducing gas bubbles into the slurry with no or minimum modifications when compared to SAR by the mean of a hollow shaft connected to an impeller with holes located in the gas phase region and holes in the liquid region. At low mixing speeds, the GIR will behave as a SAR. When agitation speed is increased, the reduced local pressure created below the impeller blades becomes more significant and at the critical mixing speed for gas induction, the gas bubbles overcome the hydrostatic head of the slurry and are induced through the holes on the hollow shaft into the slurry. The knowledge of the critical mixing speed for gas induction, N_{CRI} is essential to operate a Gas-Inducing Reactor. According to Lemoine et al.[14], the critical mixing speed for gas induction can be calculated by the following equation:

$$\frac{N_{CRI}^2 d_{imp.}}{g} = 0.512 \times \left(\frac{\mu_L}{\mu_{Water}}\right)^{0.146} \left(\frac{\sigma_L}{\sigma_{Water}}\right)^{-0.180} \left(\frac{\rho_L}{\rho_{Water}}\right)^{-0.265} \left(\frac{H_L}{d_T}\right) \tag{2-1}$$

The physical properties are taken at the operating temperature for the liquid whereas they are at ambient temperature for water. This correlation was developed with various reactor sizes (up to 1.5m) for different gas-liquid systems.

The GSR, on the other hand, the gas is sparged into the slurry by the mean of a gas distributor directly located directly the impeller. Even though this type of reactor can easily achieve high rate of absorption, its advantages should be balanced with the higher capital cost

generated by the gas compression needed to sparge the gas into reactor and the more complex structure needed for the recirculation of the gas.

In slurry reactors, it is of prime necessity to achieve complete solid suspension. The correlation developed by Zwietering[15] was used to calculate the critical mixing speed necessary to solid suspension. This critical mixing speed as defined in equation (2-2) is the speed needed so that no particles remain settled at the bottom of the reactor for more than 2 seconds.

$$N_{suspension} = \frac{s\,\nu^{0.1} d_p^{0.2} \left(g\Delta\rho / \rho_L\right)^{0.45} C_V^{0.13}}{d_{imp.}^{0.85}} \tag{2-2}$$

ν is the kinematic viscosity, $\Delta\rho$ is the density difference between the solid and the liquid phase and s is a dimensionless coefficient depending on the reactor design ($d_T/d_{imp.}$ ratio). The Zwietering's correlation was modified by several investigators[16-20] to account for different reactor and impeller geometries, different liquid-solid systems or for multiple impellers. This correlation was, however, developed only for liquid-solid systems and does not account for any effect of the gas phase induced into the liquid. Recent work from Murugesan[21] suggests that gas bubbles might have an impact on the critical mixing speed for solid suspension.

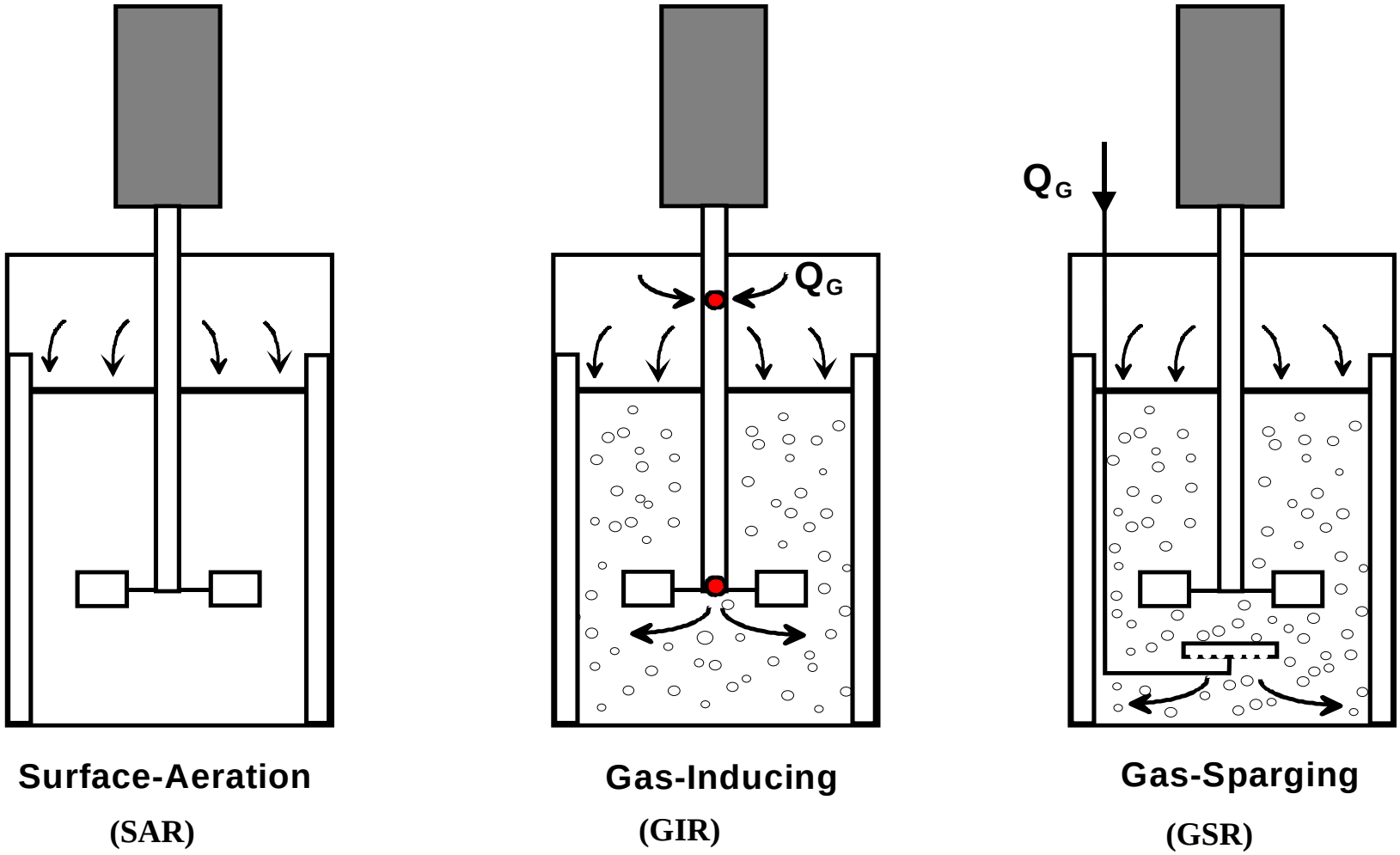

Figure 2: Operation Modes of Stirred Tank Reactors

2.3 SOLUBILITY AND MASS TRANSFER CHARACTERISTICS IN 3-PHASE AGITATED REACTORS

For the optimization of a 3-phase process, full understanding of hydrodynamics, heat and mass transfer parameters and the kinetics of the reaction is needed. For the reaction to take place in a slurry reactor, the following steps, schematically represented in Figure 3, are involved during the process:

- Step 1: Transfer of the gas-phase reactants from the gas phase bulk to the gas liquid interface through the gas film.
- Step 2: Transfer of the gas-phase reactants from the interface to the liquid bulk through the liquid film.
- Step 3: Transfer of the reactants from the liquid bulk to the liquid-solid interface.
- Step 4: Transfer of the reactants from the liquid-solid interface to the catalyst particle surface through the liquid-solid film.
- Step 5: Adsorption and reaction of the reactants on the catalyst active sites.

The resulting products will then desorb from the catalyst surface and will transfer back to either the liquid or the gas bulk. According to the two-film theory initially developed by Lewis and Whitman[22] all these steps can be described by a pseudo steady-state mass transfer across a stagnant gas-liquid and liquid-solid interface by the following equations:

$$R_S = k_G a(P_G - P^*) \tag{2-3}$$

$$R_S = k_L a(C^* - C_L) \tag{2-4}$$

$$R_S = k_S a_P (C_L - C_S) \tag{2-5}$$

P_G and P^* in equation (2-3) are the gas phase partial pressure and the pressure at equilibrium, respectively, defined as:

$$P^* = C^* He \tag{2-6}$$

where C^* is the equilibrium solubility and He is Henry's Law constant.

The kinetic rate of reaction is given by Equation (2-7) below:

$$R_S = K_r a_P C_S \tag{2-7}$$

Combining Equations (2-3), (2-4) and (2-5) for the rate of mass transfer with the kinetic rate of reaction (Equation (2-7)), the overall rate of reaction can be written as follows:

$$R_S = \frac{C_G - C_S}{\frac{1}{k_G a He} + \frac{1}{k_L a} + \frac{1}{k_S a_P} + \frac{1}{K_r a_P}} \tag{2-8}$$

Since the gases used are pure and that the vapor of the liquid in the gas phase is small, the gas phase resistance term can be neglected as well as the resistance term for the solid phase due to the small size of particles utilized. It can be deduced that the liquid phase mass transfer and the kinetics are the terms governing the overall rate of reaction. This study, however, will focus on the determination of the volumetric liquid-side mass transfer coefficient, $k_L a$. In the following, the effects of the main operating variables (pressure, temperature, mixing speed, solid concentration) as well as system's physical properties on $k_L a$ are presented.

2.3.1 Effect of Operating Parameters on the Solubility C^*

As it can be seen in Equation (2-4), the equilibrium solubility, C^* is a parameter of prime importance for determining the rate of mass transfer in gas-liquid-solid processes. Table 2

presents a literature review for the solubility of gases in organic or paraffinic liquids systems under high temperature and high pressure conditions. It was found that, for most of these gas-liquid systems, the solubility appeared to increase linearly with pressure and therefore follows Henry's law within the pressures investigated. The C^* of gases in organic liquids was also reported[23, 24] to decrease with increasing molecular weight/carbon number of organic liquid in homologous hydrocarbon series. Depending on the gas-liquid system considered as well as the temperature interval studied, C^* values can either increase or decrease with increasing temperature for example, the solubilities for Ar, H_2, N_2, He and CO in n-paraffins were reported[25-33] to increase with increasing temperature whereas those for CO_2, CH_4, C_2H_6, C_2H_4, and C_3H_8 were reported to decrease[24, 25, 30, 32]. Several investigators[30, 32, 34-38] measured the solubility of different gases in the same organic liquid (mostly in n-paraffins) and reported the following order for the solubility values:

$$C^*_{He}<C^*_{H2}<C^*_{N2}<C^*_{CO}<C^*_{CH4}<C^*_{CO2}<C^*_{C2H4}<C^*_{C2H6}<C^*_{C3H8}$$

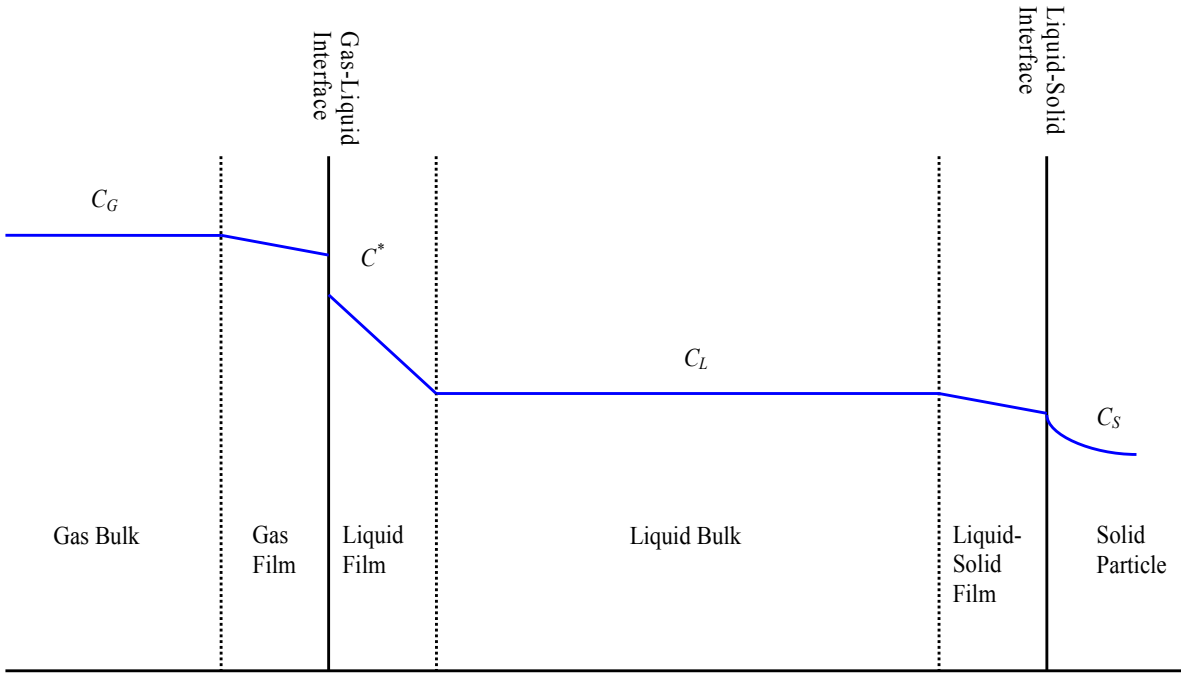

Figure 3: Concentration Profile in a 3-Phase Reactor

2.3.2 Volumetric Liquid-Side Mass Transfer Coefficient, k_La in GIR

As previously discussed, one of the major resistance term in Equation (2-8) is the volumetric liquid-side mass transfer coefficient, k_La. The k_La is traditionally measured by either chemical methods or physical methods such as monitoring the physical absorption of the gas of interest with an appropriate probe (species-sensitive probes (O_2, H_2, etc.) or pressure transducers).

k_La values have been reported in literature[23, 38-40] to be strongly dependent on the gas-liquid-solid system and operating conditions used; and therefore the following sections present the effect of process operating variables (pressure, temperature, mixing speed and solid concentration) and system properties (liquid nature, surface tension, viscosity and gas nature) on k_La.

2.3.3 Effect of Pressure on k_La in GIR

A literature review on the effect of pressure on the volumetric liquid-side mass transfer coefficient is given in Table 3, and as can be seen, k_La values are strongly dependent on the gas-liquid system used and on the range of pressure investigated. For instance, k_La was found to increase[23, 38, 41-46], to remain unaffected[31, 47-51] or even decrease[52] with increasing pressure.

Most of these investigators related the effect of pressure on k_La to the variation of the physical properties of the gas-liquid system because of the increased gas solubility, which decreases both surface tension and viscosity. Due to these conflicting impacts of viscosity and surface tension on k_La, the resultant impact may result in no effect, an increase or a decrease of k_La depending on the degree of change of the actual physical properties of the gas-liquid system.

2.3.4 Effect of Temperature on k_La in GIR

The effect of temperature on k_La is shown in the literature review given in Table 4. In the same manner as for the effect of pressure, increasing the temperature can also produce an increase[31, 38, 41, 43, 46, 47, 49, 51], have no or little effect[42] or decrease[43] k_La values.

It is reported that k_La is mainly affected by the temperature due to the resulting strong impact on liquid physico-chemical properties. With increasing temperature, the liquid viscosity and surface tension decrease resulting in an increase of the average bubble size and consequently decrease the interfacial area, a. Increasing temperature will also increase the diffusivity of the gas into the liquid and subsequently k_L since it is proportional to the diffusivity to power 0.5 to 1.0. Thus, the effects on a and k_L could lead to an increase, a decrease or no effect on k_La depending on the system and operating conditions used.

2.3.5 Effect of Mixing Speed on k_La in GIR

A literature review on the effect of mixing speed on k_La is presented in Table 5. Increasing mixing speed is reported[23, 38, 41-49, 51, 53-57] to strongly enhance the volumetric liquid-side mass transfer coefficient. This behavior can be readily explained by the increased amount of gas induced into the liquid and therefore higher gas holdup and interfacial area are obtained when increasing mixing speed. Also, increasing mixing speed will increase the shear rate applied at the gas-liquid interface which can reduce the liquid film thickness and will, according to the two-film model, increase k_L. Several investigators[38, 53-55] noticed, however, that no significant k_La enhancement is provided when reaching high mixing speeds (greater than 1200 rpm) in small size reactors. This observed asymptotic trend of k_La at high mixing speed in some systems can be

attributed to the fact that the pumping capacity of the impeller reaches a maximum and would not produce further change in gas holdup and therefore no further enhancement of k_La values.

2.3.6 Effect of Solid Concentration on k_La in GIR

As reported in the literature review presented in Table 6, adding solid particles to the liquid can have contradictory effects on k_La. Several studies showed that when adding a small amount of solid particles, little effect[47, 58] on k_La and even an increase[38, 42, 48, 49, 59-62] of k_La values could be observed, whereas at high solid concentrations, k_La values drastically decreased[38, 42, 43, 48, 49, 59] with increasing solid concentration.

Low solid concentrations of small particles have only a limited impact on the overall slurry viscosity and can even hinder the coalescence tendency or promote breakup of gas bubbles by interacting directly with the gas-liquid interface, resulting in stable or increased values of the volumetric liquid-side mass transfer coefficient. On the contrary, high solid concentrations are more likely to increase to a greater extent the overall slurry viscosity which will promote gas bubbles coalescence which decreases the gas-liquid interfacial area a. Increasing bubble size, on the other hand, can increase the mass transfer coefficient k_L and accordingly k_La could increase decrease or independent of solid concentration based on its impact on both a and k_L.

2.3.7 Effect of Liquid Nature on k_La

A literature review on the effect of liquid nature is presented in Table 7. When considering homologous hydrocarbon series, such as increasing the carbon number (n) in alkanes C_nH_{2n+2}, Karandikar et al.[43, 45, 46] and Chang et al.[23] reported a decrease in k_La with increasing the carbon number. This effect can be related to the increase of viscosity of the n-alkane series when increasing the carbon number.

Other investigators measured the effect of liquid physical properties on k_La. For instance, Albal et al.[48] reported that increasing the liquid phase viscosity decreases the volumetric liquid-side mass transfer coefficient, whereas they observed an increase in k_La values when decreasing the surface tension of the liquid. These effects on k_La are mainly due to the decrease of the gas diffusivity into the liquid when increasing viscosity and to the decrease in the average bubble size when decreasing surface tension.

2.3.8 Effect of Gas Nature on k_La in GIR

The effect of gas nature on k_La is quite complex. In paraffinic liquids, Chang et al.[23] and Inga[63] reported similar k_La behavior when considering gases having close diffusivities. For instance, they reported similar k_La values for N_2 and CO since carbon monoxide and nitrogen are having close diffusivities and therefore close k_L. It is, however, quite risky to explain the effect of gas nature on k_L only by considering its impact on k_L alone since an effect on the interfacial area could be possible, particularly with low molecular weight gases.

Table 2: Literature Survey on Solubility of Gases in Paraffinic Liquids

Reference	Gases	Solvent	MW	T (K)	P (bar)	System
Chou et al.[30]	H_2/CO/CH_4/CO_2/ C_2H_6/C_2H_4	Sasol wax (n-$C_{43}H_{88}$)	605	473-573	10-50	Diffusion cell (Shaking mech.)
Albal et al.[31]	H_2/CO	Gulf wax	380	348-523	10-35	Stirred reactor (SAR)
Van Vuuren et al.[32]	H_2/CO/CO_2/Ar/ CH_4/C_2H_6/C_2H_4/ C_3H_8/C_4H_{10}	Sasol Wax	464±53	433-513	3-11	Diffusion cell (Shaking mech.)
Tsai et al.[24]	CH_4/C_2H_6/CO_2	Mobil wax (n-$C_{61}H_{124}$)	857	473-573	10-50	Equilibration cell
Huang et al.[33]	CO/H_2	n-C_{20}/C_{28}/C_{36}/ Mobil F-T wax	282-857	373-573	10-50	Equilibration cell
Chou et al.[34]	CO/H_2/CO_2/CH_4/ C_2H_6/C_2H_4	n-C_{20}/C_{28}/C_{30}/C_{43}/C_{61}/C_{95}/ Sasol wax Mobil F-T wax	282-1332	-	-	Lacombe-Sanchez EOS Correlation (for heavy n-paraffin)
Gao et al.[64]	H_2/N_2/CO	n-C_{12}	170	344-410	7-132	Rocking cell
Purwanto et al.[65]	H_2/CO	H_2O/ethanol/1-octene(CO)/ acetone/acetonitrile/ ethanol+H_2O mixtures	18-112	298-323	3-20	Stirred reactor (SAR)
Twu et al.[66]	H_2	n-C_4/C_6/C_7/C_{10}	58-142	-	-	Modified Redlich-Kwong EOS correlation
Wang et al.[35]	H_2/CO/CO_2/CH_4/ C_2H_4/ C_2H_6	Heavy F-T waxes (C_{20} to C_{61})/F-T300 wax	282-857	473-573	10-40	Redlich Kwong EOS
Karandikar et al.[45]	CO/H_2/CH_4/CO_2	F-T heavy fraction	368	423-498	7-45	Stirred reactor (GIR)
Karandikar et al.[46]	CO/H_2	F-T medium fraction (C_{11}-C_{20})	201	423-498	10-40	Stirred reactor (GIR)
Campanella[36]	H_2/CO/CH_4/CO_2/ C_2H_6/C_2H_4	Light & heavy n-paraffins n-$C_{20}H_{42}$/n-$C_{28}H_{58}$/n-$C_{36}H_{74}$ Sasol wax ($C_{43}H_{88}$) Mobil wax ($C_{61}H_{124}$)	282-506	-	-	Correlation based on fluctuation solution theory

Table 2 (Cont'd)

Reference	Gases	Solvent	MW	T (K)	P (bar)	System
Huang et al.[67]	H_2/CO	n-$C_{20}H_{42}$/n-$C_{28}H_{58}$/ n-$C_{61}H_{124}$	282-857	373-573	10-50	Equilibration cell
Mandagaran et al.[37]	$H_2/CO/CO_2/CH_4/C_2H_6$	n-$C_{20}H_{42}$/n-$C_{36}H_{74}$/ n-Alkane/methylnaphtalene crude oils/coal-derived liquids	-	-	-	Correlation using the lattice-gas model
Breman et al.[68]	$H_2/CO/CO_2/H_2O$/ n-C_2H_6 to C_6H_{14}/ CH_3OH/C_2H_5OH/ 1-C_3H_7OH/ 1-C_4H_9OH/ 1-$C_5H_{11}OH$/ 1-$C_6H_{13}OH$	Tetraethylene glycol ($C_8H_{18}O_5$)/n-$C_{16}H_{34}$/ n-$C_{28}H_{58}$/1-$C_{16}H_{33}OH$/ phenanthrene ($C_{14}H_{10}$)/	178-394	293-553	0.6-55	Stirred reactor (SAR)
Chang et al.[23]	CO	n-C_6H_{14}/n-$C_{10}H_{22}$/n-$C_{14}H_{30}$	86-198	328-428	1-50	Stirred reactor (GIR)
Darwish et al.[69]	CH_4	n-$C_{20}H_{42}$/n-$C_{28}H_{58}$/ n-$C_{36}H_{74}$/n-$C_{44}H_{90}$	282-618	323-423	9-107	Rocking cell
Srivatsan et al.[70]	CO	n-$C_{10}H_{22}$/n-$C_{20}H_{42}$/ n-$C_{28}H_{58}$/n-$C_{36}H_{74}$	142-506	311-423	10-102	Rocking cell
Campanella[71]	$H_2/CO/CO_2$	n-paraffins C_{20}-C_{44}	282-618	-	-	Correlation using a lattice-gas model
Miller et al.[50]	H_2/CO	n-$C_{28}H_{58}$	394	528	10-30	Stirred reactor (SAR)
Peter et al.[72]	$H_2/CO/CO_2$	Krupp wax	345	379-573	Up to 980	Pressure chamber
Deimling et al.[43]	CO/H_2	F-T heavy/medium/light	114-368	373-523	10-40	Stirred reactor (SAR)

Table 2 (Cont'd)

Reference	Gases	Solvent	MW	T (K)	P (bar)	System
Inga[63]	$H_2/CO/N_2/CH_4/C_2H_4$	Hexane mixture: 2 methyl pentane(6.73%)/ 3 methyl pentane(14.17%)/ hexane(64.55%)/ methylcylopentane(14.55%)	85.88	398-303	5-25	Stirred reactor (SAR)
Matsumoto[73]	H_2/CO	n-$C_{28}H_{58}$/phenanthrene/ fomblin YR (perfluorinated polyether)	178-394	353-553	2.5-7	Equilibrium cell
Tekie et al.[41]	N_2/O_2	Cyclohexane	78	330-430	7-35	Stirred reactor
Ghosh et al.[25]	$CH_4/C_2H_6/CO/H_2$	n-Alkanes (up to C_{16})/ 1-alkenes (C_2 to C_{16})	28-226	-	-	Statistical Associating Fluid Theory EOS
Ronze et al.[26]	H_2	Cyclohexane/Gas oil	78	298-675	Up to 40	Stirred reactor (GIR)
Hichri et al.[47]	H_2	2-propanol/o-cresol	60-108	303-393	0-30	Stirred reactor (GIR)
Behkish et al.[74]	$H_2/CO/N_2/CH_4$	Isopar-M (C_{10}-C_{16})/ hexane mixture	85.88-192	298	1.7-8	SBCR
Alghamdi[38]	$H_2/CO/N_2$/He	Isopar-M (C_{10}-C_{16})/ PAO-8 (C_{30}-C_{70})	192-640	373-473	7-35	GIR
Tong et al.[27]	N_2	n-$C_{10}H_{22}$/n-$C_{20}H_{42}$/ n-$C_{28}H_{58}$/n-$C_{36}H_{74}$	142-506	323-423	Up to 180	Equilibrium cell
Park et al.[28]	CO	Benzene/naphthalene/ Phenanthrene/pyrene	78-202	323-433	Up to 233	Equilibrium cell
Park et al.[29]	H_2	n-$C_{10}H_{22}$/n-$C_{20}H_{42}$/ n-$C_{28}H_{58}$/n-$C_{36}H_{74}$	142-506	323-423	Up to 174	Equilibrium cell

Table 3: Literature Survey on the Effect of Pressure on k_La

Reference	Gas	Liquid/Slurry	Operating Conditions	Reactor	Remarks
Hichri et al.[47]	H_2	2-propanol/o-cresol/ mixture (2/3 2-propanol+ 1/3 o-cresol)/ Pyrex beads ($40<d_p<300\mu m$)	303-393K, 800-1500 RPM, TD 5 cm, 0-30 bar, solid up to 5 vol.%	GIR	No influence of P
Sridhar et al.[55]	N_2	Cyclohexane	297-423K, 480-1800 RPM, 1-10 bar, TD 13 cm	GSR	P↑ a↑ ε_G↑ no significant increase after 10 atm
Teramoto et al.[75]	H_2/He/N_2/ CO_2/Ar	Ethanol/p-xylene/water	273K, 2-100 bar, 150-1400 RPM, TD 5.6 cm	SAR	No effect of P on k_L for H_2O and ethanol For p-xylene P↑ k_L slightly↓
Albal et al.[48]	He/O_2	Glycerin/water+CMC/ glass beads (75-150μm)/ oil shale particles	295K,13.8-96.5 bar, 400-1000 RPM, TD 10.2 cm, Solid up to 30 vol%	SAR	No influence of P
Dietrich et al.[49]	N_2/H_2	Ethanol/water/ hydrogenation mixture/ Ni Raney particles (10-15μm)	293-353K, 10-50 bar, TV 0.5L	GIR	k_La independent of P
Albal et al.[31]	H_2/CO	Gulf wax, MW 380	348-523K, 10-35 bar, 800-1000 RPM	SAR	k_La independent of P
Tekie et al.[41]	N_2/O_2	Cyclohexane	330-430K, 7-35 bar, 400-1200 RPM	GIR/SAR	P↑ k_La slightly↑
Inga et al.[42]	H_2/CO/N_2/ CH_4/C_2H_4	Hexane mixture/ Iron oxide catalyst	298-373K, 2-25 bar, 400-1200 RPM	SAR	P↑ k_La↑ (H_2/CO/N_2) No effect or slight decrease for (CH_4/C_2H_4)
Miller et al.[50]	H_2/CO	n-Octacosane (n-$C_{28}H_{58}$)/ iron-based catalyst	523K, 10-30 bar, 250-1750 RPM, TV 0.3L	SAR	Effect of P not significant

Table 3 (Cont'd)

Reference	Gas	Liquid/Slurry	Operating Conditions	Reactor	Remarks
Deimling et al.[43]	H_2/CO	F-T light(C_6-C_{11})/ F-T medium (C_{12}-C_{21})/ F-T heavy($\geq C_{22}$)/solid: glass bed (125-177μm)	373-523K, 10-40 bar, TV 2.0L, 800-1100 RPM, Solid up to 30 wt.%	SAR	P↑ k_La↑
Lekhal et al.[44]	H_2/CO	n-Octene/ethanol/water	323K, 10-150 bar, TV 0.6L, 1100-2500 RPM	GIR	Poor effect of P on k_La
Karandikar et al.[46]	H_2/CO	F-T medium (C_{11}-C_{22}) M.W. 201.5	423-498K, 10-40 bar, TV 4L, 700-1200 RPM	GIR	P↑ k_La↑↑ Effect of H_2O: ↑ k_La values for CO ↓ k_La values for H_2
Karandikar et al.[45]	H_2/CO/ CH_4/CO_2	F-T heavy ($\geq C_{22}$) M.W. 368.5	423-498K, 10-40 bar, TV 4L, 700-1200 RPM	GIR	P↑ k_La↑↑ Effect of H_2O: ↑ k_La for $CO/H_2/CH_4/CO_2$ at 700 RPM ↓ k_La for H_2/CO_2 at 1000-1200 RPM No clear effect on k_La for CO/CH_4
Chang et al.[23]	CO	n-hexane/n-decane/ n-tetradecane	328-428K, 1-50 bar, 800-1200 RPM, TV 4L	GIR	P↑ k_La slightly↑
Chen et al.[51]	O_2	water	293-313K, 1-1.2 bar, 900-1300 RPM, TD 29 cm	GIR	k_La independent of P
Alghamdi[38]	H_2/CO/N_2/He	Isopar-M (C_{10}-C_{16})/ PAO-8 (C_{30}-C_{70})/ solid Al_2O_3	373-473K, 7-35 bar, 800-1200 RPM, solid up to 50 wt.%	GIR	k_La slightly increase with P
Maalej et al.[52]	N_2	Water	293K, 1-100 bar, TV 1.6L	GSR	P↑ k_La↓

Table 4: Literature Survey on the Effect of Temperature on k_La

Reference	Gas	Liquid/Slurry	Operating Conditions	Reactor	Remarks
Hichri et al.[47]	H_2	2-propanol/o-cresol/ mixture (2/3 2-propanol+ 1/3 o-cresol)/ Pyrex beads ($40<d_p<300\mu m$)	303-393K, 800-1500 RPM, TD 5 cm, 0-30 bar, solid up to 5 vol.%	GIR	T↑ k_La↑
Sridhar et al.[55]	N_2	Cyclohexane	297-423K, 480-1800 RPM, 1-10 bar, TD 13 cm	GSR	Effect of T on a is Complex
Dietrich et al.[49]	N_2/H_2	Ethanol/water/ hydrogenation mixture/ Ni Raney particles (10-15μm)	293-353K, 10-50 bar, TV 0.5L	GIR	T↑ k_La↑
Albal et al.[31]	H_2/CO	Gulf wax, MW 380	348-523K, 10-35 bar, 800-1000 RPM	SAR	T↑ k_La↑
Tekie et al.[41]	N_2/O_2	Cyclohexane	330-430K, 7-35 bar, 400-1200 RPM	GIR/SAR	T↑ k_La↑
Inga et al.[42]	H_2/CO/N_2/ CH_4/C_2H_4	Hexane mixture/ Iron oxide catalyst	298-373K, 2-25 bar, 400-1200 RPM	SAR	Very small effect of temperature on k_La
Deimling et al.[43]	H_2/CO	F-T light(C_6-C_{11})/ F-T medium (C_{12}-C_{21})/ F-T heavy($\geq C_{22}$)/solid: glass bed (125-177μm)	373-523K, 10-40 bar, TV 2.0L, 800-1100 RPM, Solid up to 30 wt.%	SAR	T↑ k_La↑ (for F-T light & heavy) T↑ k_La↓ (for F-T medium)
Karandikar et al.[46]	H_2/CO	F-T medium (C_{11}-C_{22}) M.W. 201.5 +effect of water	423-498K, 10-40 bar, TV 4L, 700-1200 RPM	GIR	T↑ k_La↑ For F-T liquid saturated with water
Chen et al.[51]	O_2	water	293-313K, 1-1.2 bar, 900-1300 RPM, TD 29 cm	GIR	T↑ k_La↑
Alghamdi[38]	H_2/CO/N_2/He	Isopar-M (C_{10}-C_{16})/ PAO-8 (C_{30}-C_{70})/ solid Al_2O_3	373-473K, 7-35 bar, 800-1200 RPM, solid up to 50 wt.%	GIR	T↑ k_La↑

Table 5: Literature Survey on the Effect of Mixing Speed on k_La

Reference	Gas	Liquid/Slurry	Operating Conditions	Reactor	Remarks
Chang et al.[23]	CO	n-hexane/n-decane/ n-tetradecane	328-428K, 1-50 bar, 800-1200 RPM, TV 4L	GIR	N↑ k_La↑
Hsu et al.[54]	O_3	Water	Ambient conditions, 500-1600 RPM	GIR	N↑ k_La↑ Level off at 1400 RPM (ε_G↑ but more coalescence)
Hichri et al.[47]	H_2	2-propanol/o-cresol/ mixture (2/3 2-propanol+ 1/3 o-cresol)/ Pyrex beads ($40<d_p<300\mu m$)	303-393K, 800-1500 RPM, TD 5 cm, 0-30 bar, solid up to 5 vol.%	GIR	N↑ k_La↑↑
Sridhar et al.[55]	N_2	Cyclohexane	297-423K, 480-1800 RPM, 1-10 bar, TD 13 cm	GSR	N↑ a↑, reaches asymptotic value at high N
Albal et al.[48]	He/O_2	Glycerin/water+CMC/ glass beads (75-150μm)/ oil shale particles	295K,13.8-96.5 bar, 400-1000 RPM, TD 10.2 cm solid up to 30 vol%	SAR	N↑ k_La↑
Dietrich et al.[49]	N_2/H_2	Ethanol/water/ hydrogenation mixture/ Ni Raney particles (10-15μm)	293-353K, 10-50 bar, TV 0.5L	GIR	N↑ k_La↑
Tekie et al.[41]	N_2/O_2	Cyclohexane	330-430K, 7-35 bar, 400-1200 RPM	GIR/SAR	N↑ k_La ↑ for both operating modes. N↑ ε_G ↑, a↑, no effect on Bubble size
Inga et al.[42]	$H_2/CO/N_2/CH_4/C_2H_4$	Hexane mixture/ Iron oxide catalyst	298-373K, 2-25 bar, 400-1200 RPM	SAR	N↑ k_La↑
Ledakowicz et al.[56]	$H_2/CO/N_2/CO_2$	Vestowax SH105	1-60 bar, 453-553 K, TV 1L	SAR	N↑ k_La↑

Table 5 (Cont'd)

Reference	Gas	Liquid/Slurry	Operating Conditions	Reactor	Remarks
Lekhal et al.[44]	H_2/CO	n-Octene/ethanol/water	323K, 10-150 bar, TV 0.6L, 1100-2500 RPM	GIR	N↑ k_La ↑↑
Karandikar et al.[46]	H_2/CO	F-T medium (C_{11}-C_{22}) M.W. 201.5 +effect of water	423-498K, 10-40 bar, TV 4L, 700-1200 RPM	GIR	N↑ k_La ↑↑ Effect of H_2O: ↑ k_La values for CO ↓ k_La values for H_2
Karandikar et al.[45]	H_2/CO/ CH_4/CO_2	F-T heavy ($\geq C_{22}$) M.W. 368.5 + effect of water	423-498K, 10-40 bar, TV 4L, 700-1200 RPM	GIR	N↑ k_La↑↑ Effect of H_2O: ↑ k_La for CO/H_2/CH_4/ CO_2 at 700 RPM ↓ k_La for H_2/CO_2 at 1000-1200 RPM No clear effect on k_La for CO/CH_4
Deimling et al.[43]	H_2/CO	F-T light(C_6-C_{11})/ F-T medium (C_{12}-C_{21})/ F-T heavy($\geq C_{22}$)/solid: glass bed (125-177μm)	373-523K, 10-40 bar, TV 2.0L, 800-1100 RPM, Solid up to 30 wt.%	SAR	N↑ k_La↑↑
Hsu et al.[53]	O_3	Water	290-303K, 600-1300 RPM, TD 29 cm	GIR	N↑ k_La↑, levels off above 1000 RPM
Chen et al.[51]	O_2	water	293-313K, 1-1.2 bar, 900-1300 RPM, TD 29 cm	GIR	N↑ k_La↑
Linek et al.[57]	O_2	Water +0.5M Na_2SO_4	293K, 250-850 RPM, TD 29 cm	GSR	N↑ k_La↑
Alghamdi[38]	H_2/CO/N_2/He	Isopar-M (C_{10}-C_{16})/ PAO-8 (C_{30}-C_{70})/ solid Al_2O_3	373-473K, 7-35 bar, 800-1200 RPM, solid up to 50 wt.%	GIR	N↑ k_La↑

Table 6: Literature Survey on the Effect of Solid Concentration on k_La

Reference	Gas	Liquid/Slurry	Operating Conditions	Reactor	Remarks
Hichri et al.[47]	H_2	2-propanol/o-cresol/ mixture (2/3 2-propanol+ 1/3 o-cresol)/ Pyrex beads ($40<d_p<300\mu m$)	303-393K, 800-1500 RPM, TD 5 cm, 0-30 bar, solid up to 5 vol.%	GIR	$C_S\uparrow$ low effect on k_La. At $40<d_p<200\mu m$ no k_La influence
Joosten et al.[59]	He/N_2	Kerosene/sieved fraction of polypropylene/sugar/ glass beds, ($53<d_p<250\mu m$)	TV 6.1L, Solids up to 45 vol.%	GSR	$k_La\uparrow$ by 10-20% at low Cs $k_La\downarrow$ at higher C_S
Albal et al.[48]	He/O_2	Glycerin/water+CMC/ glass beads (75-150μm)/ oil shale particles	295K,13.8-96.5 bar, 400-1000 RPM, TD 10.2 cm solid up to 30 vol%	SAR	$C_S\uparrow$ (2-5 vol%) $k_La\uparrow$ by 10-30% Further $C_S\uparrow$ $k_La\downarrow$
Dietrich et al.[49]	N_2/H_2	Ethanol/water/ hydrogenation mixture/ Ni Raney particles (10-15μm)	293-353K, 10-50 bar, TV 0.5L	GIR	C_S (to 3 wt%)$\uparrow$ $k_La\uparrow$ by 20% at low speed and 90% at high speed, C_S (above 3 wt%)$\uparrow$ $k_La\downarrow$
Inga et al.[42]	$H_2/CO/N_2/CH_4/C_2H_4$	Hexane mixture/ Iron oxide catalyst	298-373K, 2-25 bar, 400-1200 RPM	SAR	C_S (to 12.5 wt%)$\uparrow$ $k_La\uparrow$, $C_S\uparrow$ (above 12.5 wt%) $k_La\downarrow$
Deimling et al.[43]	H_2/CO	F-T light(C_6-C_{11})/ F-T medium (C_{12}-C_{21})/ F-T heavy($\geq C_{22}$)/solid: glass bed (125-177μm)	373-523K, 10-40 bar, TV 2.0L, 800-1100 RPM, solid up to 30 wt.%	SAR	$C_S\uparrow$ k_La significantly $\downarrow$
Ozkan et al.[76]	O_2	Water/n-butanol/ solid: $CaCO_3$/ $TiO_2/BaSO_4/Fe_2O_3$/activated C	298K, 500-700 RPM, TV 1.5L, C_S 0.1-2 vol.%	SAR	Effect of particles of $d_P\sim\delta$

Table 6 (Cont'd)

Reference	Gas	Liquid/Slurry	Operating Conditions	Reactor	Remarks
Kluytmans et al.[60]	O_2	Water +electrolyte (sodium gluconate)/ solid: carbon particles (30μm)	298K, TV 1.5L, 500-1500 RPM, solid up to 0.4 wt.%	SAR/GIR	C_S↑ k_La↑, at C_S =cst, the increase in k_La becomes smaller with N↑
Alghamdi[38]	$H_2/CO/N_2/He$	Isopar-M (C_{10}-C_{16})/ PAO-8 (C_{30}-C_{70})/ solid: Al_2O_3	373-473K, 7-35 bar, 800-1200 RPM, solid up to 50 wt.%	GIR	k_La↑ with C_S up to 12.5 wt.%. k_La↓ above
Ruthiya et al.[61]	O_2/H_2	Glucose solution/ α-methyl styrene (AMS)/ solid: SiO_2/carbon particles ($30<d_p<40$μm)	323K (glucose) 303K (AMS)	GIR	k_La↑ at low solid concentrations
Oguz et al.[58]	O_2	Water +solid (Al_2O_3, Fe_2O_3, TiO_2, ZnO, sea sand, Kieselguhr)	298K, 500-800 RPM, TV 4L, C_S up to 10 vol.% ($0.5<d_p<80$μm)	GSR	No effect of sand. C_S↑ k_La↓ for TiO_2 and ZnO, for Fe_2O_3 and Kieselguhr little effect at low C_S then k_La↓
Ruthiya et al.[62]	O_2/H_2	Glucose solution/ α-methyl styrene (AMS)/ solid: SiO_2/carbon particles ($30<d_p<40$μm)	323K (glucose) 303K (AMS), 200-700 RPM	SAR	k_La enhancement at $C_S<1kg/m^3$

Table 7: Literature Survey on the Effect of Liquid Nature on k_La

Reference	Gas	Liquid/Slurry	Operating Conditions	Reactor	Remarks
Hsu et al.[54]	O_3	Water	Ambient conditions, 500-1600 RPM	GIR	HL↓ k_La↑, HL↑ε_G ↓ Liq. Height↑Bubble size↓
Hichri et al.[47]	H_2	2-propanol/o-cresol/ mixture (2/3 2-propanol+ 1/3 o-cresol)/ Pyrex beads ($40<d_p<300\mu m$)	303-393K, 800-1500 RPM, TD 5 cm, 0-30 bar, solid up to 5 vol.%	GIR	HL↓ k_La↑, $k_La_{proanol}>k_La_{cresol}>k_La>_{mixture}$
Albal et al.[48]	He/O_2	Glycerin/water+CMC/ glass beads (75-150μm)/ oil shale particles	295K,13.8-96.5 bar, 400-1000 RPM, TD 10.2 cm Solid up to 30 vol%	SAR	μ_L↑ C^*↓ k_La↓ σ↓ k_La↑
Karandikar et al.[43, 45, 46]	H_2/CO	F-T light(C_6-C_{11})/ F-T medium (C_{12}-C_{21})/ F-T heavy($\geq C_{22}$)	373-523K,10-40 bar, TD 10.1 cm, 700-1200 rpm	SAR/GIR	Carbon No.↑ k_La↓
Chang et al.[23]	CO	n-hexane/n-decane/ n-tetradecane	328-428K, 1-50 bar, 800-1200 RPM, TV 4L	GIR	Carbon No.↑ k_La↓
Alghamdi[38]	$H_2/CO/N_2/He$	Isopar-M (C_{10}-C_{16})/ PAO-8 (C_{30}-C_{70})/ solid Al_2O_3	373-473K, 7-35 bar, 800-1200 RPM, solid up to 50 wt.%	GIR	$k_La_{Isopar-M}>k_La_{PAO-8}$

3.0 OBJECTIVE

From the preceding background and literature review, it appears clearly that the liquid-side mass transfer coefficient is one of the most important parameter, along with kinetics, which governs the overall rate of reaction of slurry processes in agitated reactors. As presented in section 2, the mass transfer data can be found in literature but most of them are unfortunately inconsistent and available for system that are not necessarily representative of typical high pressure, high temperature and high solid loading applications used in most industrial slurry processes.

The main objective of the present study is to determine the volumetric liquid-side mass transfer coefficient and gases solubility in a slurry reactor operating under Fischer-Tropsch synthesis conditions. In order to achieve this objective, the following experimental program is devised:

1. Measure the solubility, C^*, and the liquid-side volumetric mass-transfer coefficient, k_La, of syngas, hydrogen and carbon monoxide, as well as helium and nitrogen, in two different mixtures of hydrocarbons, polyalphaolefins (PAO-8) and Sasol wax, having physical properties similar to a F-T liquid, under typical operating conditions used in the industrial F-T process;
2. Study the effect of the main process variables, pressure (P), temperature (T), mixing speed (N) and solid concentration (C_S) on both solubility and volumetric liquid-side mass-transfer coefficient; and
3. Develop statistical and empirical correlations that relate the volumetric liquid-side mass-transfer coefficients with the main process variables.

The data obtained in this study can then be used to delineate the important operating variable affecting the mass transfer resistance in the slurry-phase F-T process in agitated reactors.

4.0 EXPERIMENTAL

4.1 GAS-LIQUID-SOLID SYSTEMS AND OPERATING VARIABLES USED

The gas-liquid-solid systems and the ranges of operating variables used in this study are:

Gases:	He, N_2, H_2 and CO
Liquids:	Polyalphaolefins (PAO-8), Sasol Wax
Solid:	Alumina powder, Al_2O_3
Pressure:	7 to 35 bars
Temperature:	423 to 523K
Mixing speed:	800 to 1200 RPM
Solid concentration:	0 to 50 wt%
Reactor operating mode:	Gas-Inducing Reactor (GIR)

4.2 PROPERTIES OF THE GAS PHASE

The gases used in this study (He, N_2, H_2 and CO) have a purity of 99.997%, 99.998%, 99.999% and 99.3%, respectively. Helium, nitrogen and carbon monoxide were purchased from Valley National Gases (West Mifflin, PA, USA) and hydrogen was purchased from Praxair (Danbury, CT, USA). The basic thermodynamic properties for these gases are listed in Table 8.

Table 8: Thermodynamic Properties of Gases used[77]

	MW (kg/kmol)	Tb (K)	T_C (K)	P_C (bar)	V_C (m^3/kmol)	ω -	Z_C -
N_2	28.014	77.35	126.20	33.98	0.0901	0.037	0.289
He	4.003	4.30	5.19	2.27	0.0573	-0.390	0.301
H_2	2.016	20.27	33.25	12.97	0.065	-0.216	0.305
CO	28.010	81.66	132.85	34.94	0.0931	0.045	0.292

4.3 PROPERTIES OF THE LIQUID PHASE

The two liquids used in this study were polyalphaolefin, PAO-8, purchased from Chevron (USA) and C_{80} wax purchased from Moore & Munger, Inc. which is a Sasol (South Africa) product.

4.3.1 Polyalphaolefin (PAO-8) Composition

The polyalphaolefins, also called Synfluid™, are mainly used as synthetic lubricant in the U.S. and Europe. They are usually made by oligomerization and dimerization of normal α-olefins treated with Lewis acids, as shown in Equation (4-1), to produce dimers, trimers, tetramers and other related compounds. Dimers with a terminal double bond and an alkyl group on the second carbon of the double bond can also be produced by using an aluminum alkyl catalyst. The resulting product consists of highly branched homo-polymer of the α-olefin and consequently, polyalphaolefins have much lower pour points than straight-chained hydrocarbons of the same molecular weight. PAO-8 used for this study is a 1-decene, $C_{10}H_{20}$, homo-polymer with a high viscosity index (138) indicating low change in viscosity with temperature. This product also exhibits a good thermal stability and a low vapor pressure in the range of temperature used (423 - 523K). The carbon number distribution, given by Chevron, is listed in Table 9 and Table 10.

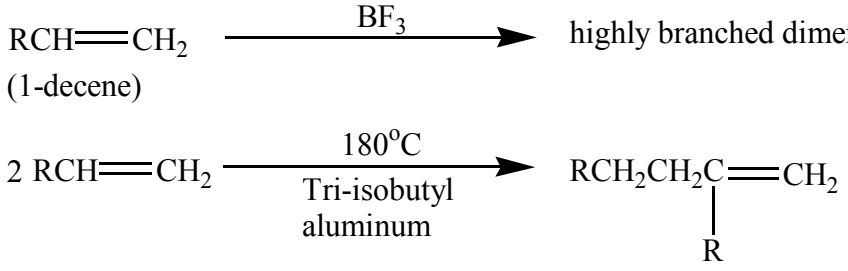

(4-1)

Table 9: PAO-8 Mass Composition

Component	Wt%
C_{30}	4
C_{40}	54
C_{50}	28
C_{60}	10.3
C_{70}	3.7

Table 10: PAO-8 Components Characterization

Component	Wt%
C_{10} trimer	4
C_{10} tetramer	54
Pentamer and higher	42

4.3.2 Sasol Wax Composition

Sasol wax, also called Paraflint™ Sasol is a wax produced from F-T process by Sasol, South Africa. This wax consists mainly of saturated and straight chain of hydrocarbons with almost no branches. Unlike PAO-8 which is a liquid at room temperature due to its highly branched homopolymer, Sasol wax is solid with a melting point around 83ºC. The molar composition of the Sasol wax is given in Figure 4; and as can be seen the hydrocarbon carbon number is ranging

from C_{17} up to C_{79} with a carbon number between C_{29} and C_{53} accounting for almost 93 mol.% of the total molar composition.

4.3.3 Molecular Weights of the PAO-8 and Sasol Wax

An average molecular weight for both hydrocarbon mixture used in this study can be calculated from the compositions given in Sections 4.3.1 and 4.3.2. The molecular weight for PAO-8 and Sasol wax were calculated using Equations (4-2) and (4-3), respectively:

$$\frac{1}{MW_{PAO8}} = \sum_{i=1}^{n} \frac{w_i}{MW_i} \tag{4-2}$$

$$MW_{Wax} = \sum_{i=1}^{n} x_i MW_i \tag{4-3}$$

where w_i and x_i represents the mass and the mole fraction of species i, respectively. The calculated molecular weights were 620 kg/kmol for PAO-8 and 568 kg/kmol for Sasol Wax.

4.3.4 Thermodynamic Parameters

The available thermodynamic properties the PAO-8 and Sasol Wax are listed in Table 11.

Table 11: Thermodynamic Properties of PAO-8 and Sasol Wax[77-83]

	MW (kg/kmol)	Tb (K)	T_C (K)	P_C (bar)	V_C (m^3/kmol)	ω -	Z_C -
PAO-8	620	703	909.64	4.56	-	1.56	-
Wax C_{80}	568	794	883.23	4.223	-	1.5384	0.2165

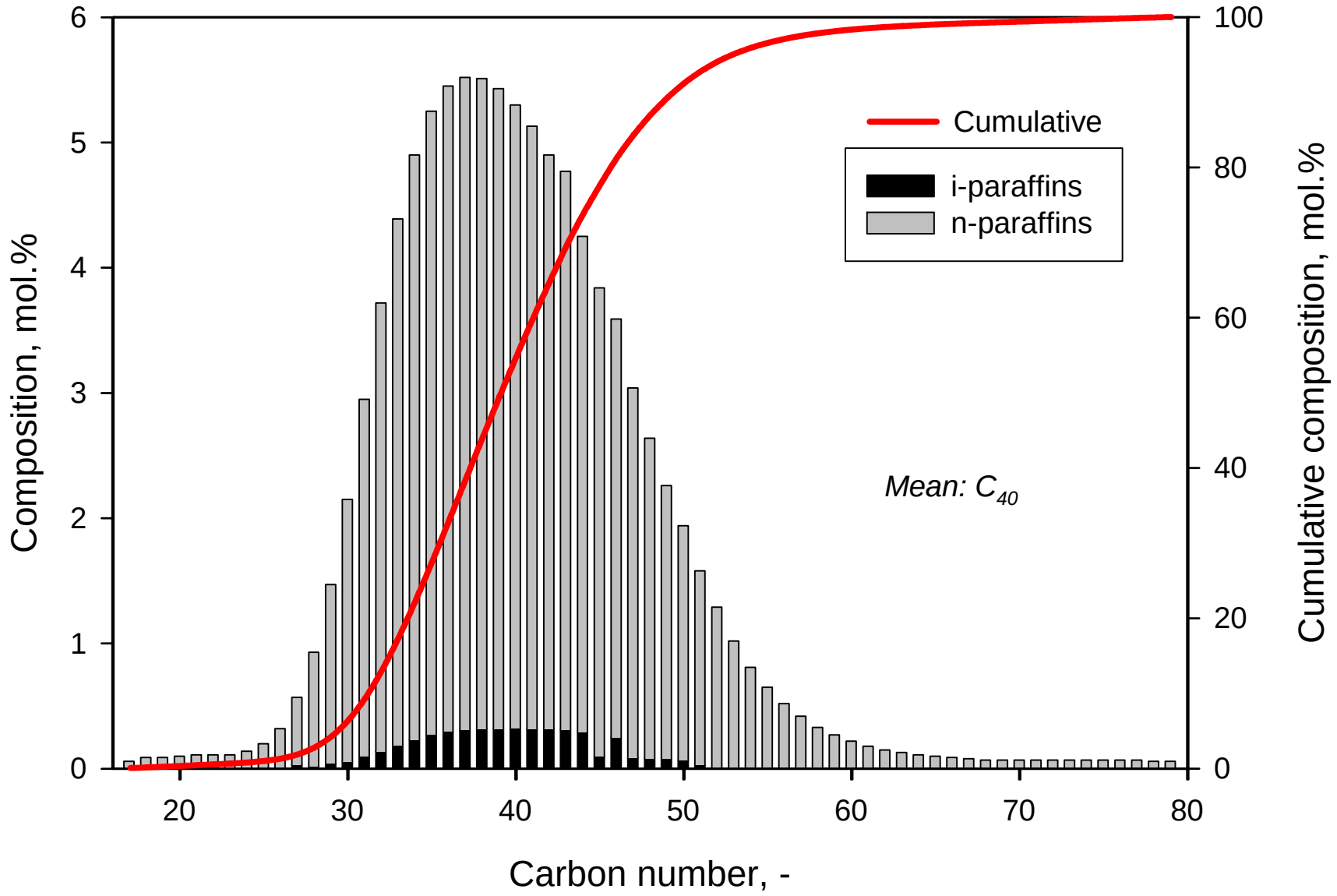

Figure 4: Molar Composition of Sasol Wax

4.3.5 Vapor Pressure of PAO-8 and Sasol wax

The vapor pressure, P^S for PAO-8 was obtained from Chevron and was correlated using the following equation:

$$P^S = 8x10^{-9} e^{0.0505T - 13.786} \quad (4\text{-}4)$$

The vapor pressure for Sasol Wax was estimated from literature data for C_{17} to C_{79} linear hydrocarbons given by Kudchadker et al.[84] and using their corresponding molar composition in the Sasol wax. The resulting vapor pressure-temperature relation can be written as:

$$\log_{10}(P^S) = 6.39159 - \frac{5165.43}{T} + \frac{164347.29}{T^2} \quad (4\text{-}5)$$

A plot of vapor pressure as a function of temperature for PAO-8 and Sasol wax is illustrated in Figure 5.

4.3.6 Liquid Density of PAO-8 and Sasol wax

The liquid density, ρ_L for PAO-8, given by equation (4-6), was correlated as a function of temperature using data provided by Chevron.

$$\rho_L = 1012.7 - 0.6238 \times T \quad (4\text{-}6)$$

The density of Sasol wax was measured in our laboratory under a wide range of temperatures (400 to 480K). The resulting data were then correlated as a function of temperature by the following expression:

$$\rho_L = 959.082 - 0.513\,T \quad (4\text{-}7)$$

A plot of liquid density as a function of temperature for PAO-8 and Sasol wax is shown in Figure 6.

4.3.7 Liquid Viscosity of PAO-8 and Sasol wax

The viscosity, μ_L, for PAO-8, given by equation (4-8), was correlated as a function of temperature using data provided by Chevron.

$$\mu_L = 1.1068e^{-0.0143T} \tag{4-8}$$

For Sasol wax, the liquid viscosity was calculated according to the corresponding-states group-contribution method from Liang et al.[85] using the following equations:

$$\ln\left(\frac{\mu_L}{\mu_c}\right) = -3.29835 + \frac{1.27666}{T_r} \tag{4-9}$$

$$\mu_c = 0.0411\left(\frac{MW^{1/2}(10000P_c)^{2/3}}{T_c^{1/6}}\right) \tag{4-10}$$

Where μ_c, T_c and P_c are the critical properties of the liquid, and T_r is the reduced temperature. Using these relations along with the molecular composition of the Sasol wax, the following liquid viscosity-temperature relation can be obtained:

$$\ln(\mu_L) = -7.7104 + \frac{1127.58}{T} \tag{4-11}$$

The effect of temperature on the viscosity is presented in Figure 7 for PAO-8 and Sasol wax.

4.3.8 Liquid Surface Tension of PAO-8 and Sasol wax

The surface tension of PAO-8 was estimated using equation (4-12).

$$\sigma_m^r = \sum_{j=1}^{n} x_j \sigma_j^r \tag{4-12}$$

A value of r =1 is recommended[77] for most hydrocarbons mixture and the surface tensions for each pure compound, σ_j, were calculated using the correlation given by Marano et al.[79, 86] as follow:

$$Y = Y_{\infty,0} + \Delta Y_{\infty}(n - n_0) - \Delta Y_0 \exp(-\beta(n - n_0)^{\gamma}) \quad (4\text{-}13)$$

with ΔY_0 and ΔY_{∞} dependent on temperature as follows:

$$\Delta Y_0 or Y_{\infty,0} = A + BT + CT^2 \quad (4\text{-}14)$$

Table 12: Coefficients for Equations (4-13) and (4-14)

Surface tension (10^{-3}N/m)			
n_0	ΔY_{∞}	β	γ
0.236 483	0	2.511 846	0.201 325

Surface tension (10^{-3}N/m)		
	ΔY_0	ΔY_{∞}
A	627.213	73.8715
B	-0.882 888	-0.177 123
C	0.002 681 88	$1.545\ 17.10^{-4}$

For Sasol wax, the liquid surface tension was calculated using the Macleod-Sugden correlation[77, 87-89] and the Weinaug-Katz modification of this equation:

$$\sigma^{1/4} = \sum_{i=1}^{n} [P_i] \left(x_i \frac{\rho_L}{MW_L} - y_i \frac{\rho_V}{MW_V} \right) \quad (4\text{-}15)$$

where $[P_i]$ is the Parachor of the pure component. Tabulated Parachor values can be found in literature[77, 89] or can be calculated via a group contribution method, a summary of these values for C_{17} to C_{79} linear hydrocarbons present in the Sasol wax is given in Table 13. The ρ_L and ρ_V are the Sasol wax liquid and vapor density, respectively with their corresponding molecular weight MW_L and MW_V. x_i and y_i are the molar fraction of the compound considered in either the liquid or the gas phase (in the case of Sasol wax, the gas phase term was neglected due to the low vapor pressure at the temperature interval used).

The resulting equation was obtained to express the dependency of the liquid surface tension on the temperature for Sasol wax:

$$\sigma_L = 57.3204 - 0.10685 \times T + 0.00005496 \times T^2 \quad (4\text{-}16)$$

A plot of the liquid surface tension as a function of temperature for PAO-8 and Sasol wax is presented in Figure 8.

Table 13: Parachor Values for Components in Sasol Wax

Component	$[P_i]$	Component	$[P_i]$	Component	$[P_i]$
n-C_{17}	715.5	n-C_{38}	1561.8	n-C_{59}	2408.1
n-C_{18}	755.8	n-C_{39}	1602.1	n-C_{60}	2448.4
n-C_{19}	796.1	n-C_{40}	1642.4	n-C_{61}	2488.7
n-C_{20}	836.4	n-C_{41}	1682.7	n-C_{62}	2529
n-C_{21}	876.7	n-C_{42}	1723	n-C_{63}	2569.3
n-C_{22}	917	n-C_{43}	1763.3	n-C_{64}	2609.6
n-C_{23}	957.3	n-C_{44}	1803.6	n-C_{65}	2649.9
n-C_{24}	997.6	n-C_{45}	1843.9	n-C_{66}	2690.2
n-C_{25}	1037.9	n-C_{46}	1884.2	n-C_{67}	2730.5
n-C_{26}	1078.2	n-C_{47}	1924.5	n-C_{68}	2770.8
n-C_{27}	1118.5	n-C_{48}	1964.8	n-C_{69}	2811.1
n-C_{28}	1158.8	n-C_{49}	2005.1	n-C_{70}	2851.4
n-C_{29}	1199.1	n-C_{50}	2045.4	n-C_{71}	2891.7
n-C_{30}	1239.4	n-C_{51}	2085.7	n-C_{72}	2932
n-C_{31}	1279.7	n-C_{52}	2126	n-C_{73}	2972.3
n-C_{32}	1320	n-C_{53}	2166.3	n-C_{74}	3012.6
n-C_{33}	1360.3	n-C_{54}	2206.6	n-C_{75}	3052.9
n-C_{34}	1400.6	n-C_{55}	2246.9	n-C_{76}	3093.2
n-C_{35}	1440.9	n-C_{56}	2287.2	n-C_{77}	3133.5
n-C_{36}	1481.2	n-C_{57}	2327.5	n-C_{78}	3173.8
n-C_{37}	1521.5	n-C_{58}	2367.8	n-C_{79}	3214.1

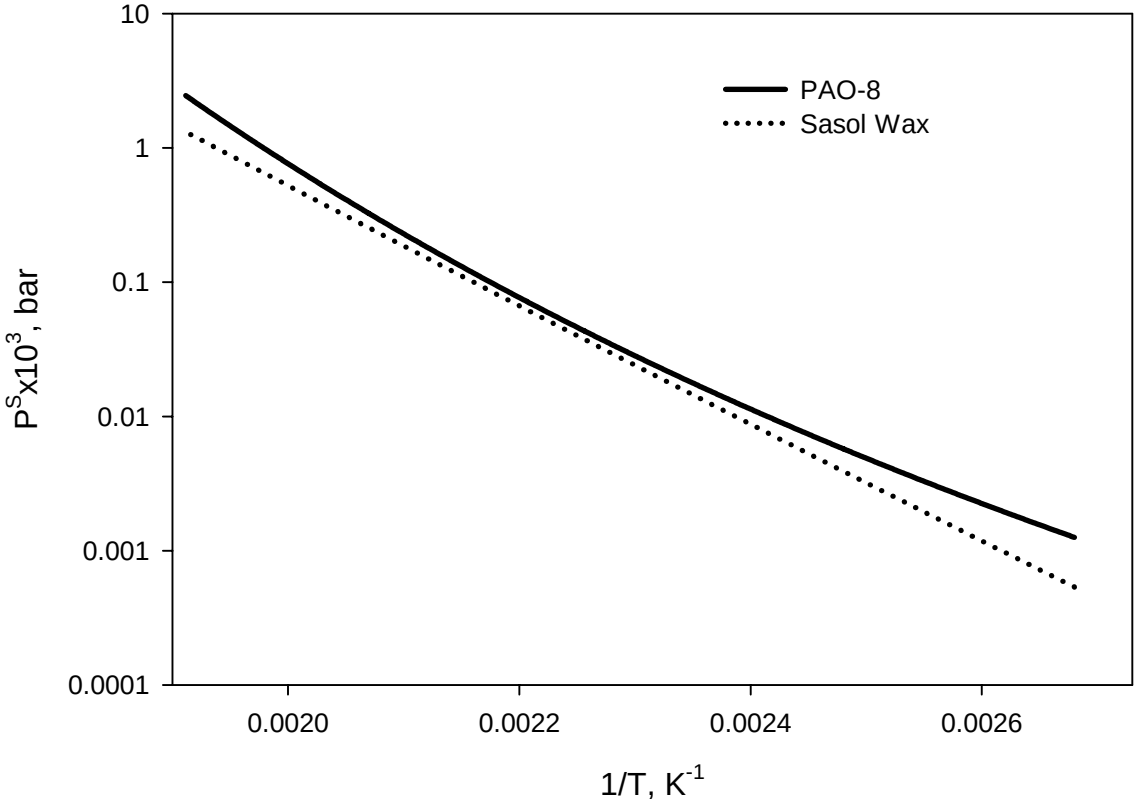

Figure 5: Effect of Temperature on the Vapor Pressure

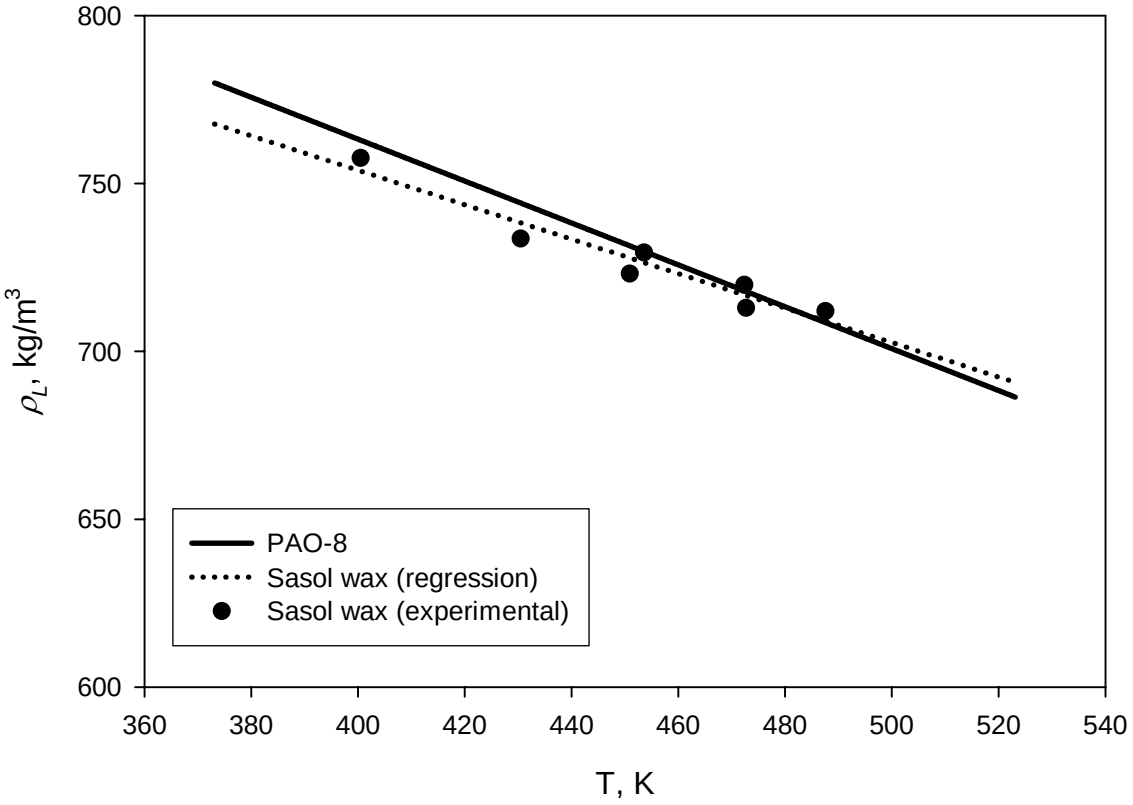

Figure 6: Effect of Temperature on Liquid Density

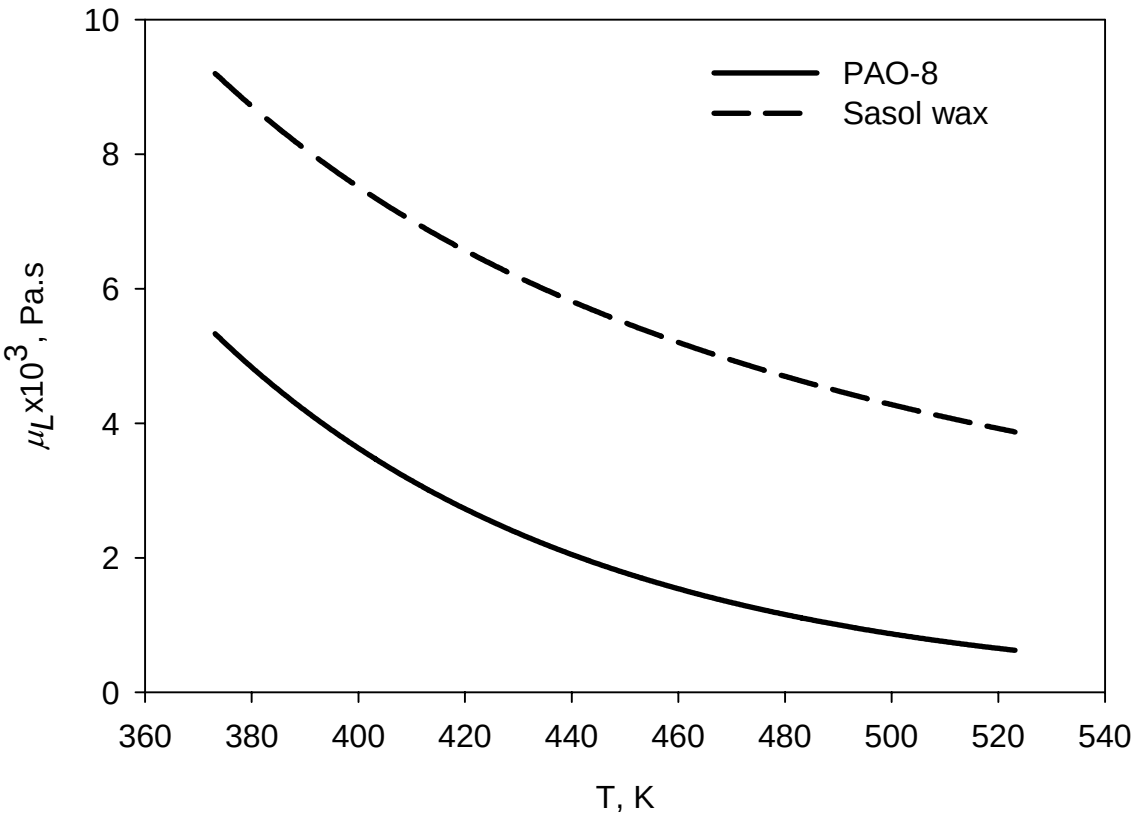

Figure 7: Effect of Temperature on Liquid Viscosity

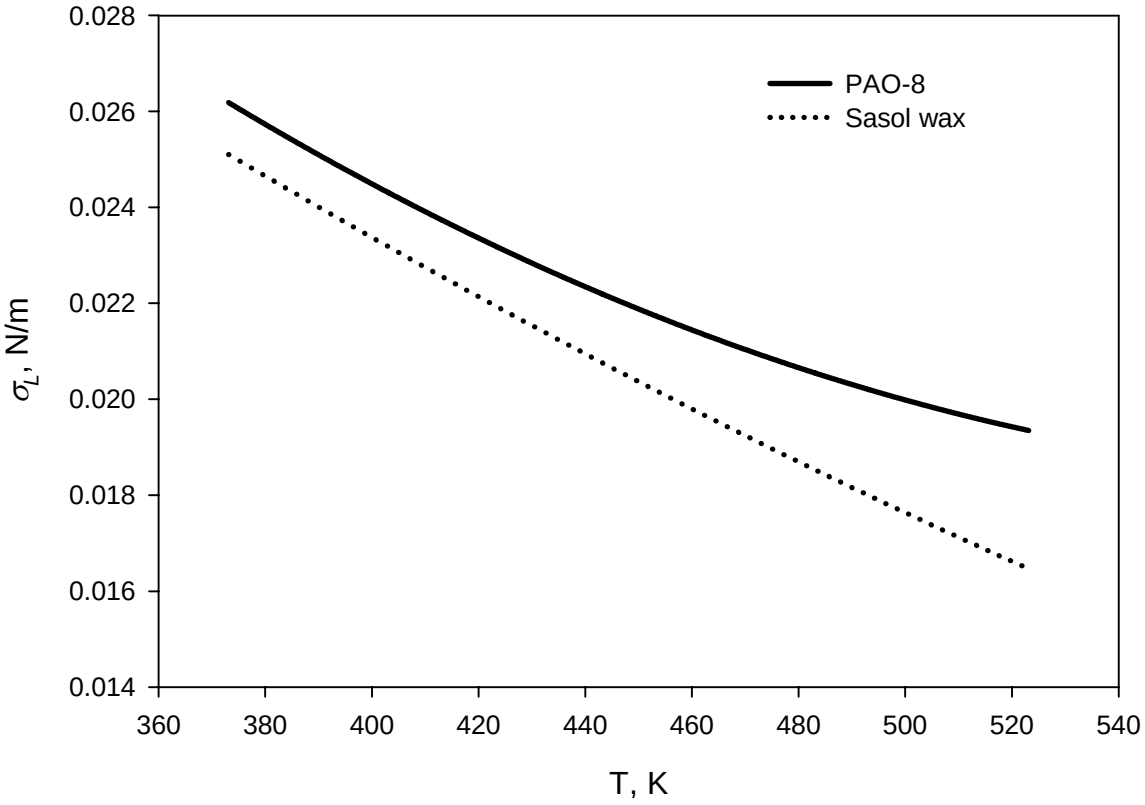

Figure 8: Effect of Temperature on Liquid Surface Tension

4.3.9 Gas-Liquid Diffusivity

The diffusivities of H_2, N_2, He and CO in PAO-8 and Sasol wax were calculated using the Wilke and Chang[77, 90] equation.

$$D_{AB} = 1.1728 \times 10^{-16} \frac{(\lambda\, MW_B)^{0.5} T}{\mu_L \upsilon_A^{0.6}} \tag{4-17}$$

A and B represent the gas and the liquid, respectively, λ, the association factor of the solvent (λ = 1) and v_A is the gas molar volume. A plot representing the gas-liquid diffusivity of all 4 gases in PAO-8 and Sasol wax is shown in Figure 9.

4.4 PROPERTIES OF THE SOLID PHASE

The solid particles used in this study are an aluminum oxide Al_2O_3 purchased from Engelhard (Beachwood, OH, USA). The aluminum oxide powder was analyzed using a Scanning Electron Microscope (SCM). Snapshots of Alumina powder with different magnifications are shown in Figure 10. Image analysis to determine each particle diameter was carried out with BioScan Optimas Software 4.1, and the resulting particle size distribution is shown in Figure 11. The mean particle size was found to be 32.33 μm and, based on Equation (4-18), the Sauter mean particle diameter was 42.37 μm.

$$d_S = \frac{\sum_{i=1}^{N} n_i d_{P,i}^3}{\sum_{i=1}^{N} n_i d_{P,i}^2} \tag{4-18}$$

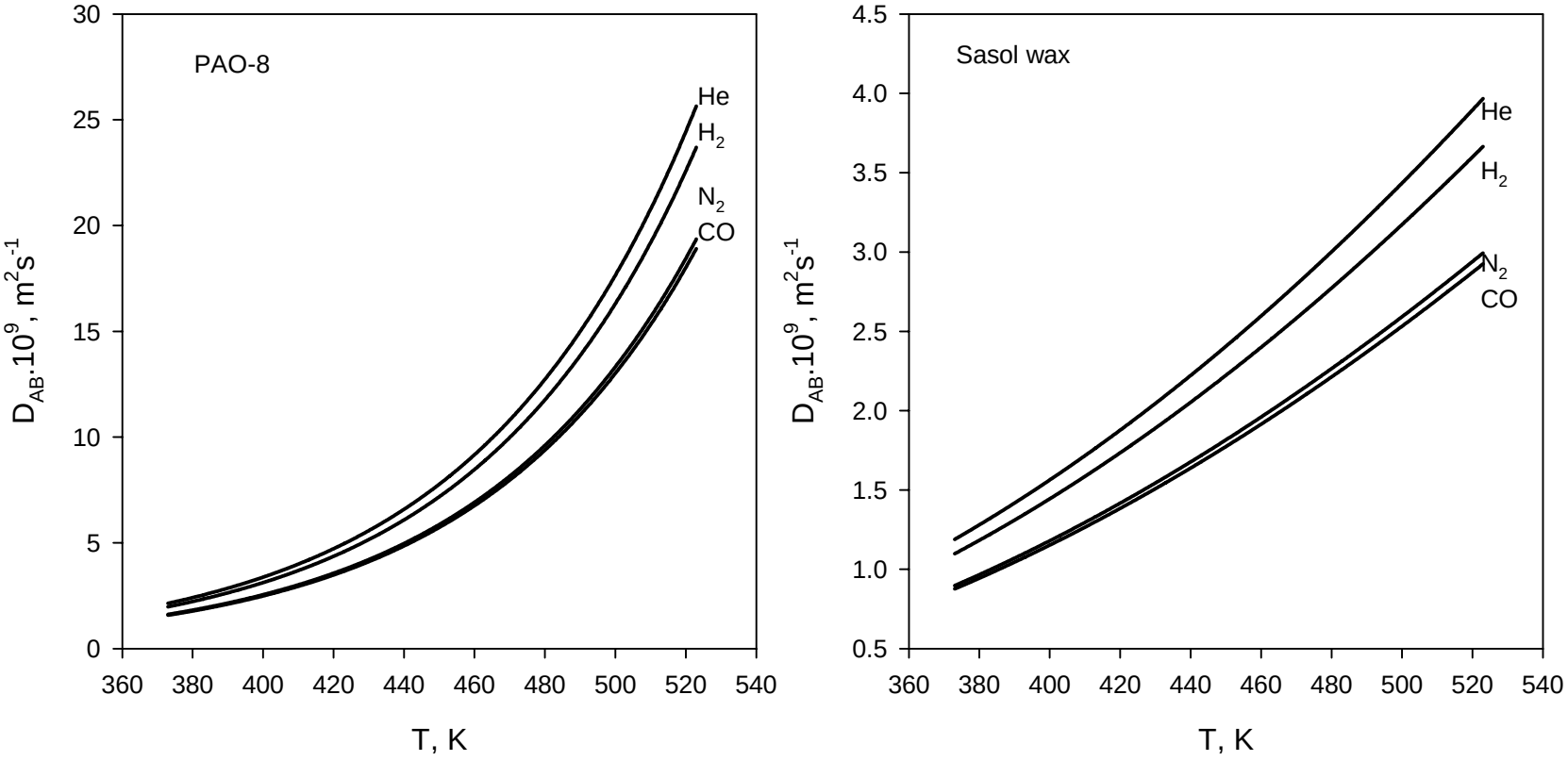

Figure 9: Effect of Temperature on the Gas-Liquid Diffusivity

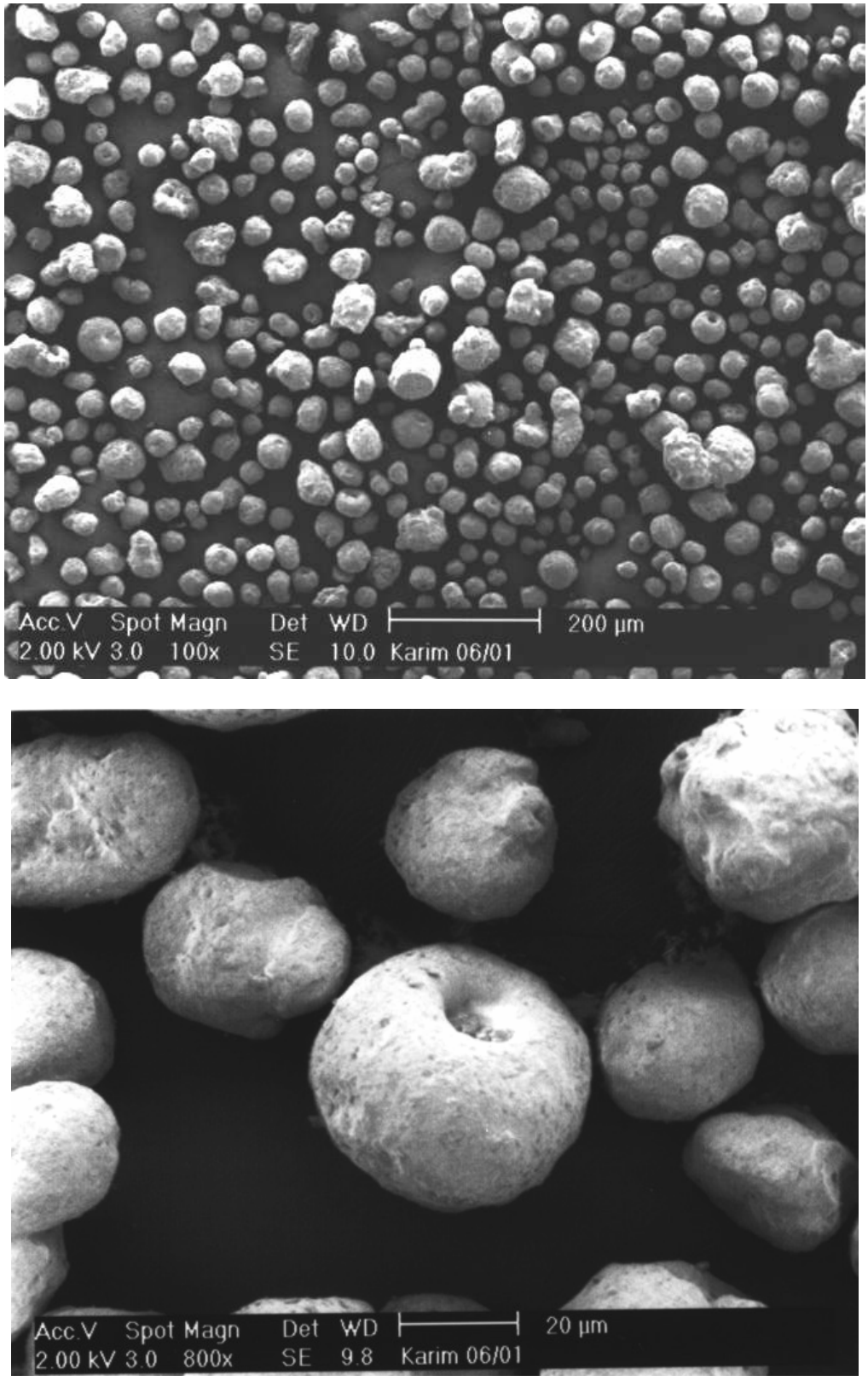

Figure 10: SEM of Alumina Particles

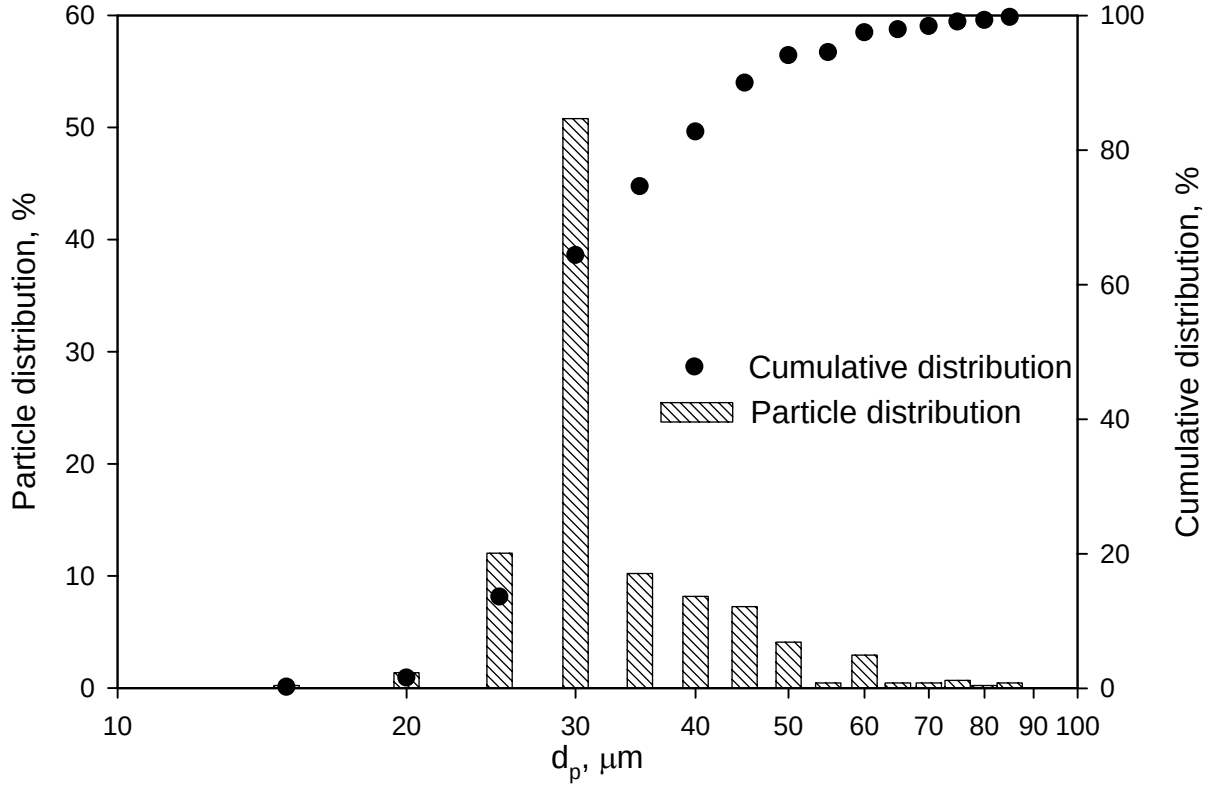

Figure 11: Alumina Powder Particle Size Distribution

4.5 SLURRY PROPERTIES

4.5.1 Slurry Density

The slurry density, ρ_{SL}, is estimated for both PAO-8 and Sasol wax liquids using the following equation:

$$\rho_{SL} = \frac{m_{cat.} + m_L}{(\frac{m_{cat.}}{\rho_{cat.}}) + (\frac{m_L}{\rho_L})} \tag{4-19}$$

ρ_L is calculated from Equations (4-6) and (4-7) given in the preceding section and $\rho_{cat.}$, the alumina density is 3062 kg/m^3. Figure 12 shows different values of slurry densities as a function of temperature for both PAO-8 and Sasol wax.

4.5.2 Slurry Viscosity

Several correlations can be found in literature to predict the slurry viscosity; a summary of the correlations available is given in Table 14; and a plot of these equations is depicted in Figure 13. In this study, the equation proposed by Barnea et al.[91] was used to calculate the slurry viscosity in this study because it was developed using several literature data for different liquids (densities from 848 to 1000 kg.m^{-3} and viscosities from 0.628 to 4.59 Pa.s) containing wide ranges of solid concentrations and particles types (densities from 1,603 to 7,740 kg.m^{-3} and particle diameter from 0.013 to 5 mm). The slurry viscosities for PAO-8 and Sasol wax at various solid concentrations are also given in Figure 13.

Table 14: Slurry Viscosity Correlations

Authors	μ_{Slurry}, *Pa.s*	*Equation*	*Remarks*
Thomas[92]	$\mu_{SL} = \mu_L(1 + 2.5C_V + 10.05C_V^2 + 0.00273e^{16.6C_V})$	(4-20)	Semi-theoretical, limitation for $C_V \rightarrow 0$
Saxena et al.[93]	$\mu_{SL} = \mu_L(1 + 4.5C_V)$	(4-21)	Obtained with air-water system
Guth et al.[94, 95]	$\mu_{SL} = \mu_L(1 + 2.5C_V + 14.1C_V^2)$	(4-22)	Holds up to $C_V = 0.08$
Barnea et al.[91]	$\mu_{SL} = \mu_L \exp\left(\frac{5/3\, C_V}{1 - C_V}\right)$	(4-23)	Compilation of literature data
Roscoe[96]	$\mu_{SL} = \mu_L(1 - C_V)^{-2.5}$	(4-24)	Semi-theoretical, suspension of spheres of equal size
Einstein[97]	$\mu_{SL} = \mu_L(1 + 2.5C_V)$	(4-25)	Restricted to low concentrations
Vand[98]	$\mu_{SL} = \mu_L \exp\left(\frac{2.5C_V + 2.7C_V^2}{1 - 0.609C_V}\right)$	(4-26)	No interaction between particles

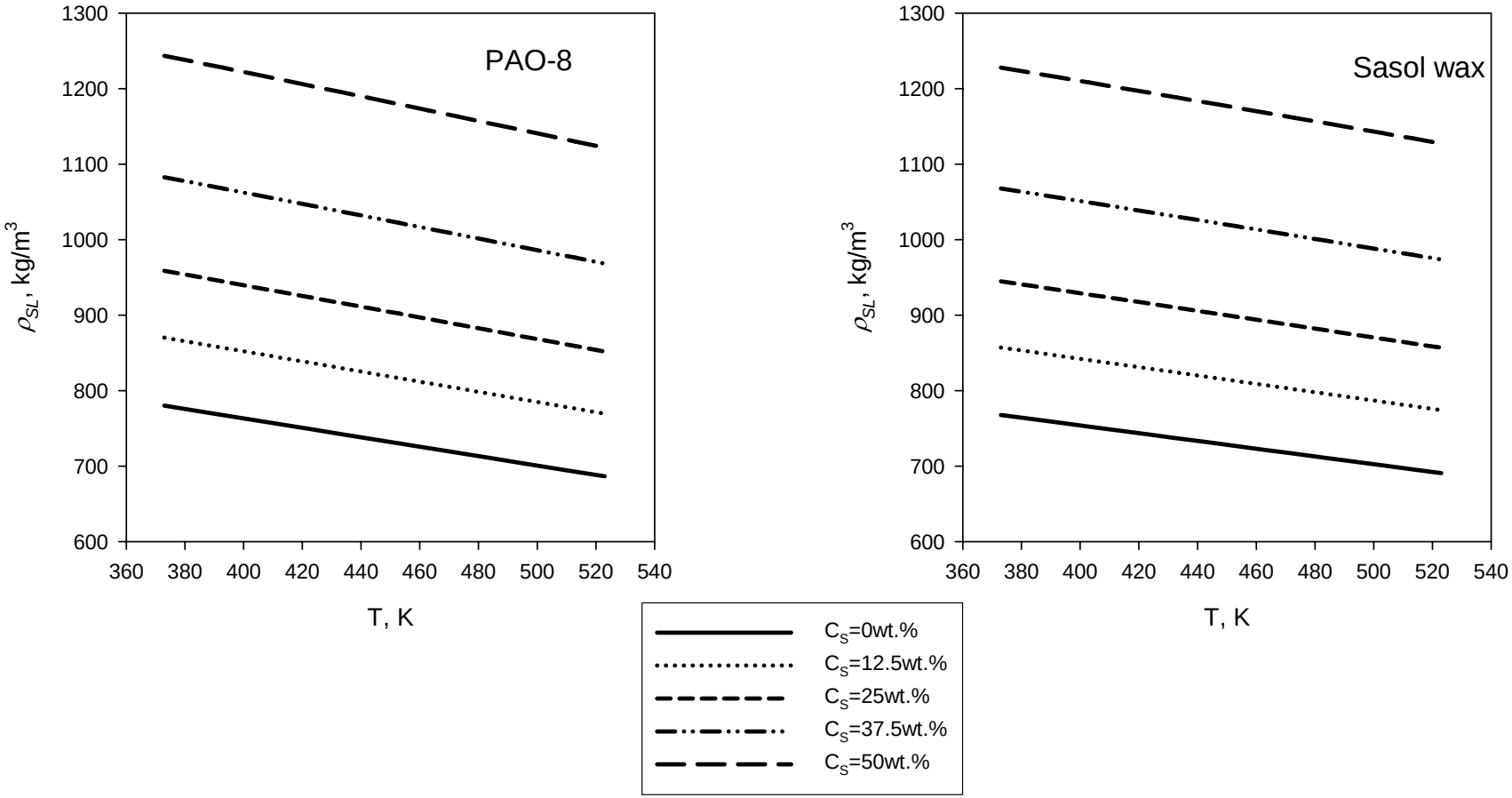

Figure 12: Effect of Temperature on Slurry Density

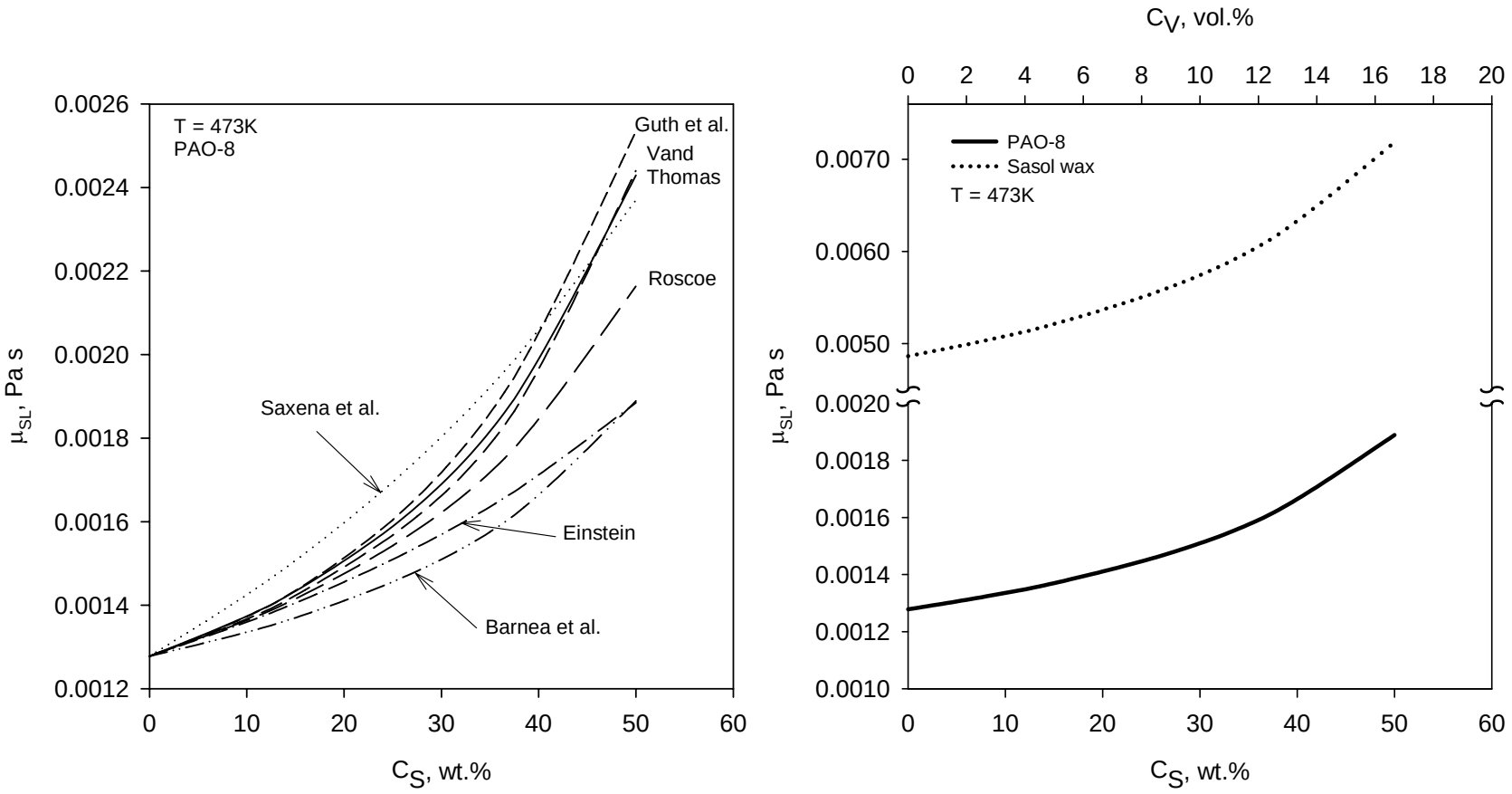

Figure 13: Slurry Viscosity Correlations

4.6 EXPERIMENTAL SETUP

The experimental setup, schematically represented in Figure 14, consists of the following main units:

1. Reactor
2. Preheater
3. Vacuum system
4. Computer and data acquisition system

4.6.1 Reactor

A one liter bolted Autoclave manufactured by Autoclave Engineers, Inc. with an effective volume of 1.028 liters operated in a gas-inducing mode is used in this study. The reactor is rated for a maximum working pressure of 5450 psi at a maximum temperature of 850 ºF. Details and dimensions are given in Figure 15 and also summarized in Table 15. The reactor is equipped with four baffles located symmetrically to avoid the formation of vortices, an internal cooling coil, an external heating jacket as well as a heating tape and thermal insulation wrapped around the upper part of the reactor to achieve a better temperature control. A hollow shaft connected to a 6 flat-blade impeller is used for mixing. Four holes of 2.4 mm diameter drilled at each end of the hollow shaft enable the reactor to be operated in a gas-inducing mode. The agitator is driven by a magnetic drive with enough capacity to avoid any eccentricity. Two thermocouples (K-type) and a Setra pressure transducer (model 205-2 0-1000 psig) are used to measure and record the change of pressure and temperature in both liquid and gas phase.

Table 15: Reactor Dimensions

Reactor inside diameter, d_T	76[(*)]
Reactor outer diameter	111
Impeller diameter	31.75
Baffle Width ($1/10^{th}$ of d_T)	7.6
Number of Baffles	4
Reactor material of construction	316 SS
Geometry	Cylindrical
Lower impeller clearance from the bottom	45
Hollow shaft length	178
Liquid height above impeller	60
Number of impellers	1
Number of blades	6
Impeller type	Flat blade disk turbine
Shaft hole diameter	2.4
Liquid height	110.2
Reactor inside depth	238
Volume of the reactor	1.028 liter

[(*)] *all dimensions are in mm unless stated otherwise*

4.6.2 Preheater

The preheater, a high-pressure vessel with an effective volume of 5.42 10^{-4} m^3, is used to heat the gas to a desired temperature before being charged into the reactor. It is maintained to the desired temperature by a furnace with an automatic temperature controller from Lindberg, USA. A radiation shielded K-type thermocouple is used to measure the temperature; and a pressure transducer from Setra (model 205-2) rated up to 3000 psig is used to record the pressure.

4.6.3 The vacuum System

A HYVAC-14, 2-stage mechanical vacuum pump from CENCO, Chicago, USA is used to vacuum the entire system to a minimum absolute pressure of 5 mm Hg. The vacuum pump is used to degas the slurry in the reactor prior the experiment; and to ensure that no gas remains in the system. A Jerguson window liquid trap is placed between the reactor and the pump to prevent

liquid entrance into the vacuum system and to monitor any possible liquid loss. The outlet of the vacuum pump is directly connected to a fume hood.

4.6.4 Data Acquisition Unit

Both thermocouples and pressure transducers are interfaced via an EXP-16 extension board linked to a DAS-8 PGA acquisition board from Metrabyte, Corp., Taunton, MA, USA connected to an Intel-based Personal Computer (PC). Programs with a Graphic User Interface developed in our laboratory are used to monitor and record the system's temperature and pressure. During the absorption, the decline of pressure is displayed as a function of time and all temperature-pressure data are stored in files.

4.7 EXPERIMENTAL PROCEDURES

In this study, the multi-step transient physical gas absorption method was used to obtain the equilibrium solubility, C^*, and the volumetric liquid-side mass transfer coefficient, k_La for H_2, CO, N_2 and He in PAO-8 and Sasol wax in the operating conditions listed in Section 4.1. This experimental procedure is similar to that reported by Chang et al.[39, 40, 99], Tekie et al.[100, 101], Fillion[102], Martinez[103] and Alghamdi[38]. The experimental procedures are given below:

1. A predetermined amount of PAO-8 or wax and, if applicable, alumina powder is charged into the reactor.
2. The reactor is closed and the liquid and the whole system are degassed.
3. The gas used (H_2, CO, N_2 or He) is charged into the preheater.
4. Both reactor and preheater are heated to the desired temperature.

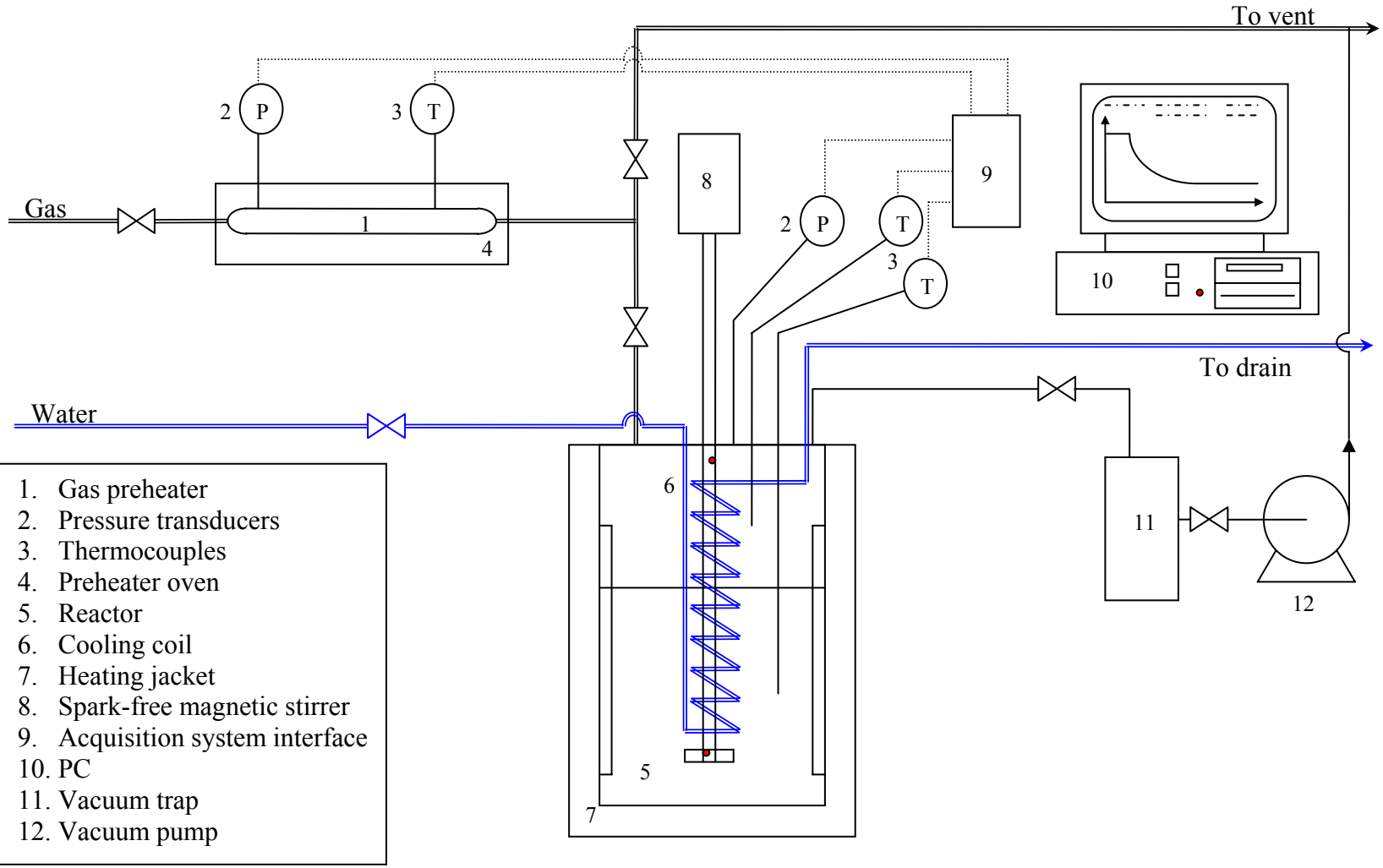

Figure 14: Schematic Diagram of the Experimental Setup

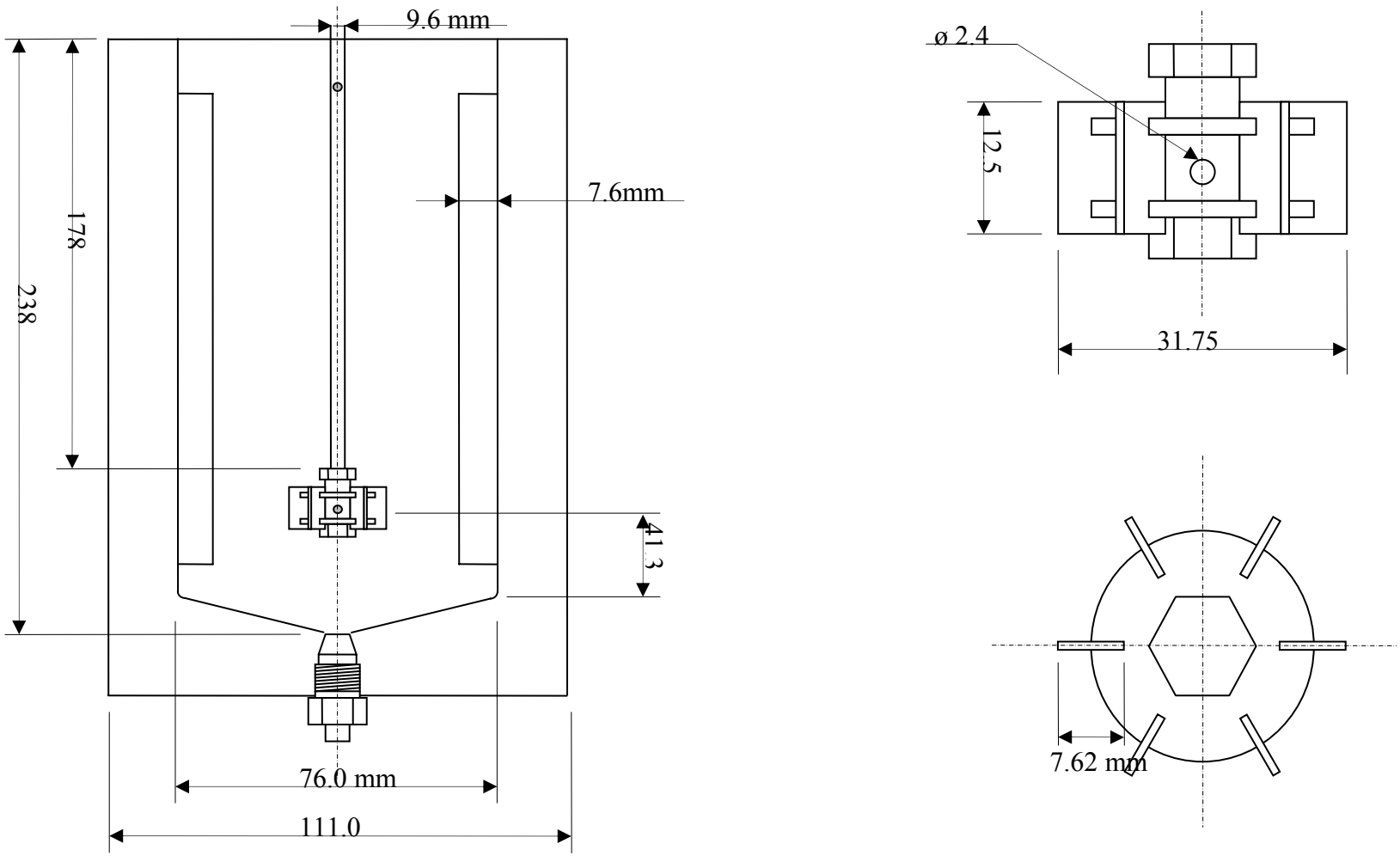

Figure 15: Reactor Dimensions and Impeller Details

5. The initial conditions (pressure and temperature) in the preheater are recorded.
6. The gas is charged into the reactor until the desired pressure is reached.
7. The data acquisition (temperature of gas and liquid/slurry phase and pressure) for the reactor is started.
8. The reactor content is stirred at a predetermined mixing speed until a thermodynamic equilibrium, characterized by a constant reactor final pressure, is reached. The reactor pressure decline is displayed and recorded as a function of time.
9. The data acquisition for the reactor is stopped and the final conditions in the preheater are recorded.
10. Steps 5 to 9 are repeated to collect multiple data points at different pressures ranging from 7 to 35 bar under the same temperature, mixing speed and liquid height as shown in Figure 16.

This experimental procedure is followed at each run with different temperature, mixing speed and solid concentration. After each run, C^* and k_La are calculated as described in the next section.

4.8 CENTRAL COMPOSITE STATISTICAL DESIGN OF EXPERIMENTS

A statistical design of experiments similar to that employed by Tekie et al.[41] and Alghamdi[38] was used in this study. The advantages of this approach is to investigate reliably the effect of the operating variables on the parameter studied (k_La) with a minimum number of experiments. Also, the produced statistical correlations generally benefit from a high degree of confidence.

In this study, the effect of 4 variables (temperature, pressure, mixing speed and solid concentration) at five levels on k_La was investigated. The resulting experimental space is a

symmetric and rotatable hypersphere with equidistant design points from the center and a radius of 2. The surface response can be described by the following equation:

$$\sum_{i=1}^{k} x_j^2 = 2^2 \tag{4-27}$$

x_j represents the coded value of each variable and is defined as:

$$x_j = 2\left[\frac{2X_i - (X_{i,L} + X_{i,H})}{X_{i,H} - X_{i,L}}\right] \tag{4-28}$$

where X_i is the value of the i-th variable and $X_{i,L}$ and $X_{i,H}$ are the lowest and highest levels of X_i. Table 16 shows the coded values for each of the process variables.

Table 16: Values and Coded Variables for the Statistical Central Composite Design

Variable	Coded Variables [x_j]	Values of Coded Variables				
		-2	-1	0	1	2
T (K)	x_1	423	448	473	498	523
C_S (wt%)	x_2	0	12.5	25	37.5	50
N (rpm)	x_3	800	900	1000	1100	1200
P (bar)	x_4	7	14	21	28	35

The distribution of experiments over the range of study is shown in Figure 17

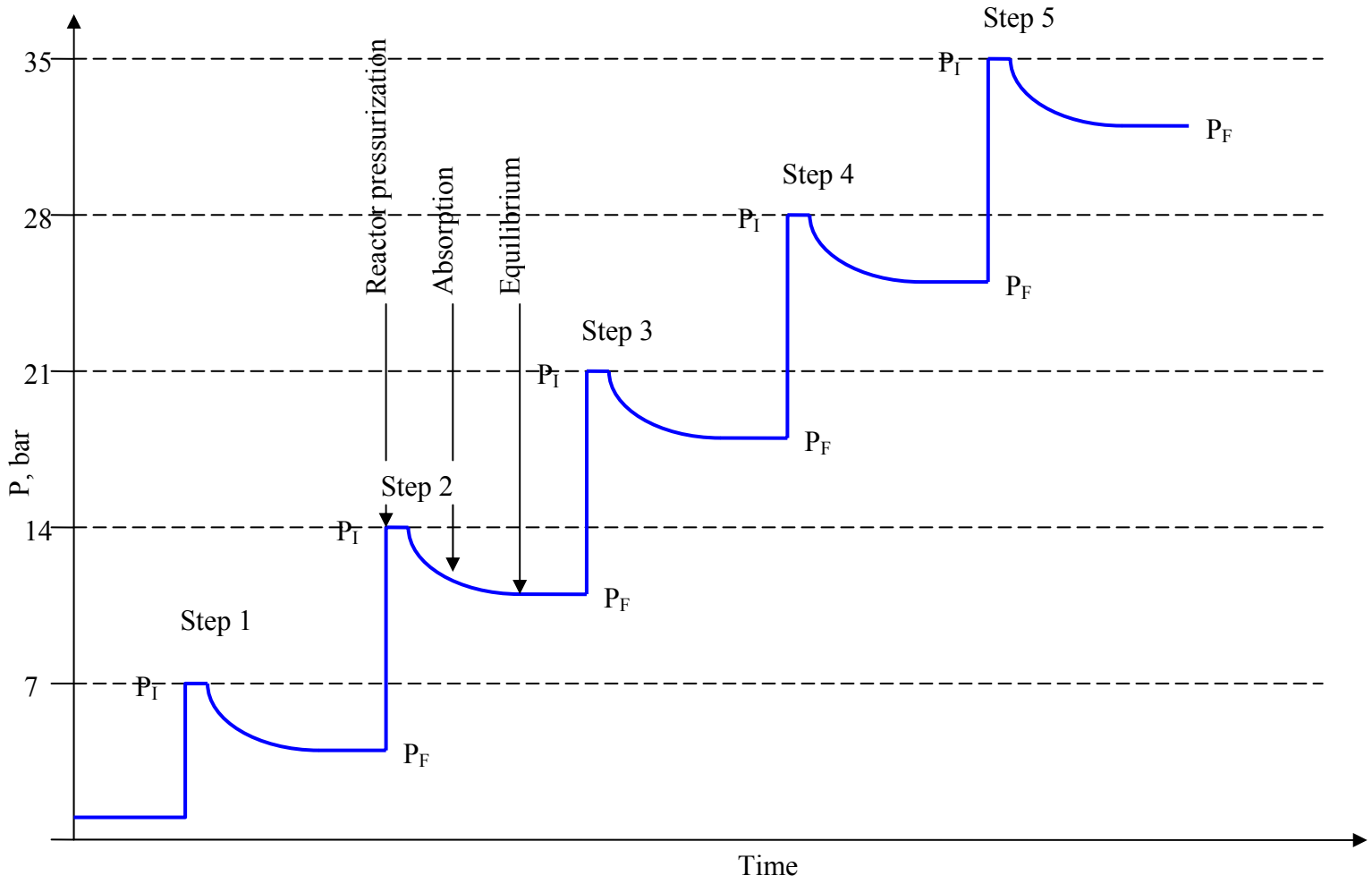

Figure 16: Schematic of the Multi-Step Procedure at Constant Temperature, Mixing Speed and Solid Concentration

P: Pressure

T: Temperature

N: Mixing speed

W: Solid loading

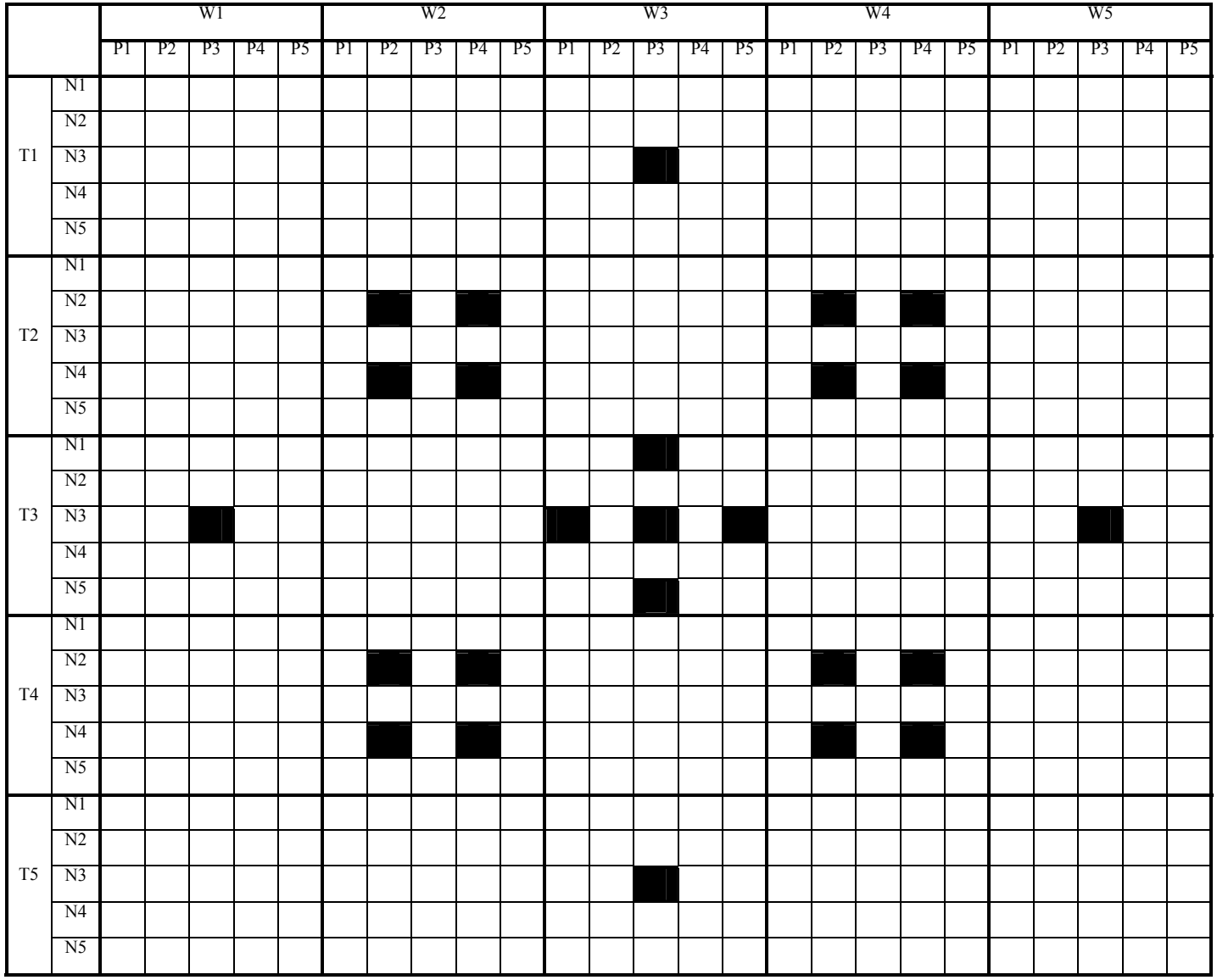

Figure 17: Distribution of the Experiments According to the Central Composite Statistical Design

5.0 CALCULATIONS

In the following section, the calculation methods for the determination of the equilibrium solubility, C^* and the volumetric liquid-side mass transfer coefficient, k_La are presented. The calculation procedures of C^* and k_La for hydrogen, carbon monoxide, helium and nitrogen in PAO-8 and Sasol wax from the experimental data collected are similar to those used by Martinez[103] and Alghamdi[38]. C^* values were calculated by building a mass balance on the preheater and reactor coupled with the Peng-Robinson Equation of State (PR-EOS); and k_La values were determined using the transient physical gas absorption technique and the two-film model theory.

The following assumptions were made:

1. In the preheater, non-ideal gas behavior is assumed and the PR-EOS can be used.
2. In the reactor, ideal behavior is assumed in the range of our operating variables.
3. The liquid and the gas phase are assumed to be well-mixed resulting in homogeneous concentrations for each phase.
4. Negligible absorption is taking place before the mixing is turned on.
5. The gas-phase mass transfer resistance is negligible compared to that of the liquid phase.
6. During the absorption, no variation of temperature is assumed.

5.1 PENG-ROBINSON EQUATION OF STATE

In the preheater, the Peng-Robinson Equation of State was used to calculate the number of moles charged into the reactor. A general form of the PR-EOS can be written as:

$$P = \frac{RT}{v-b} - \frac{a(T)}{v(v+b)+b(v-b)} \tag{5-1}$$

This equation can be expressed in terms of compressibility factor as:

$$Z^3 - (1-B)Z^2 + (A - 3B^2 - 2B)Z - (AB - B^2 - B^3) = 0 \tag{5-2}$$

where

$$A = \frac{aP}{R^2 T^2} \tag{5-3}$$

$$B = \frac{bP}{RT} \tag{5-4}$$

$$Z = \frac{Pv}{RT} \tag{5-5}$$

Only one phase is present in the preheater and the solution of equation (5-2) having the largest positive root corresponds to the gas phase. At the critical point:

$$a(T_C) = 0.45724 \ \frac{R^2 T_C^2}{P_C} \tag{5-6}$$

$$b(T_C) = 0.07780 \frac{R \ T_C}{P_C} \tag{5-7}$$

At any temperature:

$$a(T) = a(T_C)\alpha(T_R, \omega) \tag{5-8}$$

$$b(T) = b(T_C) \tag{5-9}$$

where

$$\alpha^{1/2} = 1 + \kappa(1 - T_R^{1/2}) \tag{5-10}$$

$$\kappa = 0.37464 + 1.5422\omega - 0.26992\omega^2 \tag{5-11}$$

Equation (5-2) was used to calculate the molar volume of the gas in the preheater at given temperature and pressure. The number of gas moles was obtained from the molar volume and the preheater volume as:

$$N_{1,pre} = \frac{V_{pre}}{v_{pre}} \tag{5-12}$$

5.2 CALCULATION OF C^*

The equilibrium solubility, C^*, is defined as the number of moles of gas absorbed into the liquid at thermodynamic equilibrium and is defined by:

$$C_i^* = \frac{N_{i,I} - N_{i,F}}{V_L} \tag{5-13}$$

$N_{i,I}$ is the number of moles of the gaseous species (i) in the reactor prior to absorption and $N_{i,F}$ is the number of moles of the gaseous species (i) remaining in the reactor at thermodynamic equilibrium after absorption. $N_{i,I}$ and $N_{i,F}$ can be calculated from Equations (5-14) and (5-15) as:

$$N_{i,I} = \frac{P_{i,I} V_G}{R T_{I,avg.}} \tag{5-14}$$

$$N_{i,F} = \frac{P_{i,F} V_G}{R T_{F,avg.}} \tag{5-15}$$

where

$$T_{I,avg.} = \frac{T_{I,gas} + T_{I,liq.}}{2} \tag{5-16}$$

$$T_{F,avg.} = \frac{T_{F,gas} + T_{F,liq.}}{2} \tag{5-17}$$

V_G is the volume of the gas-phase in the reactor calculated at the operating temperature as follows:

$$V_G = V_r - \left(\frac{m_L}{\rho_L} + \frac{m_{cat.}}{\rho_{cat.}} \right) \tag{5-18}$$

where m_L and m_{cat} are the masses of the liquid- and solid-phase, respectively.

5.3 CALCULATION OF k_La

k_La is calculated using the transient physical gas absorption technique. During the absorption, the decline of the reactor pressure is recorded as a function of time until a thermodynamic equilibrium is reached.

According to the two-film model theory[22], the rate of mass transfer from the solute gas to the liquid can be expressed as:

$$\frac{dn_L}{dt} = k_L a(C^* - C_L)V_L \tag{5-19}$$

The rate of solute gas uptake by the liquid can be related to the rate of change of pressure through the ideal gas law:

$$\frac{dn_L}{dt} = -\frac{V_G}{RT}\frac{dp_{i,t}}{dt} \tag{5-20}$$

C_L, the bulk concentration of the solute gas in the liquid, is obtained at any time t using a mass balance as:

$$C_L = \frac{V_G}{V_L RT}(P_{i,I} - P_{i,t}) \tag{5-21}$$

Henry's law constant is given by:

$$He = \frac{P_{i,t}}{C*} \tag{5-22}$$

When combining equation (5-19) with Equations (5-20), (5-21) and (5-22), the following equation can be obtained:

$$(-\frac{V_G}{RT})(\frac{dP_{i,t}}{P_{i,t}(\frac{V_L}{He}+\frac{V_G}{RT})-\frac{V_G P_{i,I}}{RT}}) = k_L a \cdot dt \tag{5-23}$$

Let:

$$U = P_{i,t}(\frac{V_L}{He}+\frac{V_G}{RT})-\frac{V_G P_{i,I}}{RT} \tag{5-24}$$

$$dU = dP_{i,t}(\frac{V_L}{He}+\frac{V_G}{RT}) \tag{5-25}$$

Integrating equation (5-23) between $t = 0$ and t, gives:

$$\ln\left[\frac{P_{i,t}(\frac{V_L}{He}+\frac{V_G}{RT})-\frac{V_G P_{i,I}}{RT}}{\frac{P_{i,I}V_L}{He}}\right] = -\left[\frac{V_L RT}{V_G He}+1\right]k_L a.t \tag{5-26}$$

Multiplying both numerator and denominator in the left hand side term by RT/V_G gives:

$$\ln\left[\frac{P_{i,t}(\psi+1)-P_{i,I}}{\psi P_{i,I}}\right] = -[\psi+1]k_L a.t \tag{5-27}$$

with $\Psi = (V_L RT/V_G He)$

At equilibrium, the concentration of the solute gas, C_{eq}^* is defined as:

$$C_{eq}^{*} = \frac{V_G}{V_L RT}(P_{i,I} - P_{i,F}) \tag{5-28}$$

C_{eq}^{*} can also be defined as:

$$C_{eq}^{*} = \frac{P_{i,F}}{He} \tag{5-29}$$

Equating equations (5-28) and (5-29) gives the following equation:

$$\frac{P_{i,I} - P_{i,F}}{P_{i,F}} = \frac{V_L RT}{HeV_G} = \psi \tag{5-30}$$

Combining equations (5-27) and (5-30) and multiplying by $P_{i,F}/P_{i,I}$ gives:

$$\frac{P_{i,F}}{P_{i,I}} \ln\left[\frac{P_{i,I} - P_{i,F}}{P_{i,t} - P_{i,F}}\right] = k_L a.t \tag{5-31}$$

This equation can also be written as:

$$F(P) = k_L a.t \tag{5-32}$$

When plotting the left hand side of this equation and a straight line is obtained, the slope of the line is $k_L a$. A sample calculation is provided in Appendix C.

6.0 RESULTS AND DISCUSSION

In the following sections, the gas solubility, C^* and volumetric mass transfer coefficient, k_La data are presented. These parameters were measured following the Central Composite Statistical Design of experiments within the range of operating conditions listed in section 4.1.

6.1 GAS SOLUBILITY IN PAO-8 AND SASOL WAX

The solubility values of N_2, He, CO and H_2 were measured in PAO-8 and Sasol wax in the presence and absence of solid particles in the temperature range of 423-523 K and pressure range of 7-35 bar. Figure 18 shows the reproducibility of C^* for all gases in the two different liquids; and as can be seen the solubility data were obtained with an absolute deviation of less than 7%. The error analysis on C^* along with some numerical examples are provided in Appendix B. The effects of operating variables on the gas solubility are presented in the following sections.

6.1.1 Effect of Pressure on C^*

Within the range of operating conditions used in this study, the solubility values of He, N_2, H_2 and CO in both PAO-8 and Sasol wax appeared to increase linearly with pressure as presented in Figure 19 and Figure 20. The solubility data can therefore be correlated using Henry's Law.

$$C^* = \frac{P_{r,F}}{He} \tag{6-1}$$

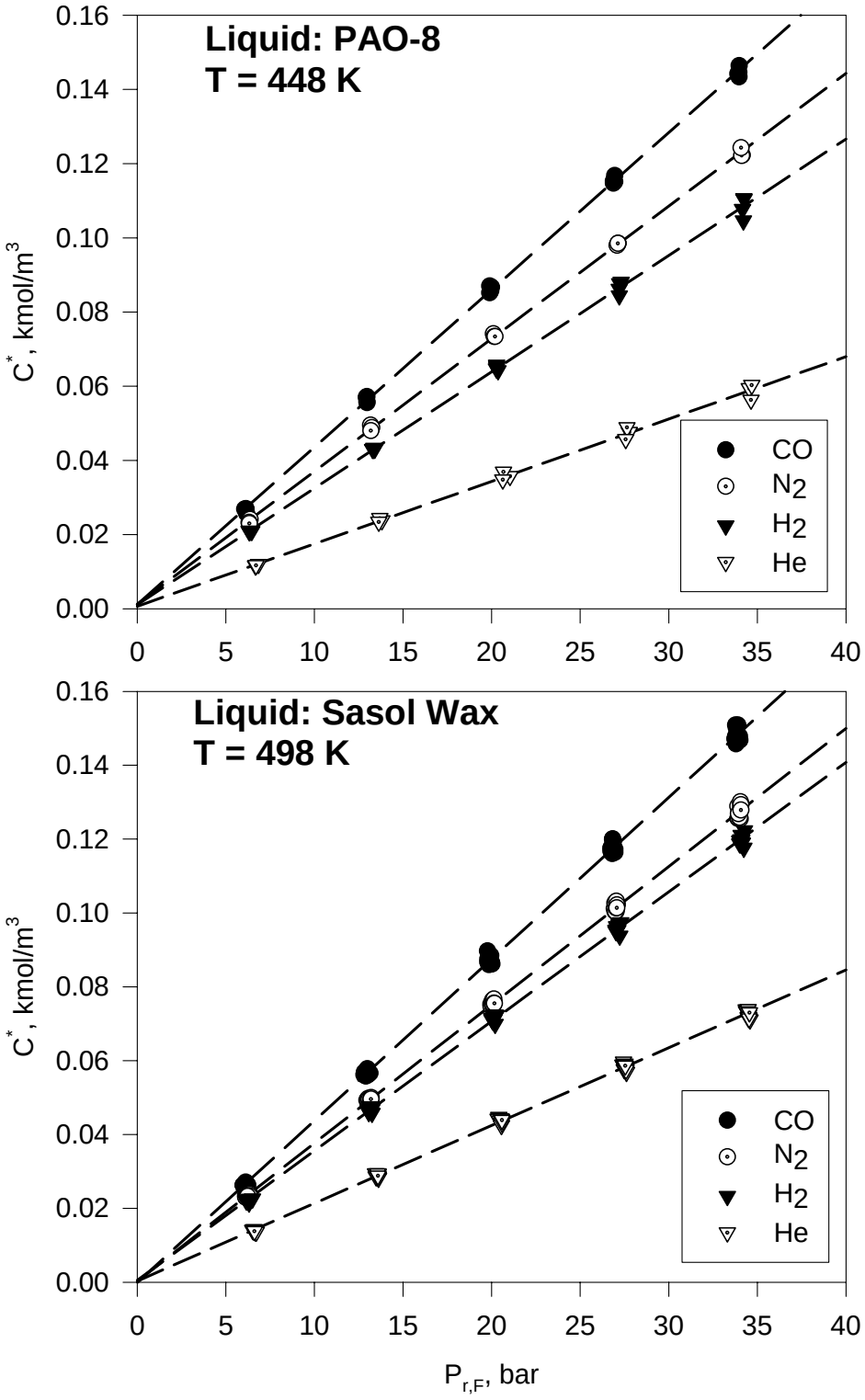

Figure 18: Reproducibility and Effect of Gas Nature on C^* Values

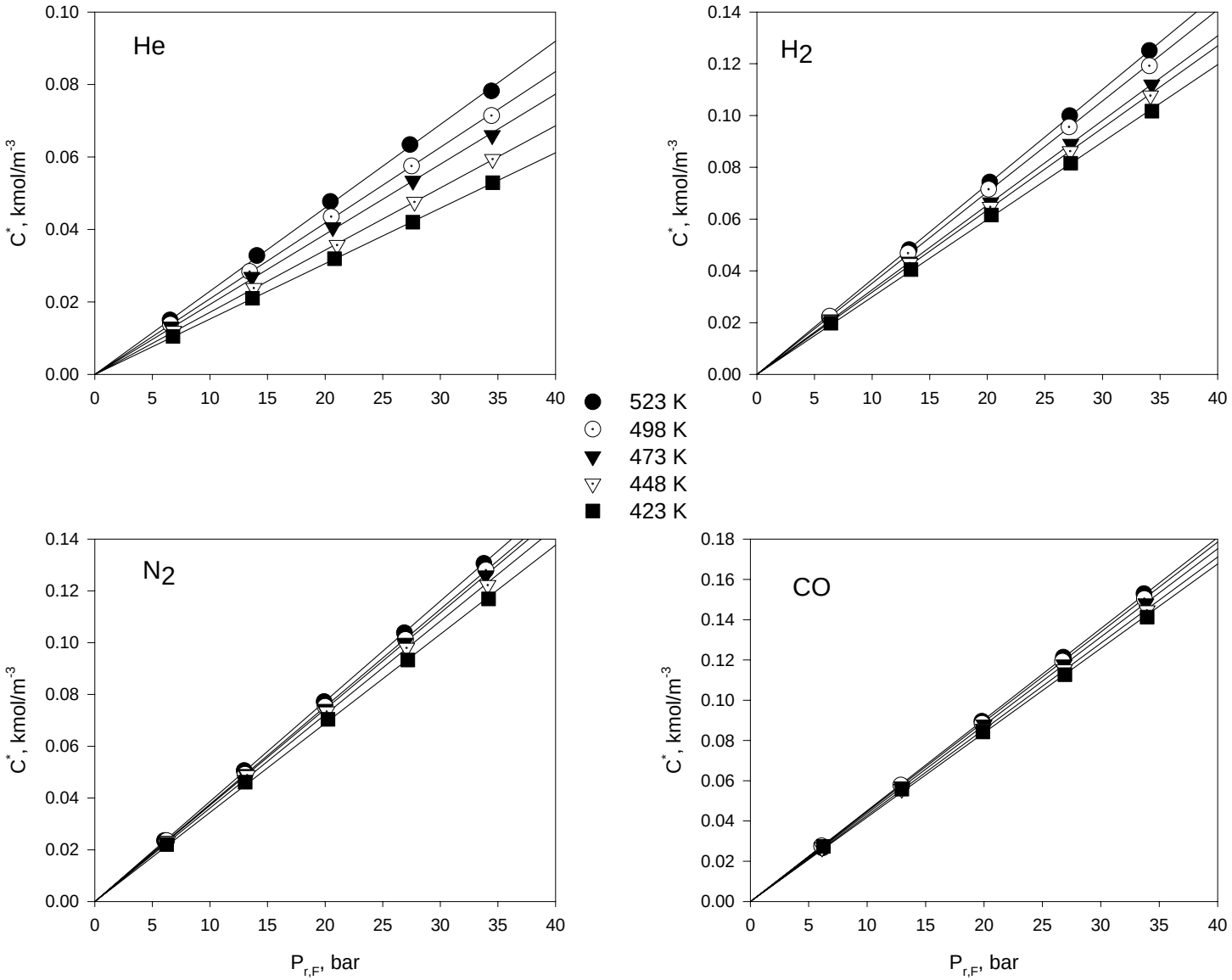

Figure 19: Effect of Pressure and Temperature on C^* for He, N_2, H_2 and CO in PAO-8

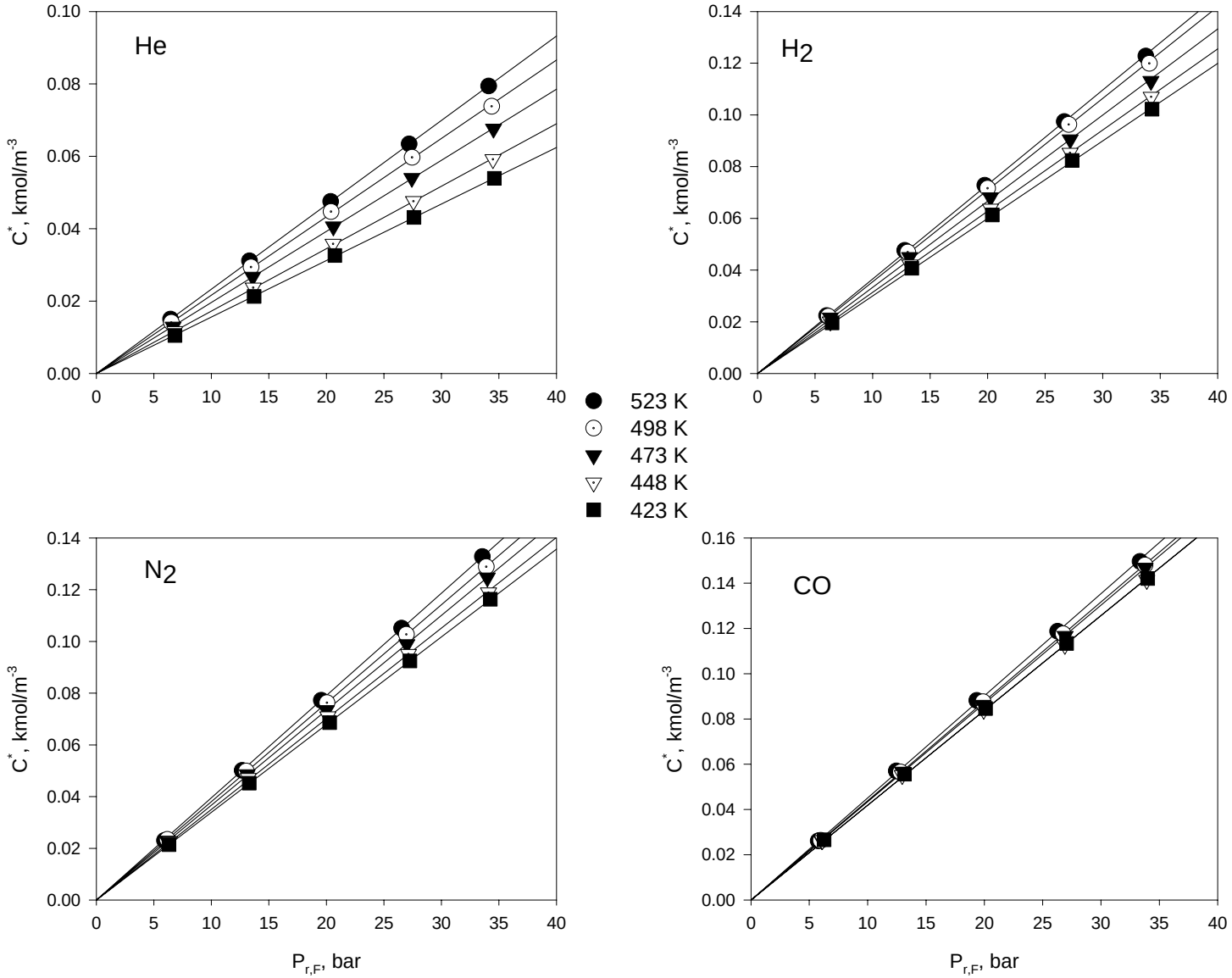

Figure 20: Effect of Pressure and Temperature on C^* for He, N_2, H_2 and CO in Sasol Wax

He is Henry's Law constant and $P_{r,F}$ is the partial pressure of the gas in the reactor after the thermodynamic equilibrium has been reached. This increase in solubility with pressure can be related to the increase of the concentration difference (driving force) between the gaseous and the liquid phases with increasing the system pressure. Similar behavior was reported in literature[23, 26, 30, 31, 38, 43, 45, 46, 50, 65, 74] for identical and different gas-liquid systems as shown in Table 2.

6.1.2 Effect of Temperature on C^*

Depending on the gas-liquid system used and the range of temperature studied, the gas solubility was reported in literature to increase[23, 27-33, 38, 41, 43, 45, 46, 64, 67-70, 73, 74, 101] or decrease[23, 30, 32, 38, 68] with increasing temperature. The effect of temperature on C^* is accounted for using the dependency of Henry's Law constant on temperature, often described with an Arrhenius-type equation[23, 32, 38, 41, 101].

$$He = H_{0a} e^{\frac{-\Delta E}{RT}} \tag{6-2}$$

H_{0a} represents the pre-exponential constant; and ΔE is the apparent activation energy of absorption.

Figure 19 and Figure 20 show the effect of temperature on the gas solubility for the 4 gases in PAO-8 and Sasol wax; and as can be seen C^* values increase with increasing temperature. The effect of temperature on the Henry's law constant is depicted in Figure 21; and the data were correlated using Equation (6-3) with R^2 greater than 97%.

$$He = H_0 e^{[A\left(\frac{1}{T}\right)^2 + B\left(\frac{1}{T}\right)]} \tag{6-3}$$

The coefficients for Equation (6-3) are listed in Table 17. It should be mentioned that similar behavior of *He* as a function of temperature was reported by Himmelblau[104] for six different gases (O_2, N_2, H_2, He, Xe and CH_4) in water from 298 K to 550 K.

Table 17: Coefficients for Henry's Law Correlation, Equation (6-3)

	PAO-8			Sasol wax		
Gas	***A***	***B***	***Ho***	***A***	***B***	***Ho***
N_2	2.173E+05	-6.575E+02	4.091E+02	-2.214E+05	1.267E+03	5.162E+01
H_2	-3.561E+04	6.076E+02	9.771E+01	-1.929E+05	1.345E+03	4.218E+01
CO	-1.295E+05	7.164E+02	8.984E+01	-3.651E+05	1.873E+03	2.287E+01
He	-4.359E+05	2.756E+03	1.091E+01	-5.442E+05	3.336E+03	5.317E+00

Over the temperature interval studied, the apparent activation energy, ΔE, was found to be a function of temperature and was estimated using Equation (6-4).

$$\frac{\Delta E}{R} = -\left[\frac{\partial \ln(He)}{\partial(1/T)}\right] \tag{6-4}$$

The resulting Henry's law constants and apparent activation energies are listed in Table 18.

6.1.3 Effect of Solid Concentration on C^*

Figure 22 and Figure 23 shows the effect of Alumina concentration on the solubility of all gases in PAO-8 and Sasol wax; and as can be concluded there is no effect of the alumina on C^* values for all gases in PAO-8 and Sasol wax under the operating conditions used.

Table 18: Henry's Law Constants and Apparent Activation Energy

Gas	T, K	PAO-8		Sasol wax	
		He, ***bar m^3/kmol***	***ΔE,*** ***kJ/kmol***	***He,*** ***bar m^3/kmol***	***ΔE,*** ***kJ/kmol***
N_2	373	-	-	314	-664
	398	-	-	308	-1284
	423	291	-3076	299	-1831
	448	278	-2599	290	-2316
	473	269	-2173	280	-2751
	498	262	-1789	269	-3141
	523	258	-1442	259	-3495
H_2	373	-	-	388	-2583
	398	-	-	366	-3123
	423	337	-3652	345	-3599
	448	318	-3730	325	-4023
	473	301	-3800	306	-4401
	498	287	-3863	289	-4741
	523	274	-3919	273	-5049
CO	373	-	-	251	+704
	398	-	-	252	-319
	423	237	-866	249	-1220
	448	233	-1150	243	-2021
	473	229	-1404	235	-2737
	498	225	-1632	226	-3382
	523	220	-1839	216	-3964
He	373	-	-	815	-3476
	398	-	-	748	-4999
	423	645	-5778	676	-6343
	448	584	-6734	605	-7537
	473	527	-7589	540	-8605
	498	476	-8359	481	-9565
	523	431	-9054	428	-10433

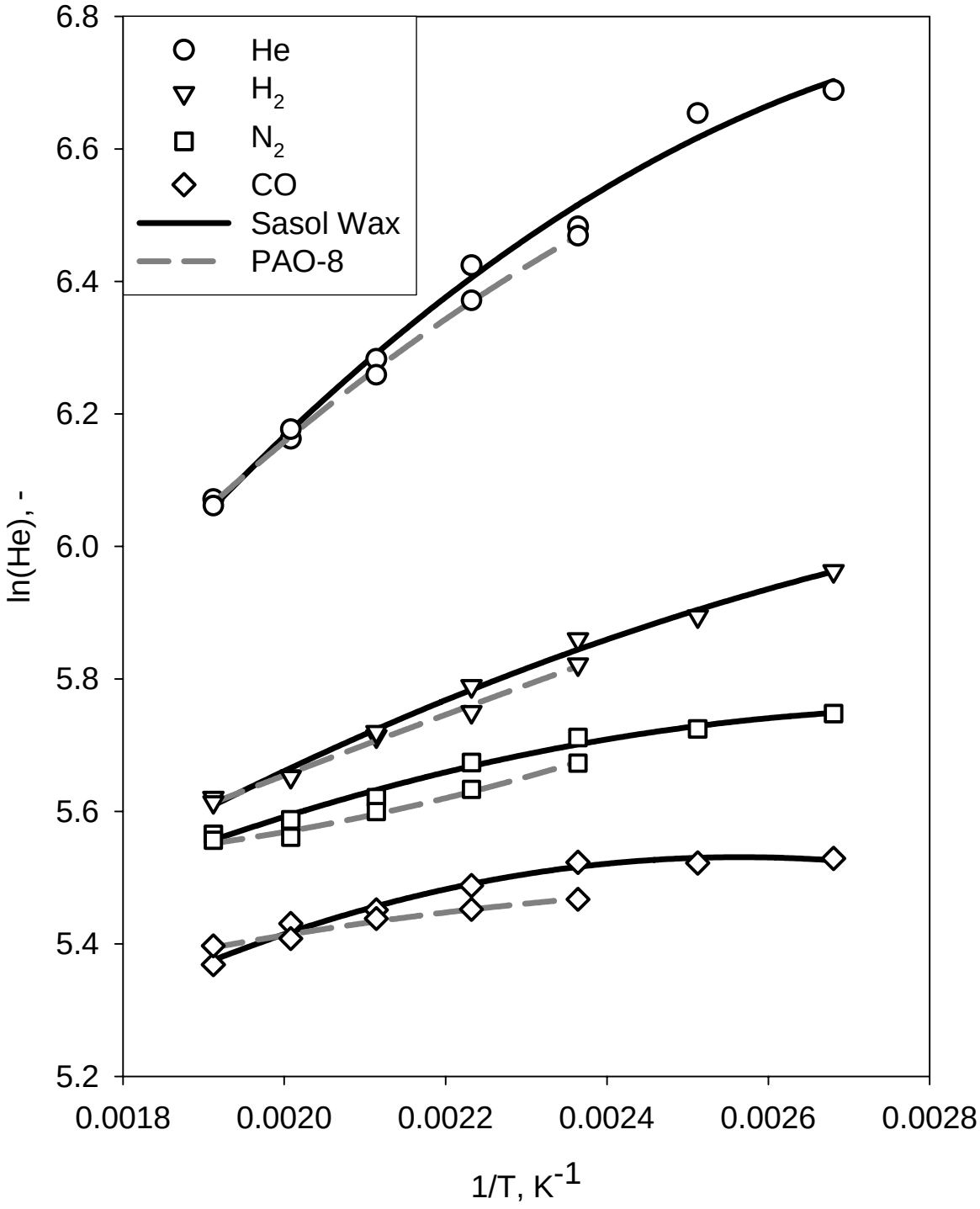

Figure 21: Effect of Temperature on Henry's Law Constants

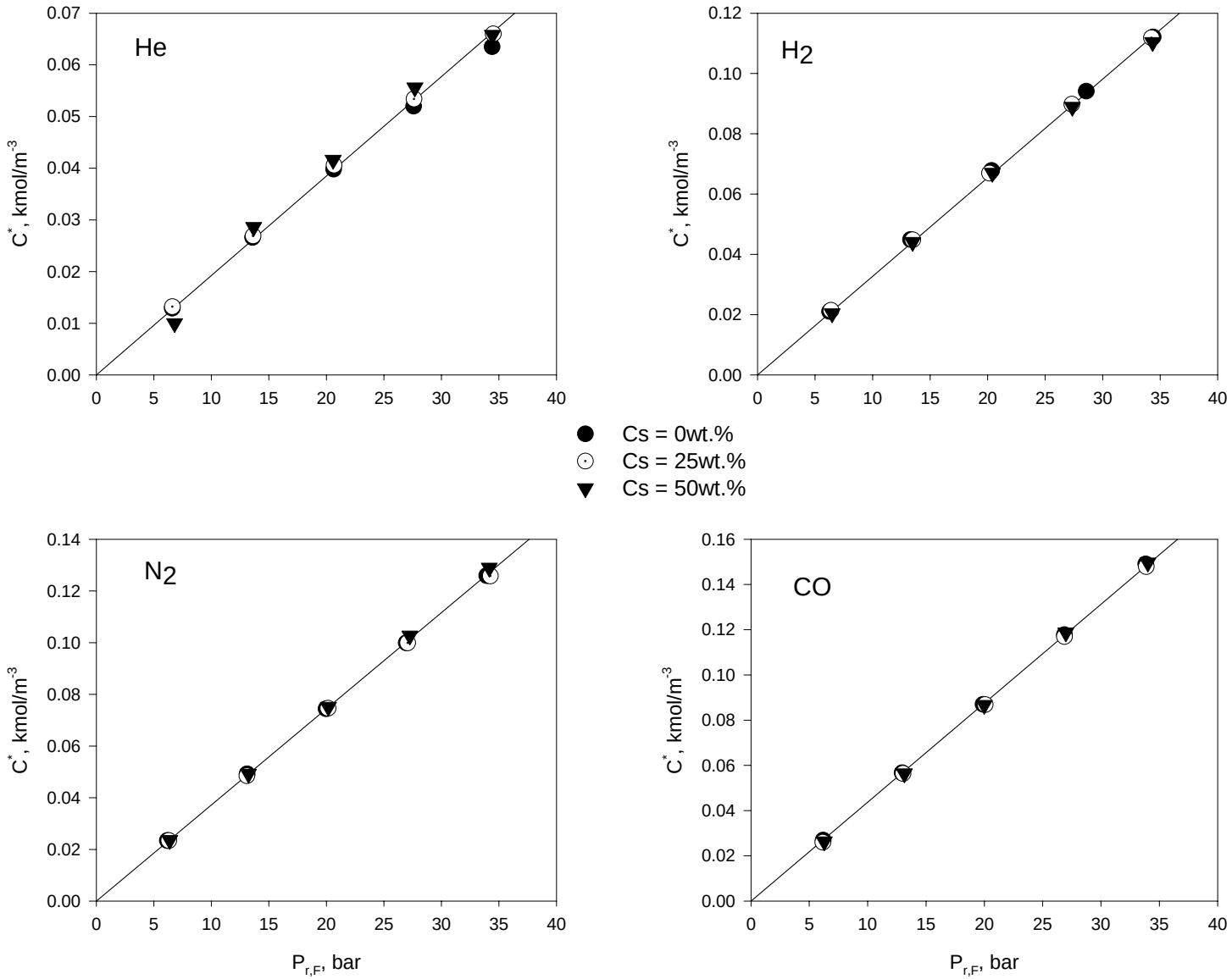

Figure 22: Effect of Solid Concentration on C^* for He, N_2, H_2 and CO in PAO-8 @ 473K

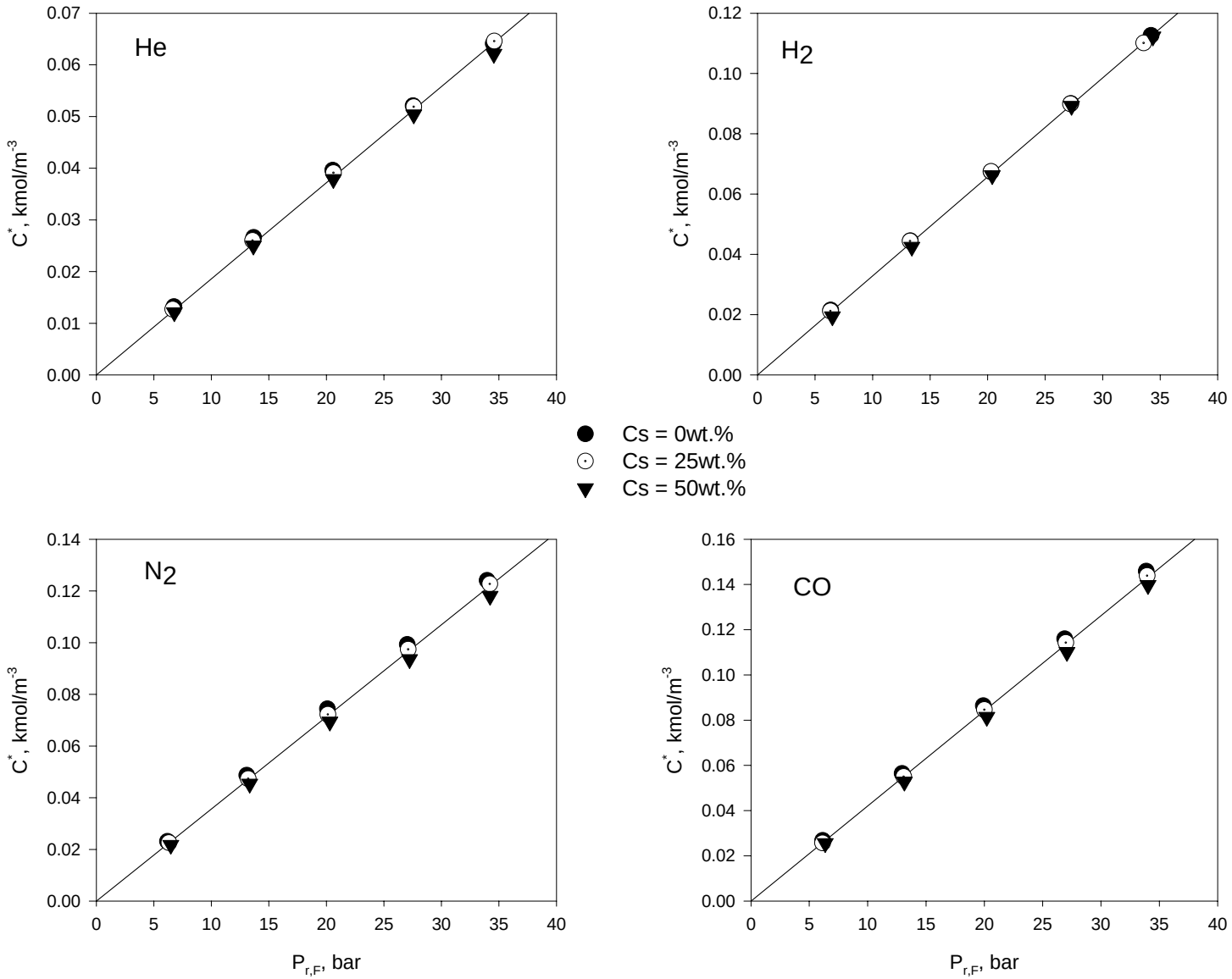

Figure 23: Effect of Solid Concentration on C^* for He, N_2, H_2 and CO in Sasol Wax @ 473K

6.1.4 Effect of Gas Nature on C^*

The effect of gas nature on solubility is also shown in Figure 18. As we can see, solubility values are following the order $C^*_{CO}>C^*_{N2}>C^*_{H2}>C^*_{He}$ for PAO-8 and Sasol wax under the similar operating conditions. This behavior can be explained using the solubility parameter (δ) concept developed by Hildebrand[105]. The solubility parameters can be calculated from the molar heat of vaporization data using Equation (6-5):

$$\delta = \sqrt{\frac{H_v - RT}{v}} \tag{6-5}$$

H_V is the molar heat of vaporization and v is the molar volume.

Using the solubility parameter values, the solubility (x_1) can then be expressed with the following equation.

$$x_1 \alpha \exp\left(- \frac{v_1^L \times (\delta_1 - \delta_2)^2 \times \phi_2^2}{RT} \right) \tag{6-6}$$

Where v_1^L is the molar volume of component 1 (gas) at temperature T; ϕ_2 is the volume fraction of component 2 (liquid); and δ_1 and δ_2 are the solubility parameters of component 1 and 2, respectively. Table 19 shows the solubility parameter values for the gases used in this study as well as those for several selected normal-hydrocarbons. The solubility parameter values for PAO-8 and Sasol wax were estimated from equation (6-5) by calculating the corresponding H_V and v values using the asymptotic behavior correlations from Marano et al.[80, 86]. According to Equation (6-6), a smaller difference between solubility parameters of the gaseous and the liquid phases should result in a higher solubility value and, thus the values of the solubility parameters listed in Table 19 can be used to explain the behavior of the solubility (C*) of the gases used in PAO-8 and Sasol wax.

Table 19: Solubility Parameter of Selected Compounds

Component	δ, $(J/m^3)^{0.5}$
He	1222[77]
H_2	6648[106]
N_2	10800[77]
CO	11700[77]
C_2H_6	12375[106]
C_3H_6	13091[106]
n-C_8H_{18}	15360[77]
n-$C_{10}H_{22}$	15538[106]
n-$C_{16}H_{34}$	15938[77]
PAO-8	16943[80, 86]
Sasol Wax	16929[80, 86]

6.1.5 Effect of Liquid Nature on C^*

Figure 21 and Figure 24 show the effect of liquid nature on Henry's Law constant and C^*, respectively. PAO-8 and Sasol wax were found to have close gas solubility values when compared under identical operating conditions. This behavior was expected since both hydrocarbon liquids have close molecular weights and average composition (around C_{40}) and very close solubility parameters as shown in Table 19

6.2 VOLUMETRIC MASS TRANSFER COEFFICIENT, k_La

The liquid-side volumetric mass transfer coefficient of N_2, He, CO and H_2 were measured in PAO-8 and Sasol wax in the presence and absence of solid particles in the temperature range of 423-523 K, pressure range of 7-35 bar and mixing speeds from 13.3 Hz to 20 Hz (800 to 1200 RPM) using the Central Composite Statistical Design of experiment. Figure 25 and Figure 26 show the reproducibility of k_La for all gases in the two different liquids; and as can be seen the

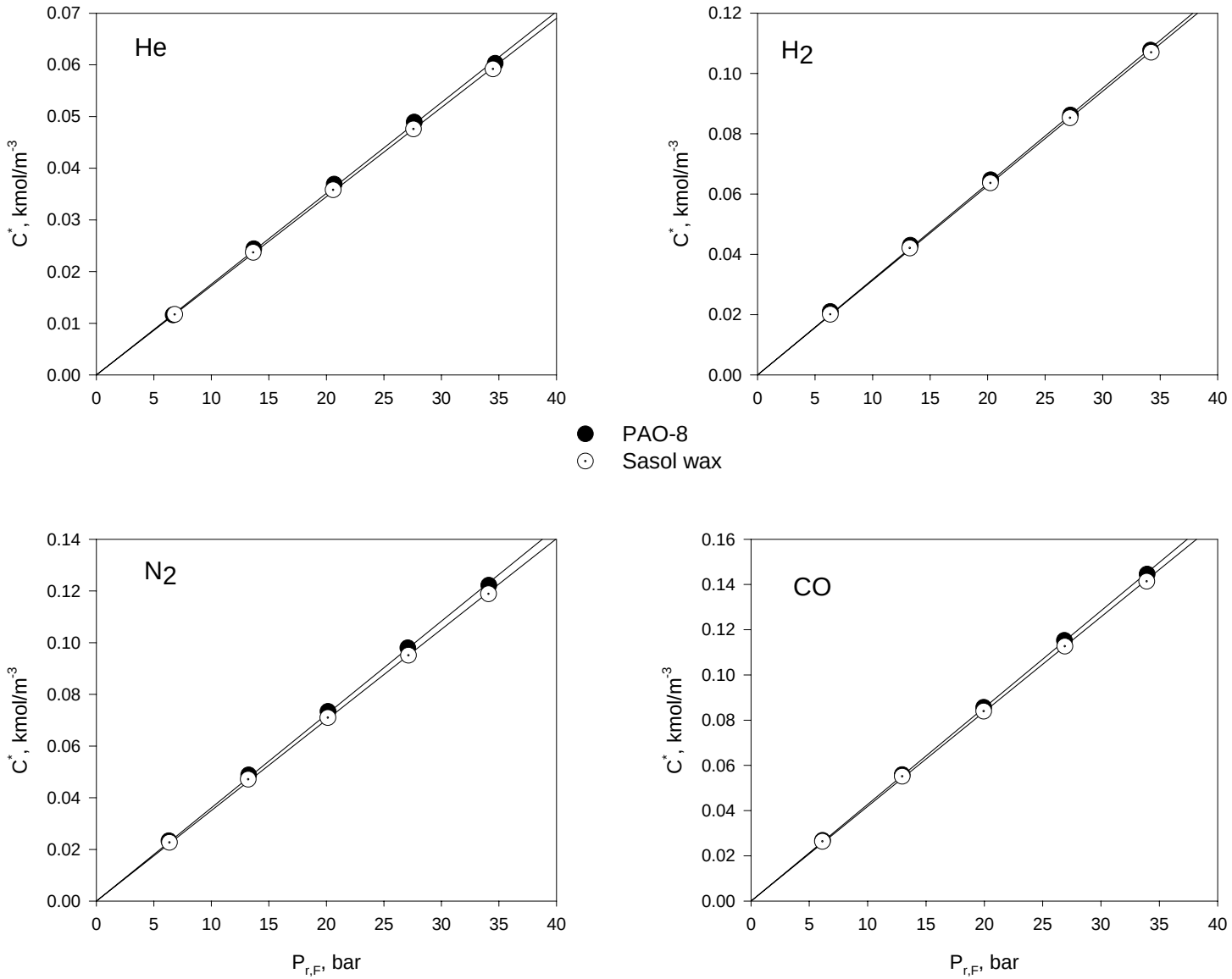

Figure 24: Effect of Liquid Nature on C^* @ 448 K

volumetric mass transfer coefficient data were obtained with an absolute deviation of less than 14%. An error analysis and sample calculations of k_La are provided in Appendix B. The effects of operating variables and system properties on k_La are presented in the following sections.

6.2.1 Effect of Mixing Speed on k_La

Figure 27 through Figure 30 show the effect of mixing speed on the volumetric liquid-side mass transfer coefficient. Increasing the mixing intensity was found to strongly enhance k_La values. This enhancement was also reported by several investigators[23, 38, 41-49, 51, 53-57] as presented in Table 5 and section 2.3.5. This increase of the volumetric mass transfer coefficient values with mixing speed can be attributed to the increase of the pumping capacity of the impeller with increasing the mixing intensity and thus more gas bubbles are induced into the liquid through the hollow shaft which increase the gas-liquid interfacial area a. Also, increasing mixing speed increases the turbulence and shear rate which decrease the liquid-film thickness and increases the mass transfer coefficient k_L. Thus, the combined effects of mixing speed on the gas-liquid interfacial area and the mass transfer coefficient should lead to the increase of k_La values.

Figure 27 through Figure 30 show that when increasing mixing speed from 800 to 1000 RPM, k_La values appear to increase by 300-550%, whereas when increasing mixing speed from 1000 to 1200 RPM, a smaller increase (130 to 200%) of k_La can be observed. The smaller increase of k_La values at higher N is related to the effect of mixing speed on the induced gas flow rate through the hollow shaft, Q_{GI}. As reported by Fillion[102] and Lemoine et al.[14], at mixing speeds greater than the critical mixing speed for gas induction, Q_{GI} increases with mixing speed until a fully developed hydrodynamic regime is reached, and then Q_{GI} becomes independent of N. Thus, increasing mixing speed after reaching the fully developed hydrodynamic did not significantly increase Q_{GI} and subsequently k_La.

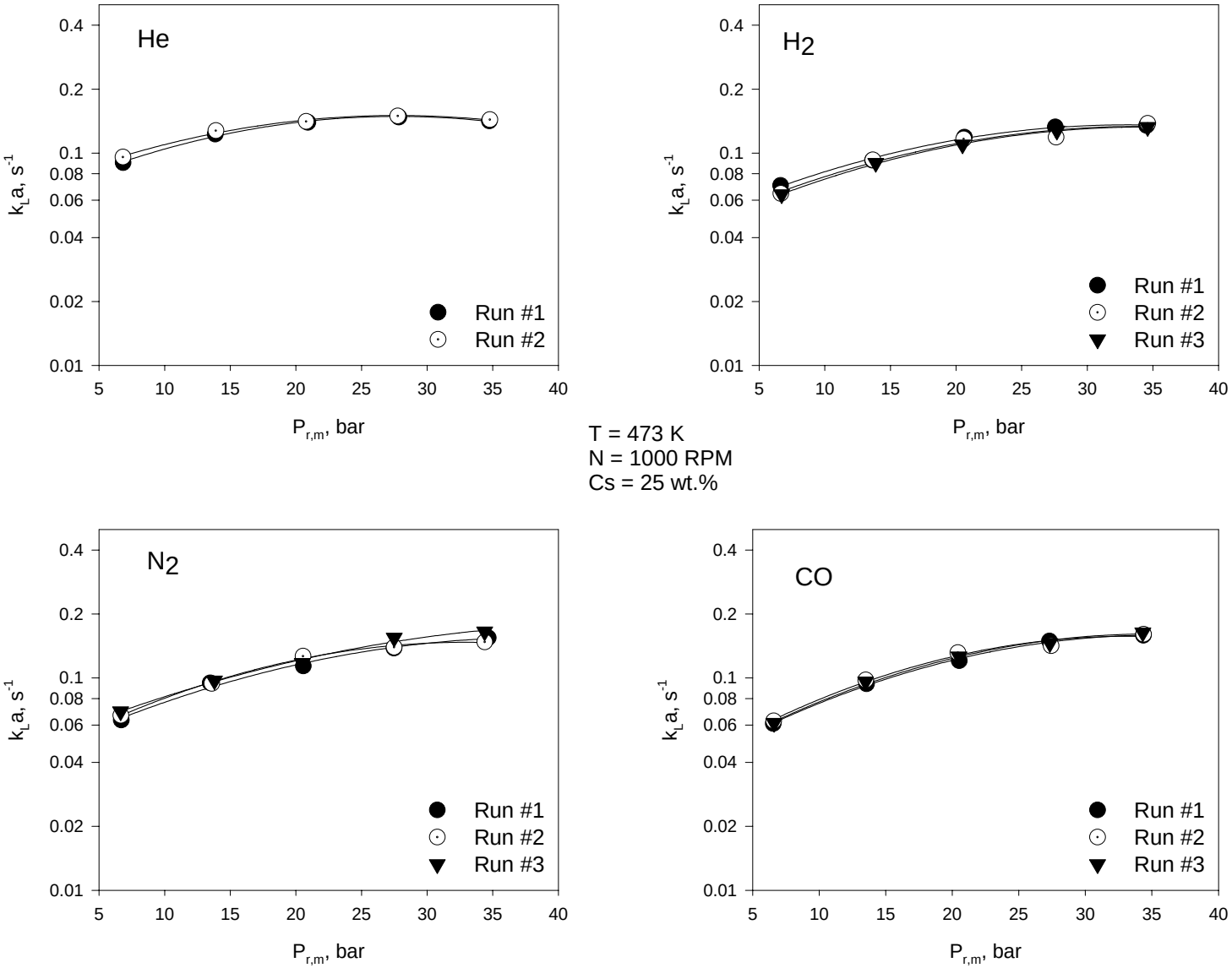

Figure 25: Reproducibility of k_La Values for He, N_2, H_2 and CO in PAO-8

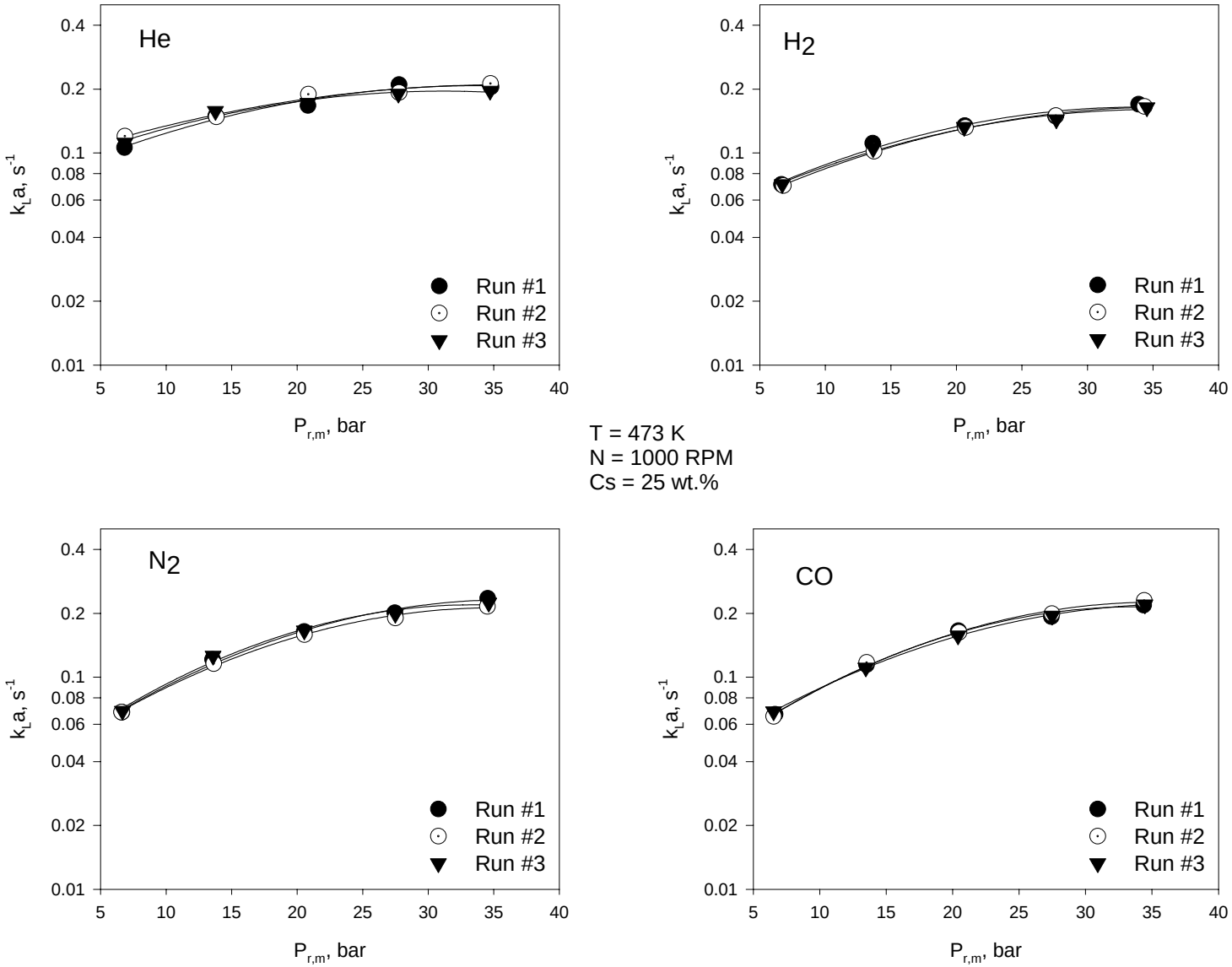

Figure 26: Reproducibility of k_La Values for He, N_2, H_2 and CO in Sasol wax

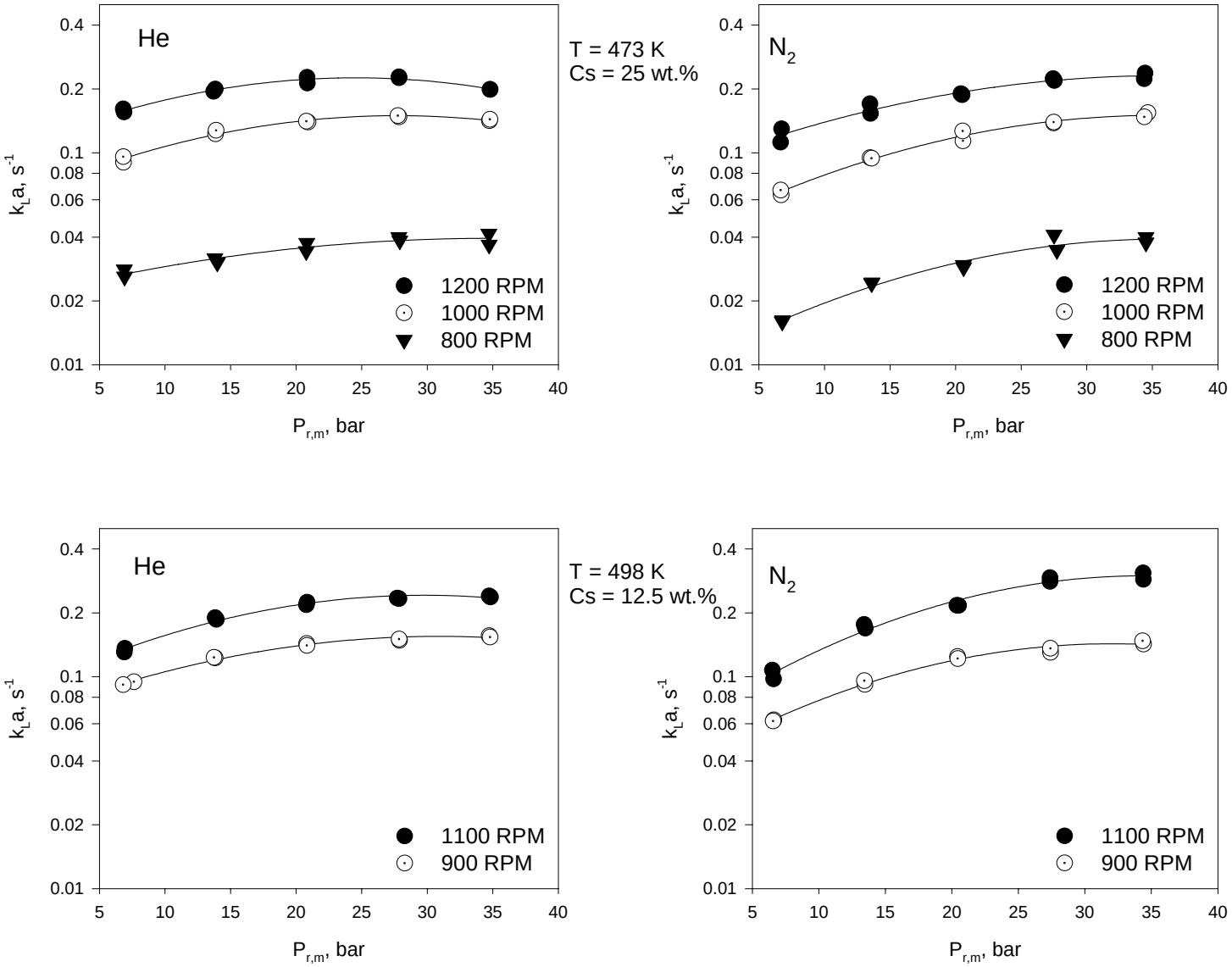

Figure 27: Effect of Mixing Speed on k_La for He and N_2 in PAO-8

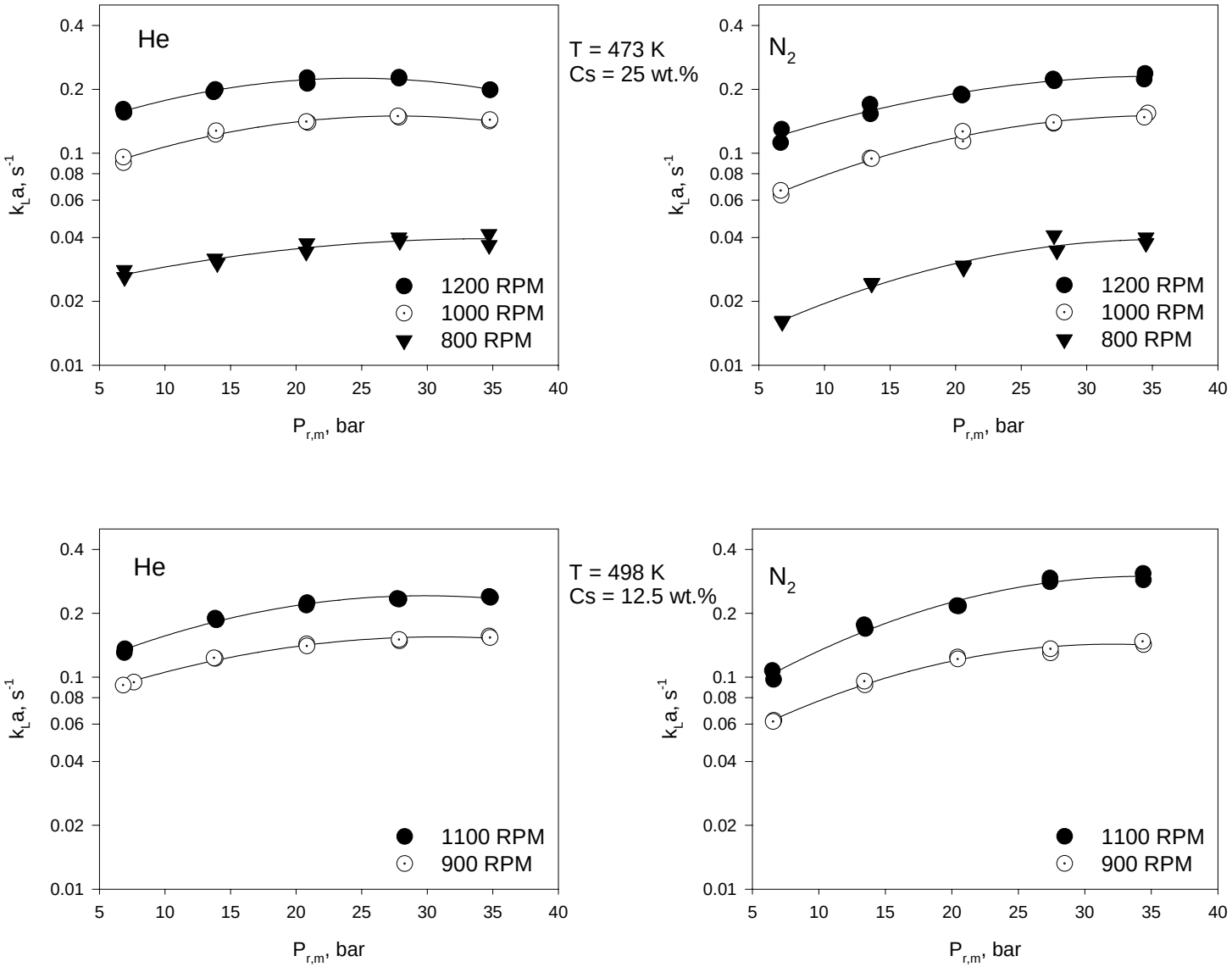

Figure 28: Effect of Mixing Speed on k_La for H_2 and CO in PAO-8

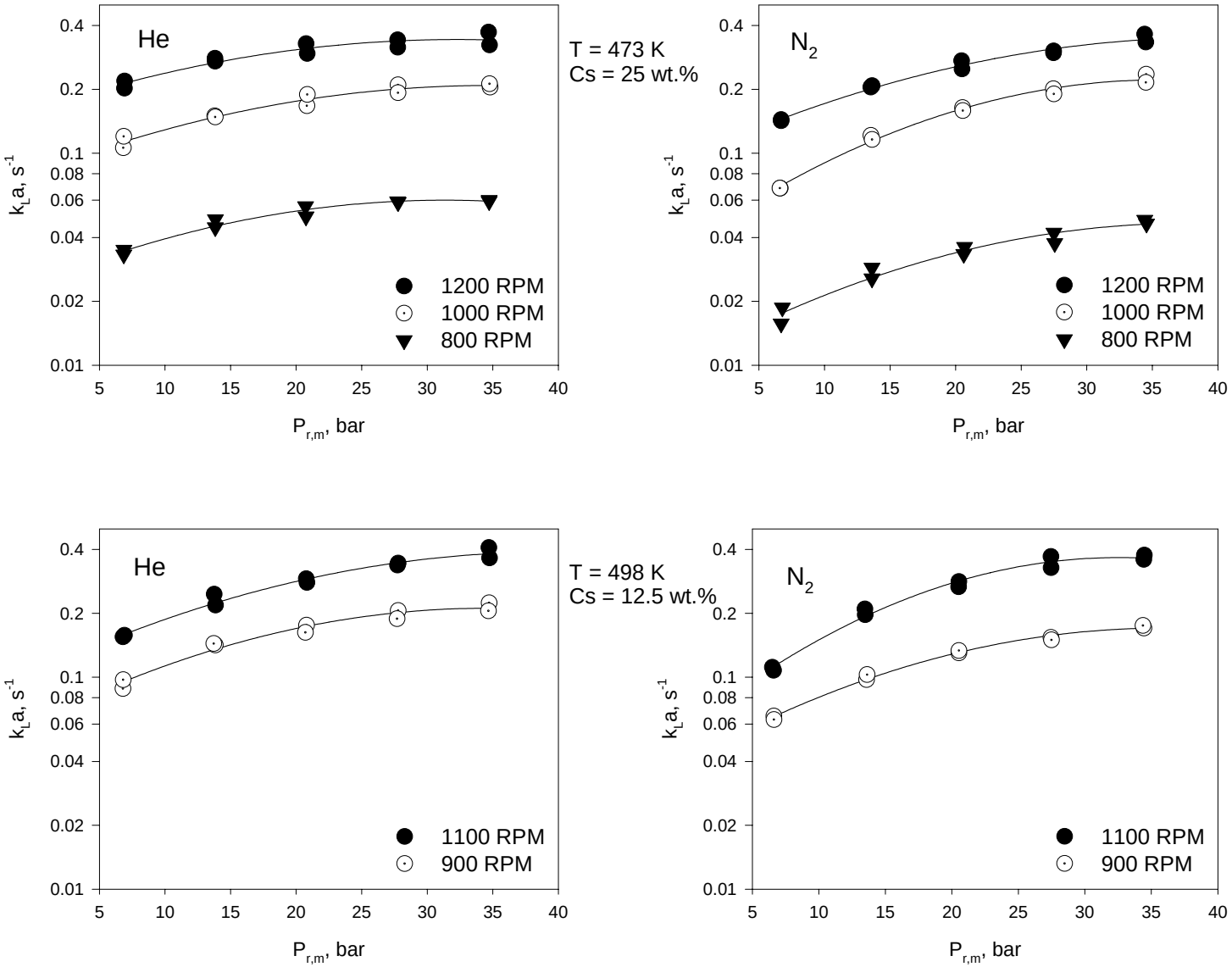

Figure 29: Effect of Mixing Speed on k_La for He and N_2 in Sasol Wax

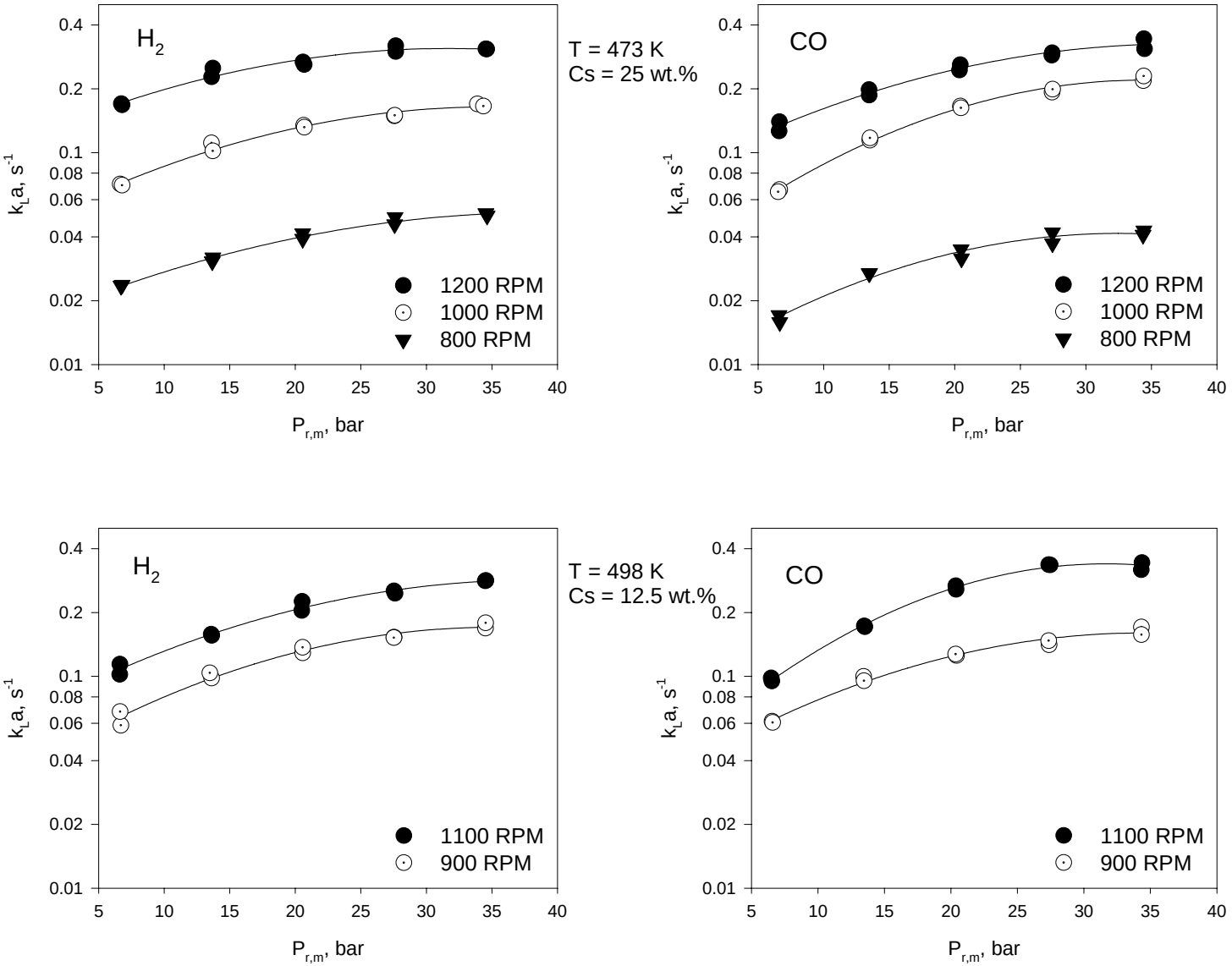

Figure 30: Effect of Mixing Speed on k_La for H_2 and CO in Sasol Wax

6.2.2 Effect of Temperature on k_La

The effect of temperature on the volumetric liquid-side mass transfer coefficient is presented in Figure 31 through Figure 34; and as can be observed increasing temperature increases k_La for all the gas-liquid-solid systems studied. This k_La behavior is in agreement with those reported by other investigators[31, 38, 42, 43, 46] for comparable gas-liquid systems, as k_La dependency on temperature was reported to be system-dependant as shown in Table 4. This increase of k_La can be attributed to the resultant effect of temperature on both k_L and a, and is usually related to the change of the liquid physico-chemical properties with temperature. In fact, increasing temperature decreases the liquid viscosity which according to Figure 9 increases the gas-liquid diffusivity and subsequently k_L, hence the latter is related to the diffusivity to power 0.5 and 1 according to the penetration theory and the two-film model, respectively. Also, the decrease of both liquid surface tension and viscosity with increasing temperature decreases the gas bubble sizes and therefore the gas-liquid interfacial area, a increases.

Figure 31 through Figure 34 show that increasing temperature from 423 to 473 K leads to a 140 to 200% increase in k_La values, whereas increasing temperature from 473 to 523 K a results only in a smaller increase in k_La values (up to 150%). This behavior can be related to the relatively smaller decrease of viscosity and surface tension within the temperature from 473 to 523 K when compared with that within the temperature range (423-473 K).

6.2.3 Effect of Pressure on k_La

The effect of pressure on k_La is strongly system-dependant hence increasing pressure may result in an increase[23, 38, 41-46], a decrease[52] or no change[31, 47-51] of k_La values as can be noticed in Table 3. Figure 25 through Figure 34 illustrate that k_La values significantly increase by about

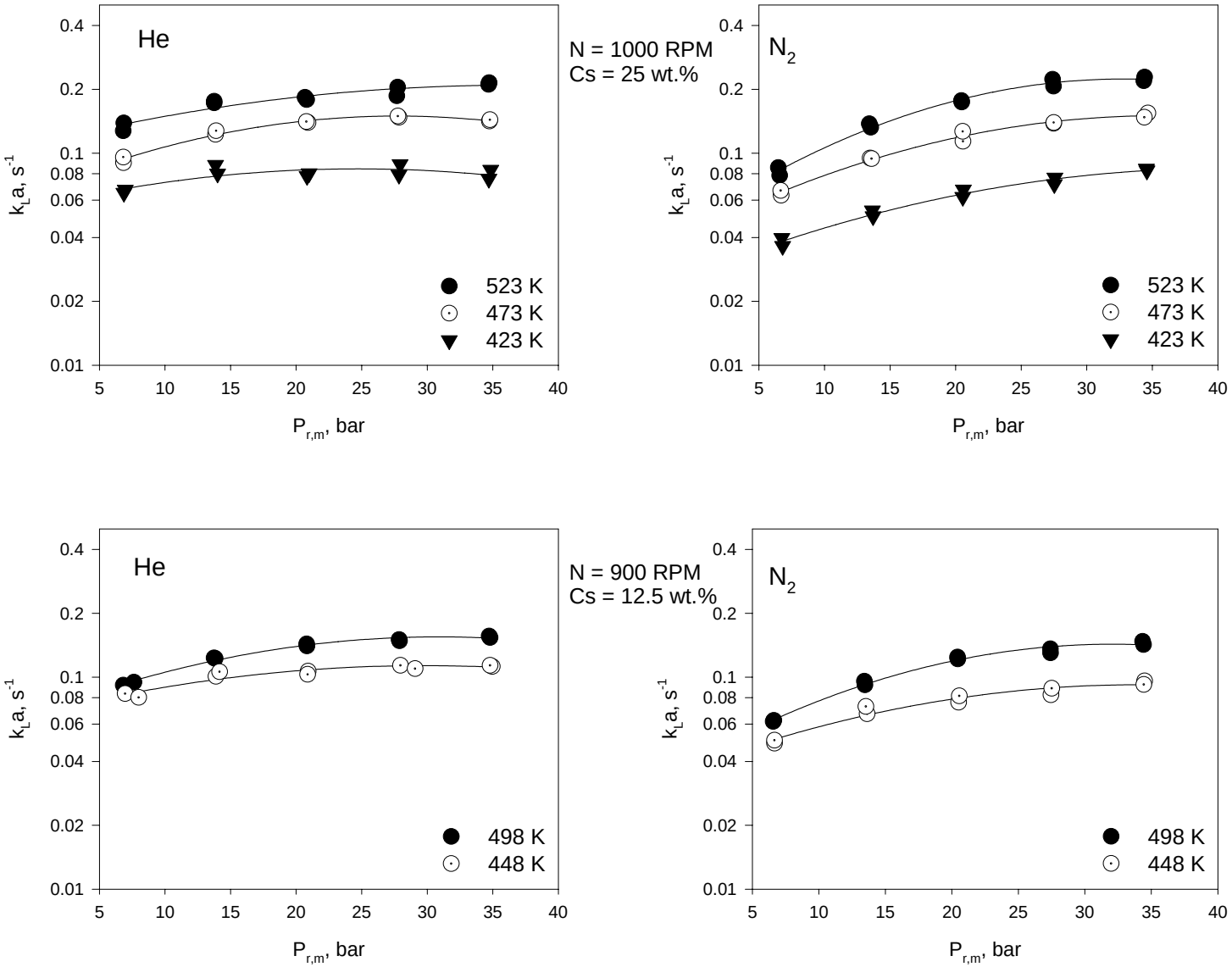

Figure 31: Effect of Temperature on k_La for He and N_2 in PAO-8

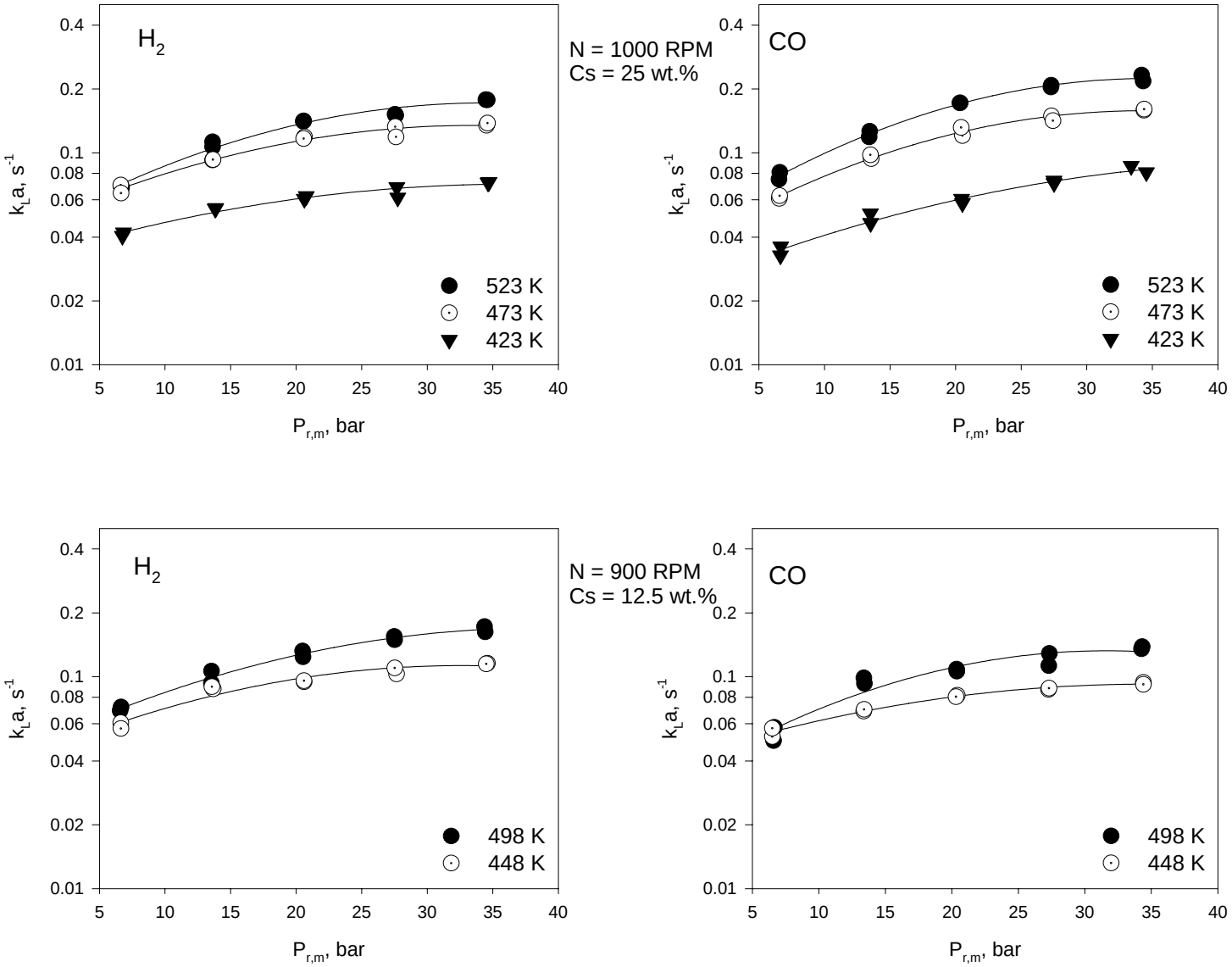

Figure 32: Effect of Temperature on k_La for H_2 and CO in PAO-8

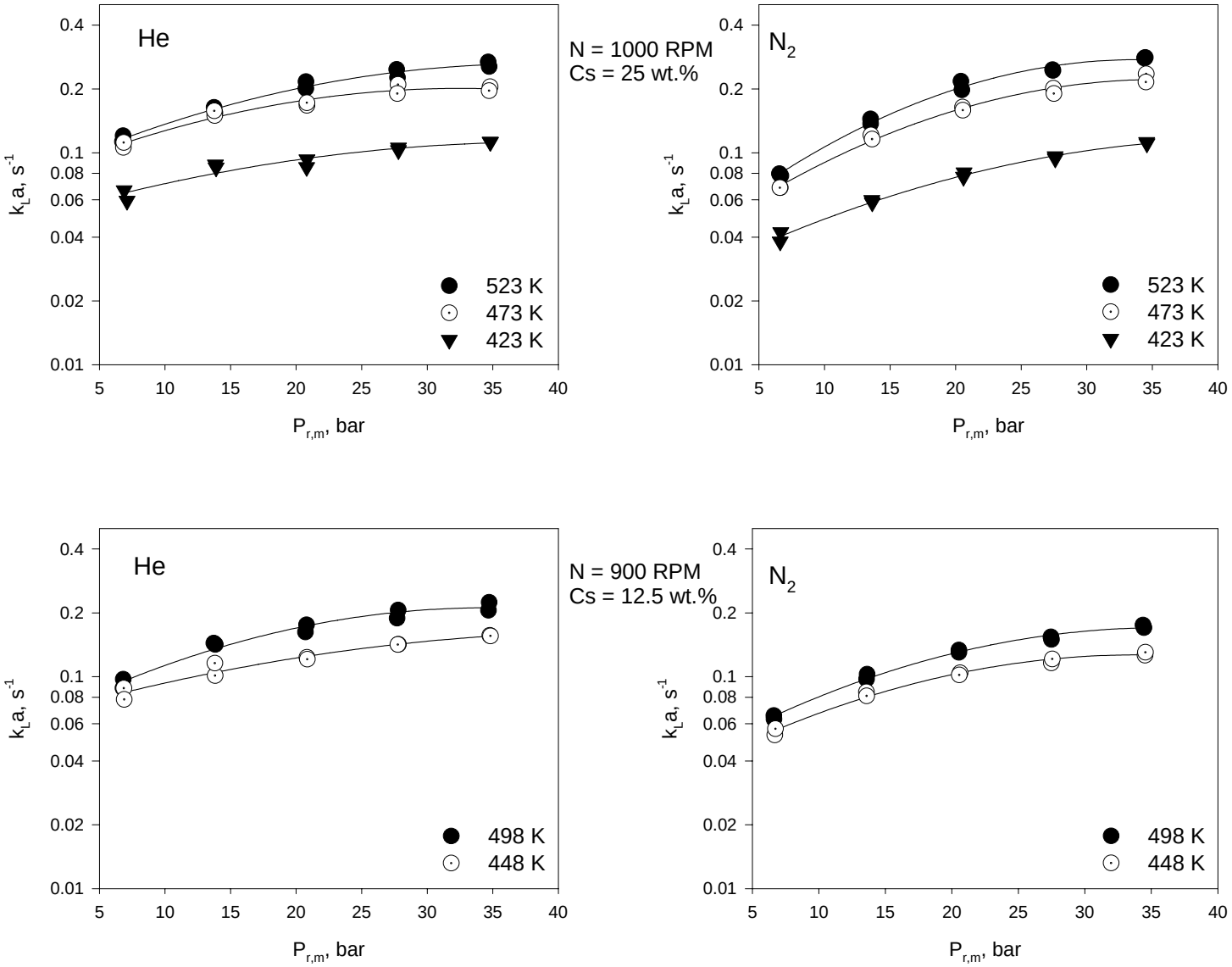

Figure 33: Effect of Temperature on k_La for He and N_2 in Sasol Wax

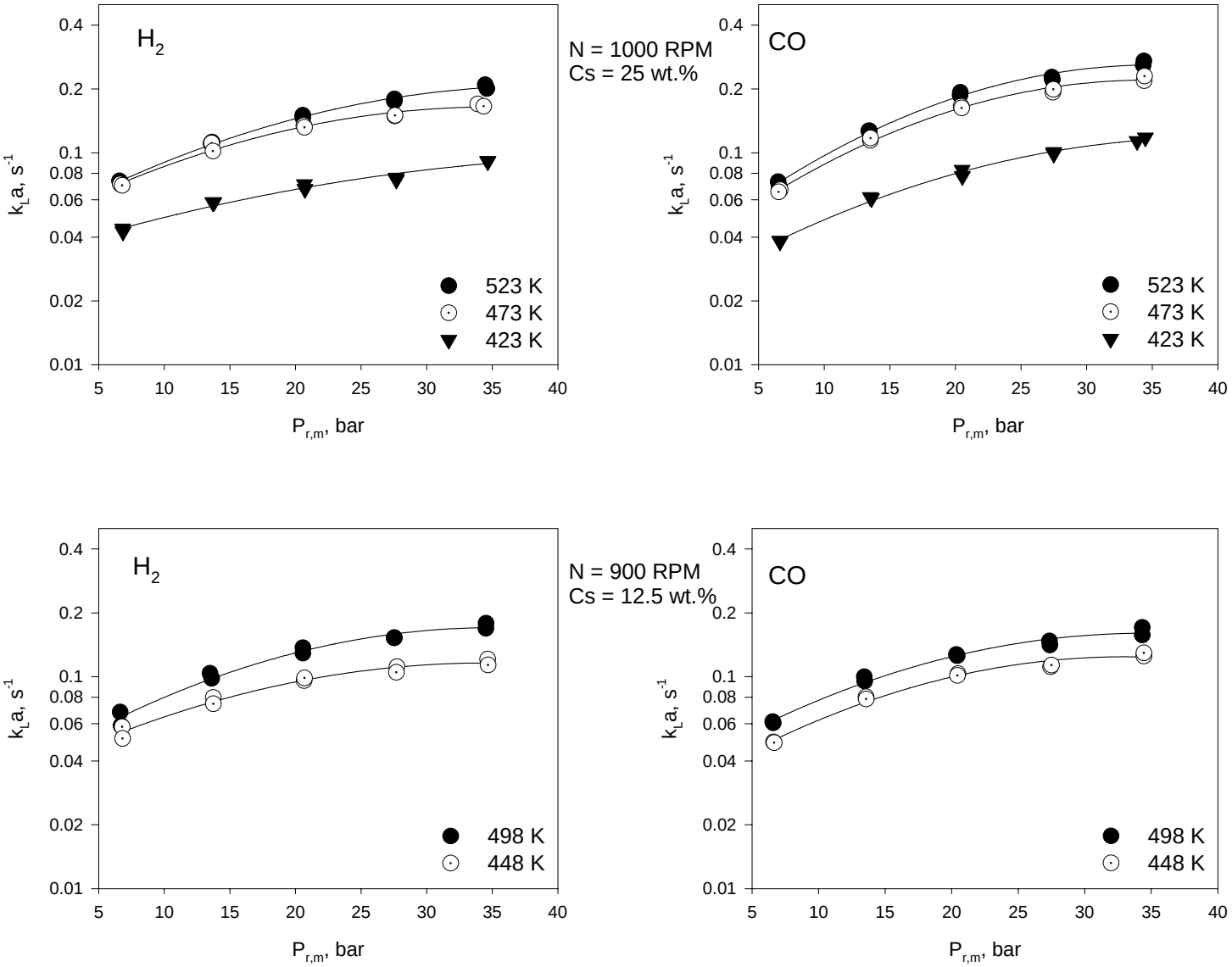

Figure 34: Effect of Temperature on k_La for H_2 and CO in Sasol Wax

250% with pressure up to 21 bar and then increase by only 140% above this pressure value. This effect can be mainly due to the change in physico-chemical properties of the gas-liquid system with increasing pressure. Increasing pressure increases the gas solubility, which decreases both liquid surface tension and liquid viscosity. Thus, both k_L and a and subsequently k_La are expected to increase with increasing pressure as with increasing temperature, mentioned in Section 6.2.2.

6.2.4 Effect of Solid Concentration on k_La

As previously shown in the literature review presented in Section 2.3.6 and Table 6, the addition of solid particles to the liquid can have different effects on k_La. Several studies showed that when adding small amount of solid particles, little effect[47, 58] or even an increase[38, 42, 48, 49, 59-62] of k_La values was observed, whereas at high solid concentrations, k_La values dramatically decreased[38, 42, 43, 48, 49, 59].

Figure 35 through Figure 38 show the effect of solid concentration on k_La for the four gases used in PAO-8 and Sasol wax. At solid concentrations below 25 wt.%, the addition of solid particles appears to have no impact or slightly decrease (less than 20%) k_La values, whereas, a sharp decrease (up to 80%) of k_La values can be observed at the highest solid loadings used (50 wt.%). Low concentrations of small solid particle could increase the mass transfer by the shuttle or grazing effect according to Kluytmans[60] who mentioned that small solid particles adsorb gas from the gas-liquid diffusion layer and desorbs it into the liquid bulk, increasing the mass transfer rate. Also, small solid loadings could create turbulences at the gas-liquid interface which decrease the effective diffusion layer and increase the mass transfer coefficient k_L and subsequently k_La. High concentrations of small particles, on the other hand, increase to a greater extent the slurry viscosity as can be observed in Figure 13, where increasing solid loadings from 0 to 25 wt.% increases the slurry viscosity by a factor of 1.1 and increasing solid loading from 25

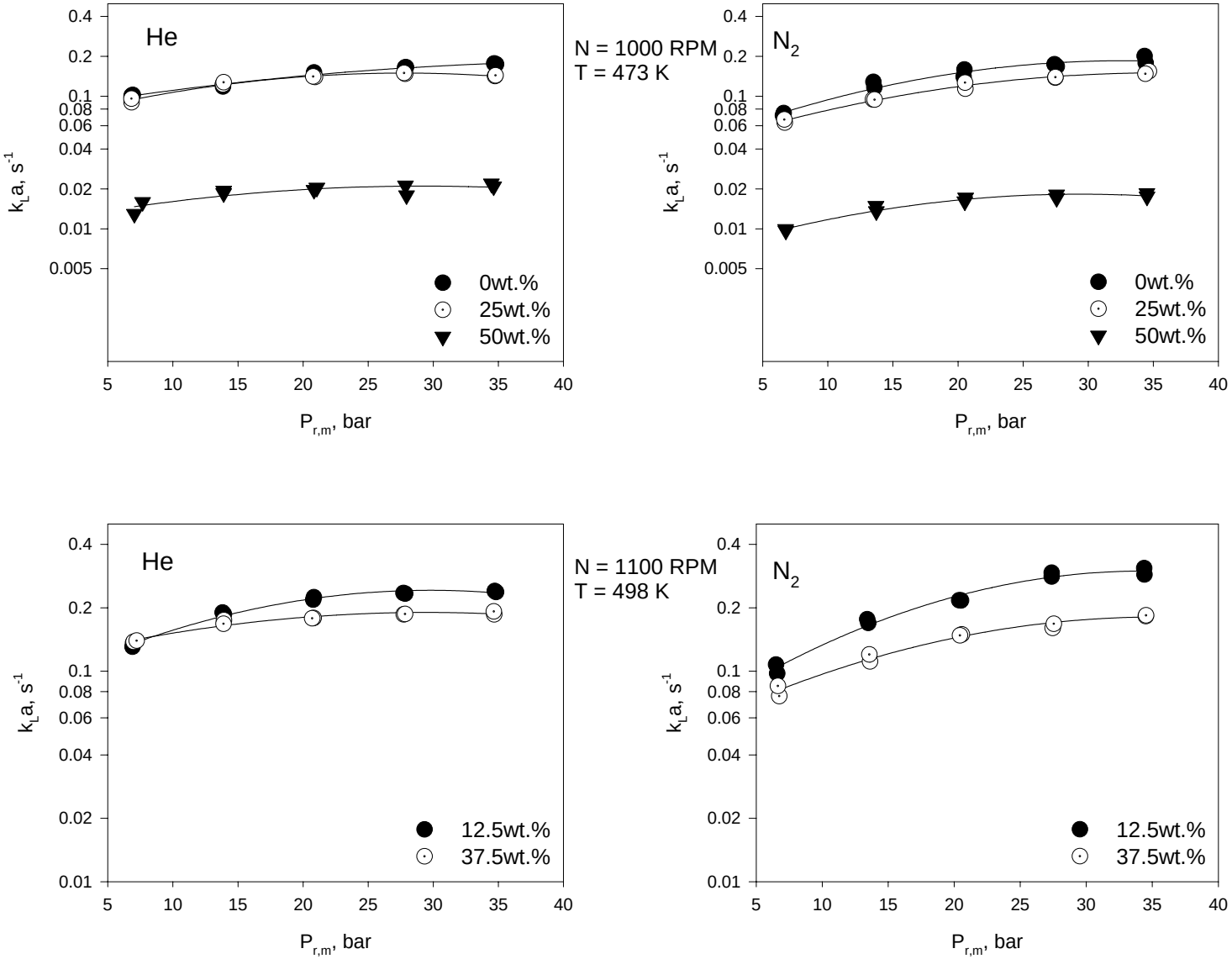

Figure 35: Effect of Solid Concentration on k_La for He and N_2 in PAO-8

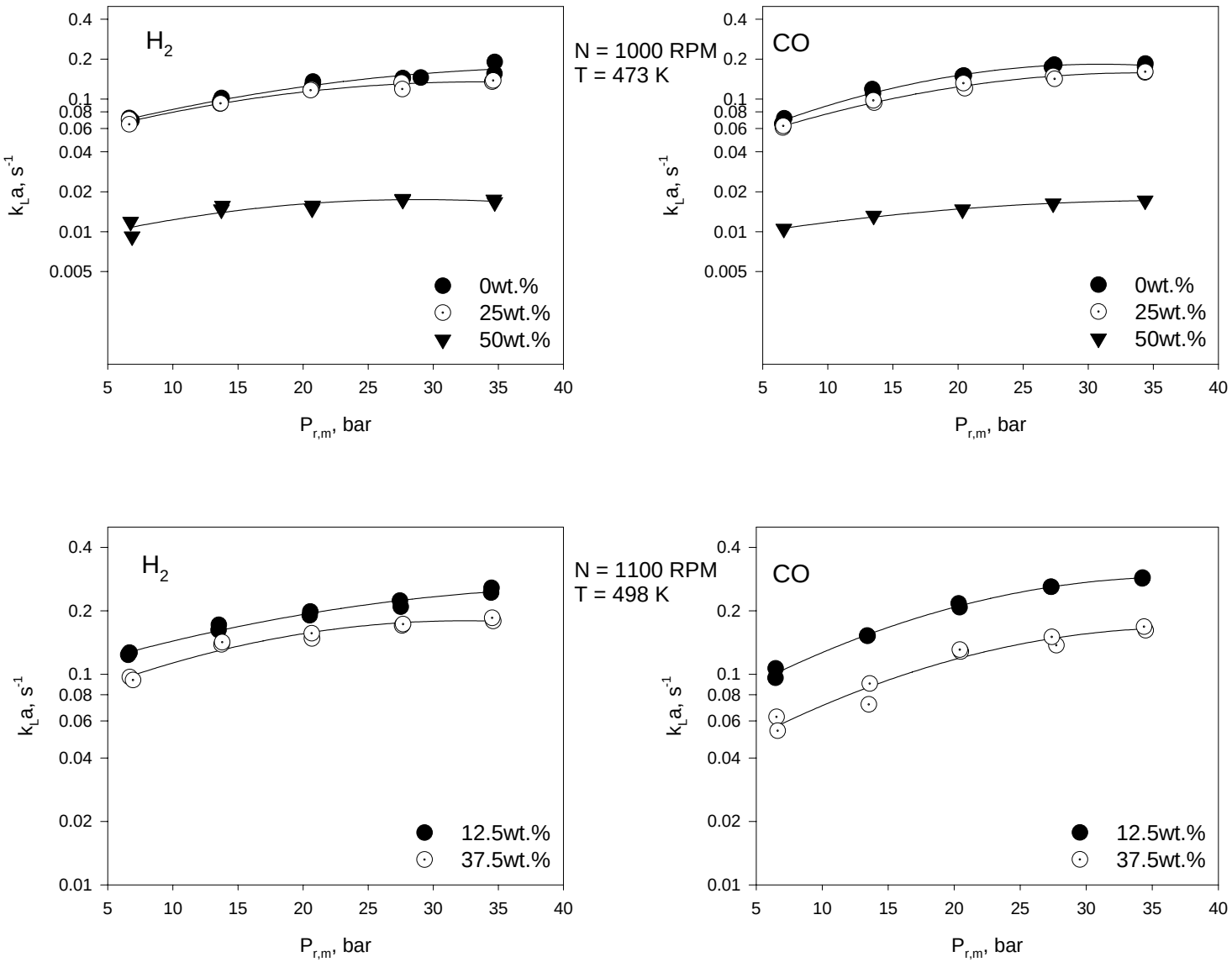

Figure 36: Effect of Solid Concentration on k_La for H_2 and CO in PAO-8

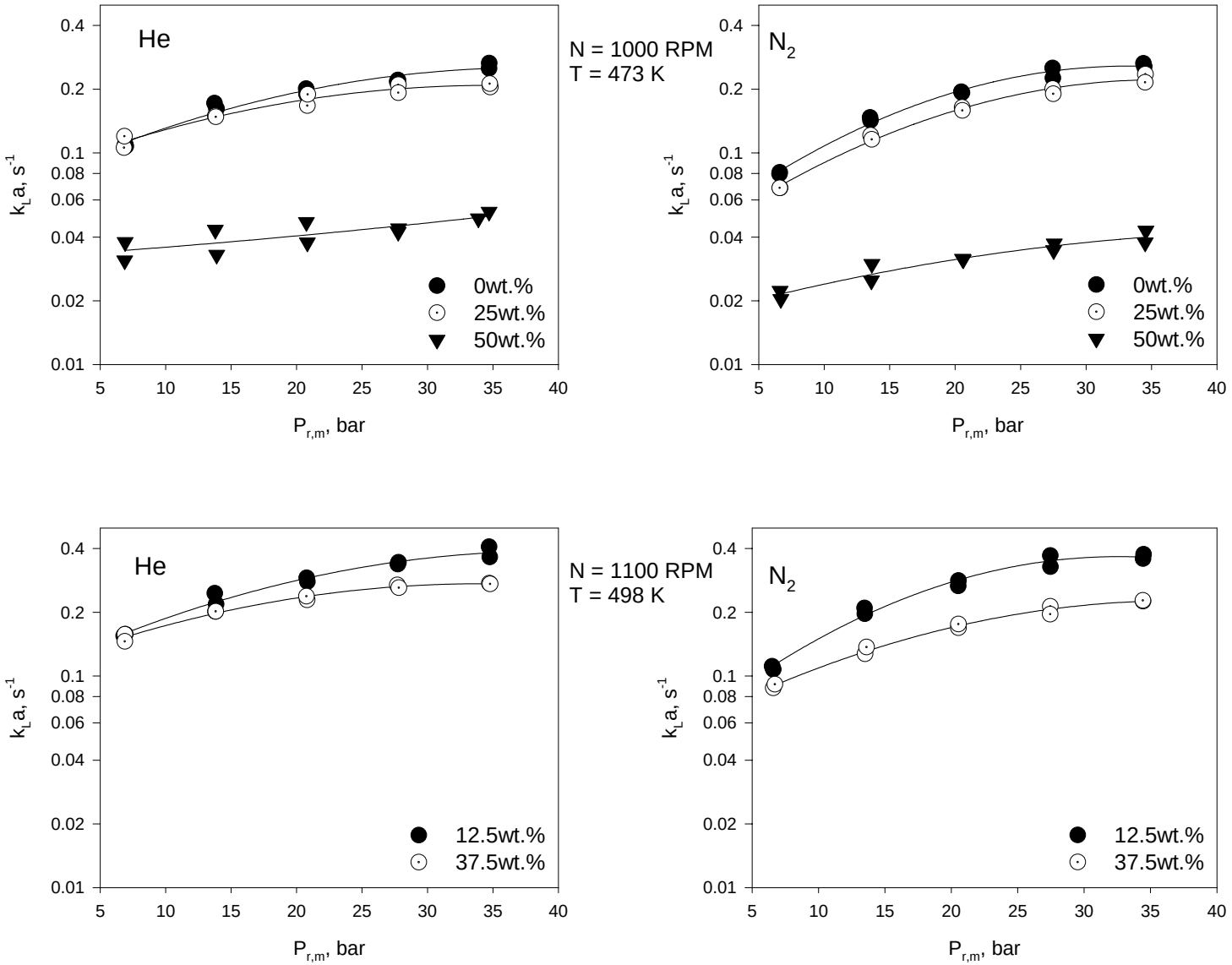

Figure 37: Effect of Solid Concentration on k_La for He and N_2 in Sasol Wax

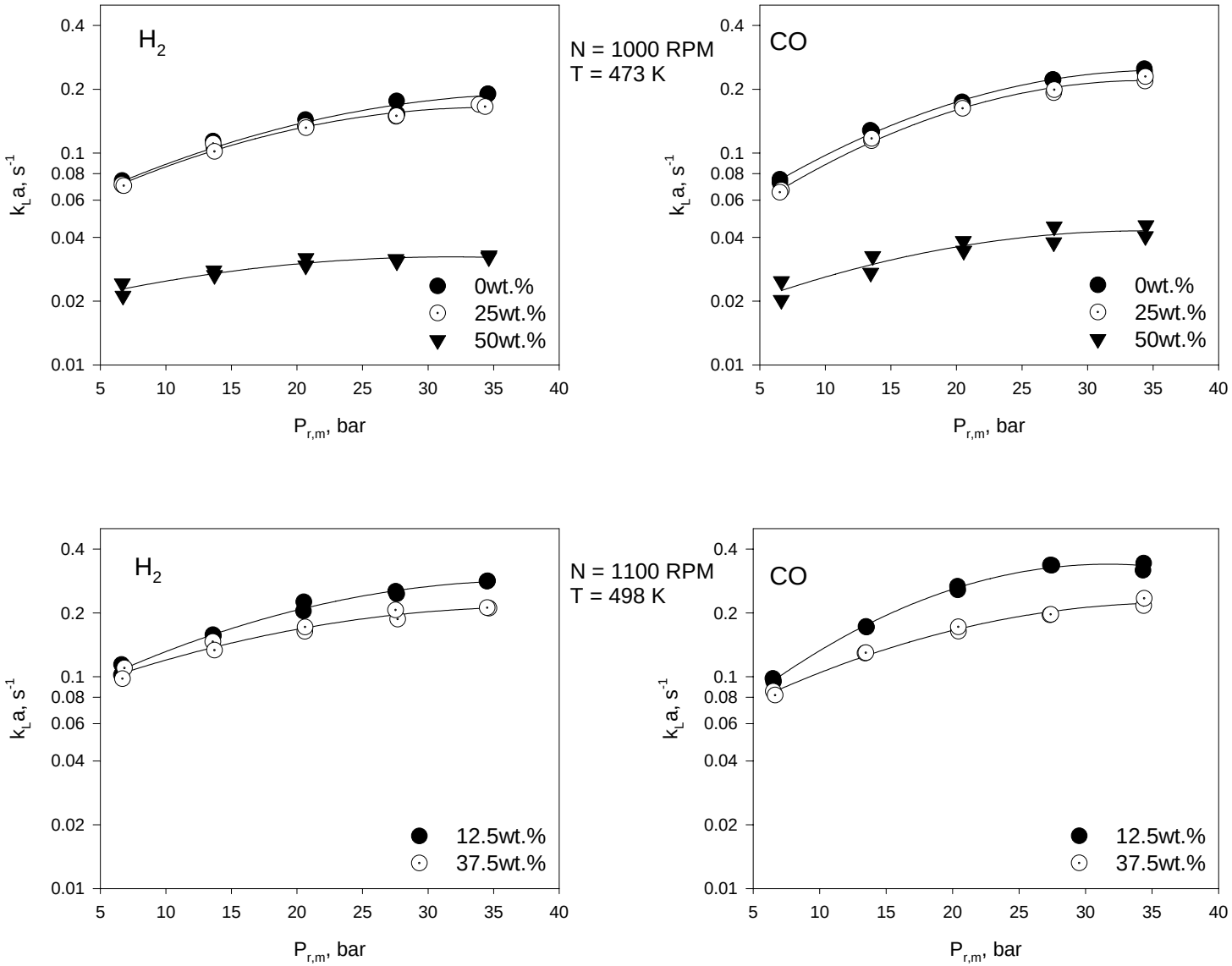

Figure 38: Effect of Solid Concentration on k_La for H_2 and CO in Sasol Wax

to 50 wt.% increases the slurry viscosity by a factor of 1.3. This increase of slurry viscosity decreases the gas diffusivity and therefore k_L hence the latter is related to the diffusivity to power 0.5 and 1 according to the penetration theory and the two-film model, respectively. Also, the increase of slurry viscosity promotes gas bubbles coalescence and decreases the gas-liquid interfacial area a. Thus, increasing solid loading decreases both k_L and a and subsequently k_La.

6.2.5 Effect of Gas Nature on k_La

As presented in Section 2.3.8, the effect of gas nature on k_La is quite complex. For instance, several investigators[23, 38, 63] reported similar k_La behavior for gases having close diffusivities, (such as N_2 and CO) and therefore close k_L. It is, however, quite risky to explain the effect of gas nature on k_La by considering its impact on k_L alone since the effect on the gas-liquid interfacial area should be considered in gas-inducing reactors.

The effect of gas nature on k_La is shown in Figure 39 and Figure 40; and as can be observed the values for nitrogen and carbon monoxide in both PAO-8 and Sasol wax are similar which can be related to the close diffusivities and molecular weights of both gases in the two liquids used. Figure 39 and Figure 40, however, show the volumetric mass transfer coefficient for helium and hydrogen are different, particularly in Sasol wax, which can be attributed to the difference between the molecular weights and diffusivities of both gases in the two liquids used as can be seen in Figure 9. It should be mentioned that in Sasol wax, the k_La values obtained for H_2 appeared to be similar to those measured for CO and N_2. This behavior is not surprising because similar k_La behavior for CO and H_2 in different F-T fractions and Gulf wax were reported by Deimling et al.[43] and Albal et al.[31], respectively, suggesting that the gas-liquid interfacial (a) has a stronger influence on k_La values than that of the mass transfer coefficient (k_L) under the operating conditions used in this study.

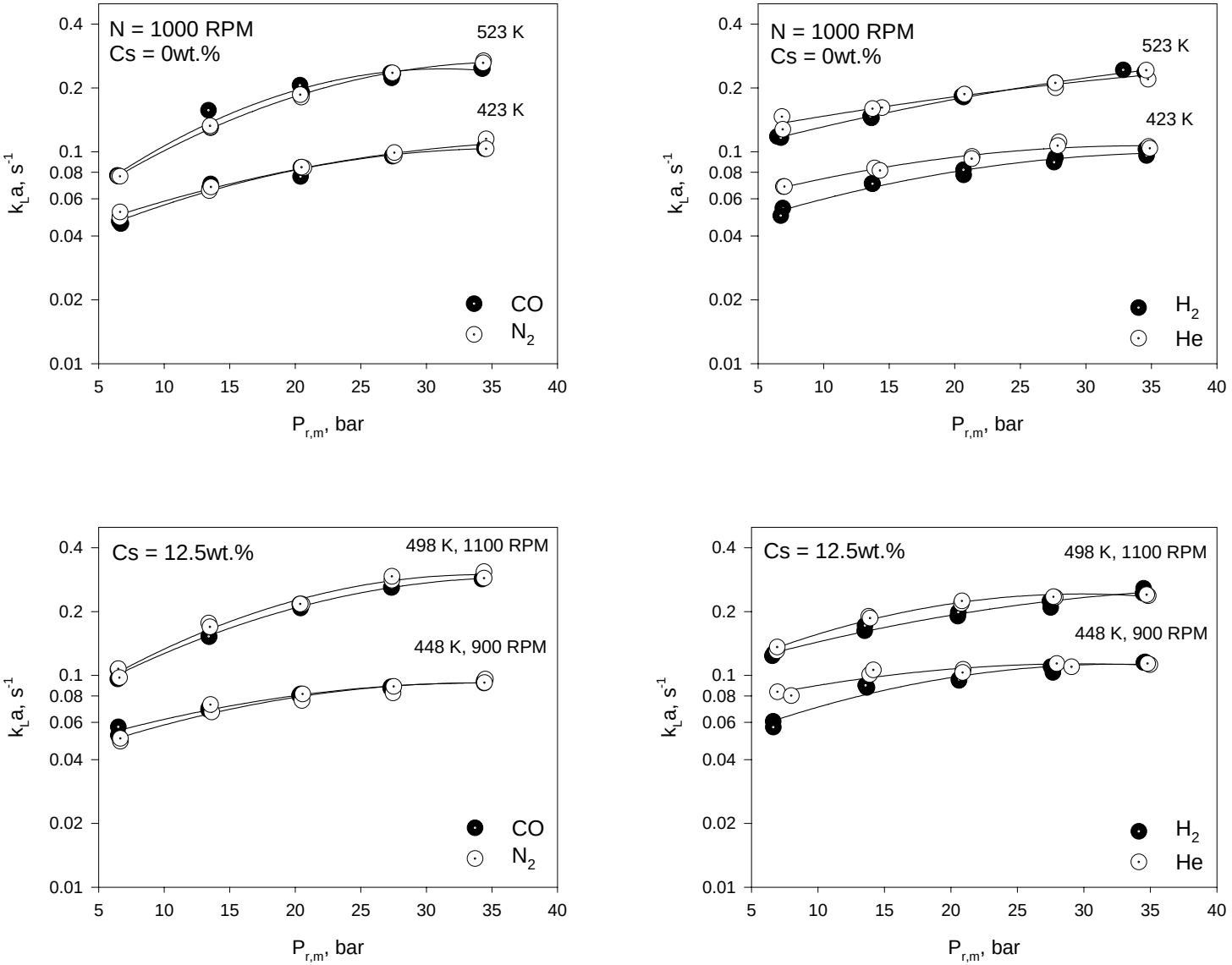

Figure 39: Effect of Gas Nature on k_La for CO, N_2, H_2 and He in PAO-8

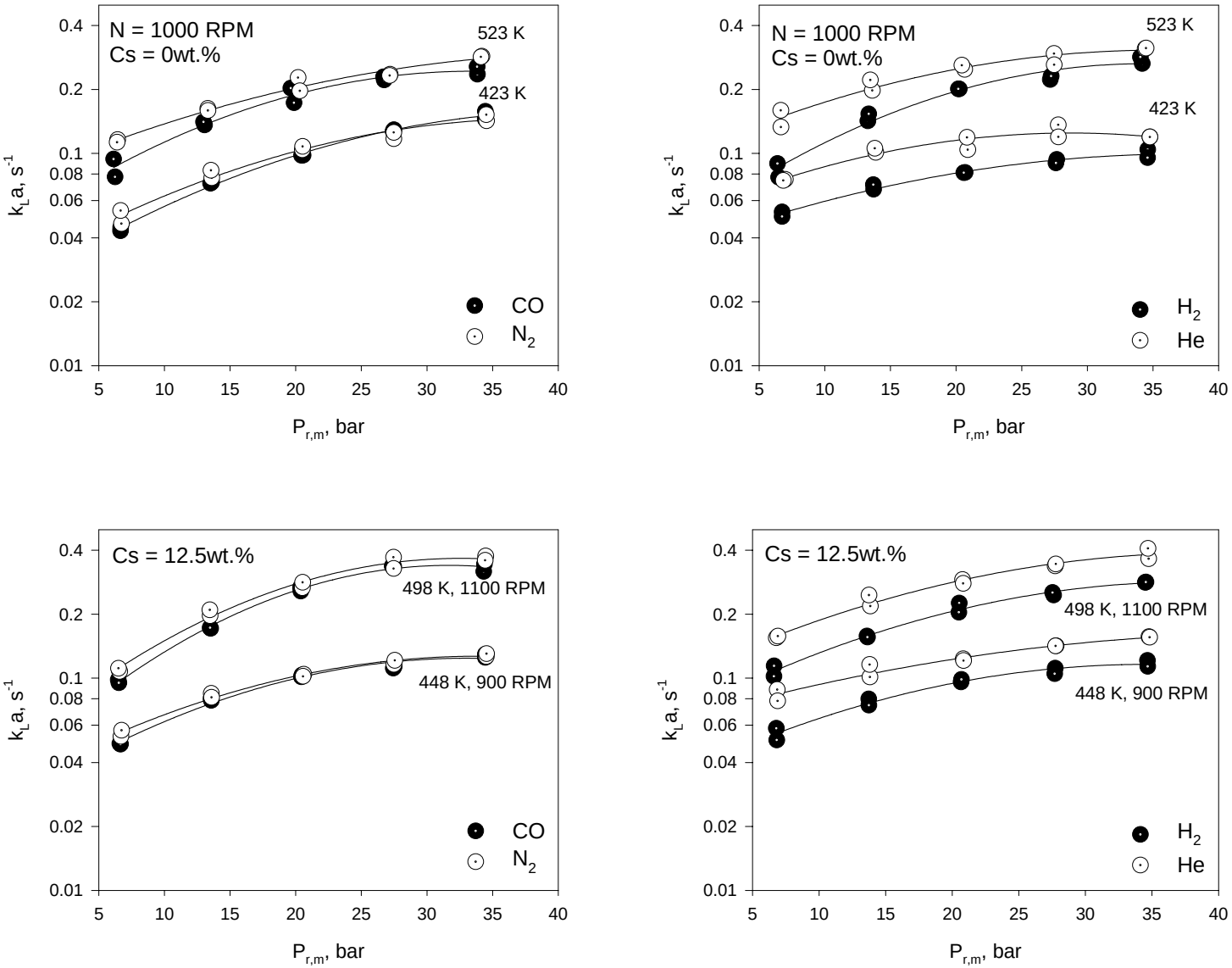

Figure 40: Effect of Gas Nature on k_La for CO, N_2, H_2 and He in Sasol Wax

6.2.6 Effect of Liquid Nature on k_La

The effect of liquid nature on k_La is given in Section 2.3.7 and Table 7. Karandikar et al.[43, 45, 46] and Chang et al.[23] reported a decrease of k_La with increasing the carbon number (n) of alkanes (C_nH_{2n+2}), which was related to the increase of viscosity with n. Also, Albal et al.[48] observed an increase in k_La values with decreasing the liquid surface tension.

Figure 41 shows that the volumetric mass transfer coefficients for the four gases in Sasol wax are 150% greater than those in PAO-8 under similar conditions. This k_La behavior cannot be explained by the effect of viscosity or diffusivity since the under the same temperature the viscosity of Sasol wax is much greater than that of PAO-8 as shown in Figure 7, which means that the mass transfer coefficient k_L for Sasol wax is greater than that of PAO-8. The k_La behavior, however, can be attributed to the fact that the surface tension of Sasol wax is lower than that of PAO-8 under the same temperature and accordingly Sasol wax could be a foaming liquid which promoted the formation of small gas bubbles with larger gas-liquid interfacial area and subsequently k_La than those with PAO-8.

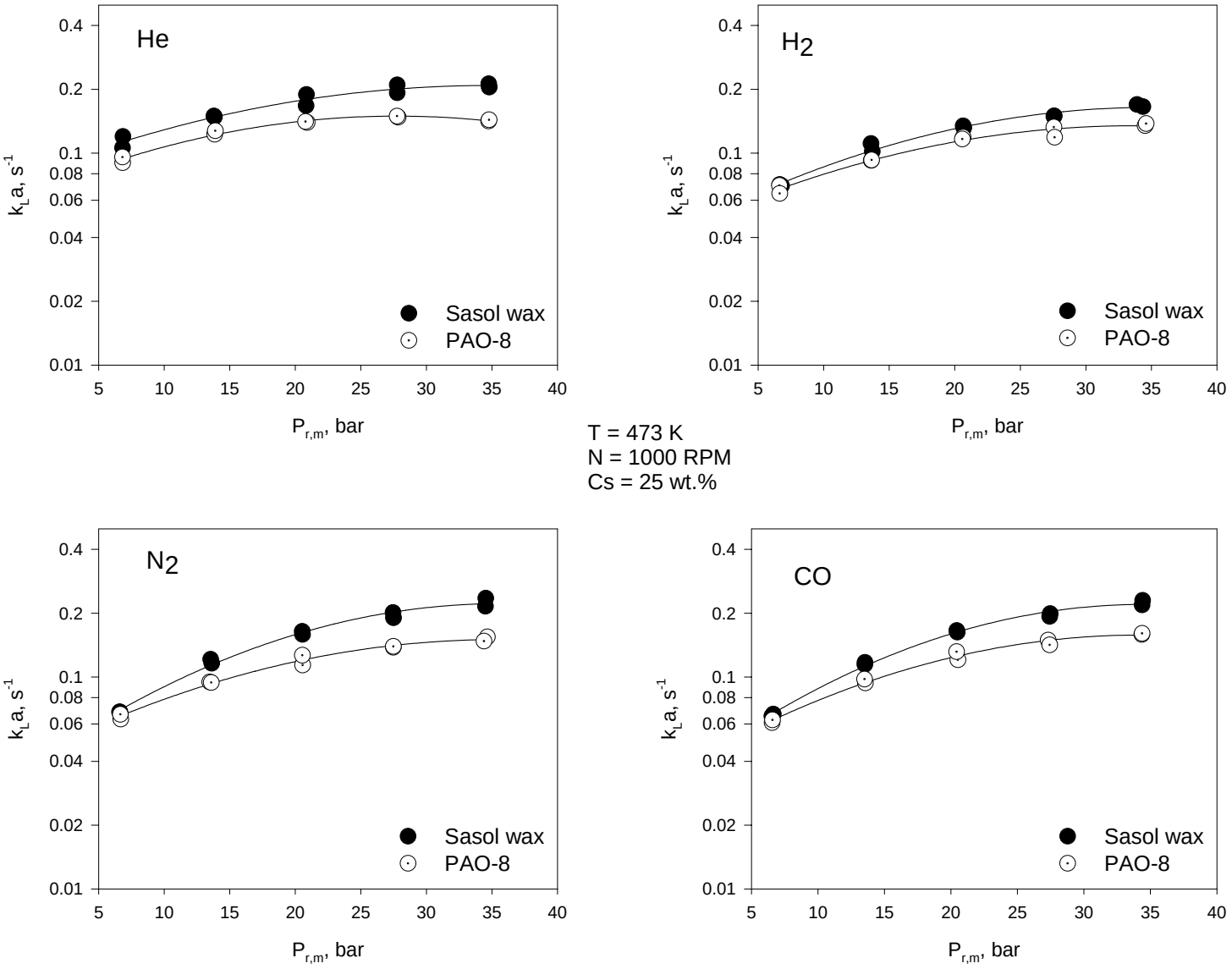

Figure 41: Effect of Liquid Nature on k_La

6.3 STATISTICAL CORRELATIONS OF k_La

The k_La experimental results obtained using the Central Composite Statistical Design are usually correlated using the following quadratic function:

$$\ln(k_L a) = \beta_0 + \sum_{i=1}^{4} \beta_i x_i + \sum_{i=1}^{4} \sum_{j \geq i}^{4} \beta_{ij} x_i x_j \tag{6-7}$$

where x_i and x_j are the coded variables and β_0, β_i and β_{ij} are constants.

In this study, in order to account for the non-linear behavior of some objective functions studied, exponential terms were added to Equation (6-7) as:

$$\ln(k_L a) = \beta_0 + \sum_{i=1}^{4} \beta_i x_i + \sum_{i=1}^{4} \sum_{j \geq i}^{4} \beta_{ij} x_i x_j + \sum_{i=1}^{4} \alpha_i e^{\gamma_i x_i} + \eta \cdot e^{\sum_{i=1}^{4} \lambda_i x_i} \tag{6-8}$$

where α_i, γ_i, η and λ_i are constants

The constants in Equation (6-8), listed in Table 20, were determined, with an R^2 greater than 97% using the least square method. A comparison between the experimental and predicted k_La values for all gases and in PAO-8 and Sasol wax is given in Figure 42; and as can be observed these correlations fit the experimental data with an average deviation of ± 20%.

To illustrate the interactions and combined effects of the operating variables on k_La, for the four gases in the two liquids used, three-dimensional response surfaces were generated and presented in Figure 43 through Figure 46. As can be seen in these figures, k_La values increase with increasing temperature at all pressures and increase with pressure at all temperatures in the Sasol wax and PAO-8. This increase of k_La values, however, is smaller at high P and T values is in agreement with the findings by Sridhar et al.[55] in Cyclohexane and Alghamdi[38] in Isopar-M.

Figure 43 through Figure 46 show that k_La values significantly increase with mixing speeds from 800 to 1050 rpm at all solid concentration used (0-50 wt%) and then tend to level-off at high mixing speeds greater than 1050 rpm which is in agreement with the data reported by Fillion[102], Alghamdi[38] and Lemoine et al.[14] in gas inducing reactors. Also, at all mixing speeds used (800-1200 rpm), increasing solid concentration from 0 up to 30 wt.% slightly decreases k_La values by 20%, whereas at solid concentration greater than 30 wt%, a dramatic decrease by about 80% of k_La can be observed. This behavior of k_La under given mixing speed and solid concentration is in agreement with the experimental findings by Dietrich et al.[49].

Table 20: Coefficients in Equation (6-8)

	PAO-8				Sasol wax			
	CO	**N_2**	**H_2**	**He**	**CO**	**N_2**	**H_2**	**He**
β_0	293.1969	-55.5174	-2.2967	-19.7220	-986.2772	-4032.1821	-143.0391	-585.8504
β_1	-	-	-	-2.6698	-9.2446	-21.4215	-4.5460	-10.5153
β_2	12.4581	0.3235	0.3160	0.2830	0.8189	1.5067	1.3448	1.5279
β_3	-	-	-0.2008	-0.2308	77.1166	171.7737	17.3559	51.7183
β_4	0.0376	-	0.0236	0.0699	-0.1018	-0.3176	-0.0708	-0.1212
β_{12}	-	-	-	-	-	-	-	-
β_{13}	-	-	-	0.0809	0.7909	0.9752	0.6355	1.0019
β_{14}	-	-	-	-	-	-	-	-
β_{23}	-	-	-	-	-	-	$1.16.10^{-4}$	-
β_{44}	0.0052	-0.0924	-0.0824	-0.0170	-0.0532	-0.0499	-	-0.0335
β_{33}	0.0585	-	-0.0757	-0.0977	-3.2514	-3.8658	-1.2735	-2.5072
β_{11}	-	-	-0.1338	-0.2564	-0.1576	-0.1398	-0.1444	-0.1988
β_{22}	-	-0.0256	-	-0.0287	-0.1621	-0.1384	-0.0586	-0.1054
α_1	416.8152	53.1879	0.1063	17.7274	-	-	-	-
α_2	-711.8844	$-4.25.10^{-13}$	$-2.82.10^{-6}$	$-2.35.10^{-12}$	-	-	-	-
α_3	-0.0689	-0.0765	$-1.02.10^{-4}$	$-8.94.10^{-11}$	-	-	-	-
α_4	-0.1983	0.3280	0.1176	$-1.24.10^{-4}$	-	-	-	-
γ_1	0.0004	0.0038	0.9590	0.1631	-	-	-	-
γ_2	0.0169	-14.0246	-6.2225	-13.1700	-	-	-	-
γ_3	1.7564	1.6539	4.7417	11.5916	-	-	-	-
γ_4	-0.6590	0.5069	0.7999	-3.3260	-	-	-	-
η	-	-	-	-	984.6260	4030.4465	141.0082	584.3003
λ_1	-	-	-	-	0.0095	0.0054	0.0333	0.0182
λ_2	-	-	-	-	$-3.91.10^{-4}$	$-2.63.10^{-4}$	$-6.49.10^{-3}$	$-1.93.10^{-3}$
λ_3	-	-	-	-	-0.0785	-0.0427	-0.1245	-0.0888
λ_4	-	-	-	-	$3.47.10^{-4}$	$1.35.10^{-4}$	$1.78.10^{-3}$	$4.56.10^{-4}$

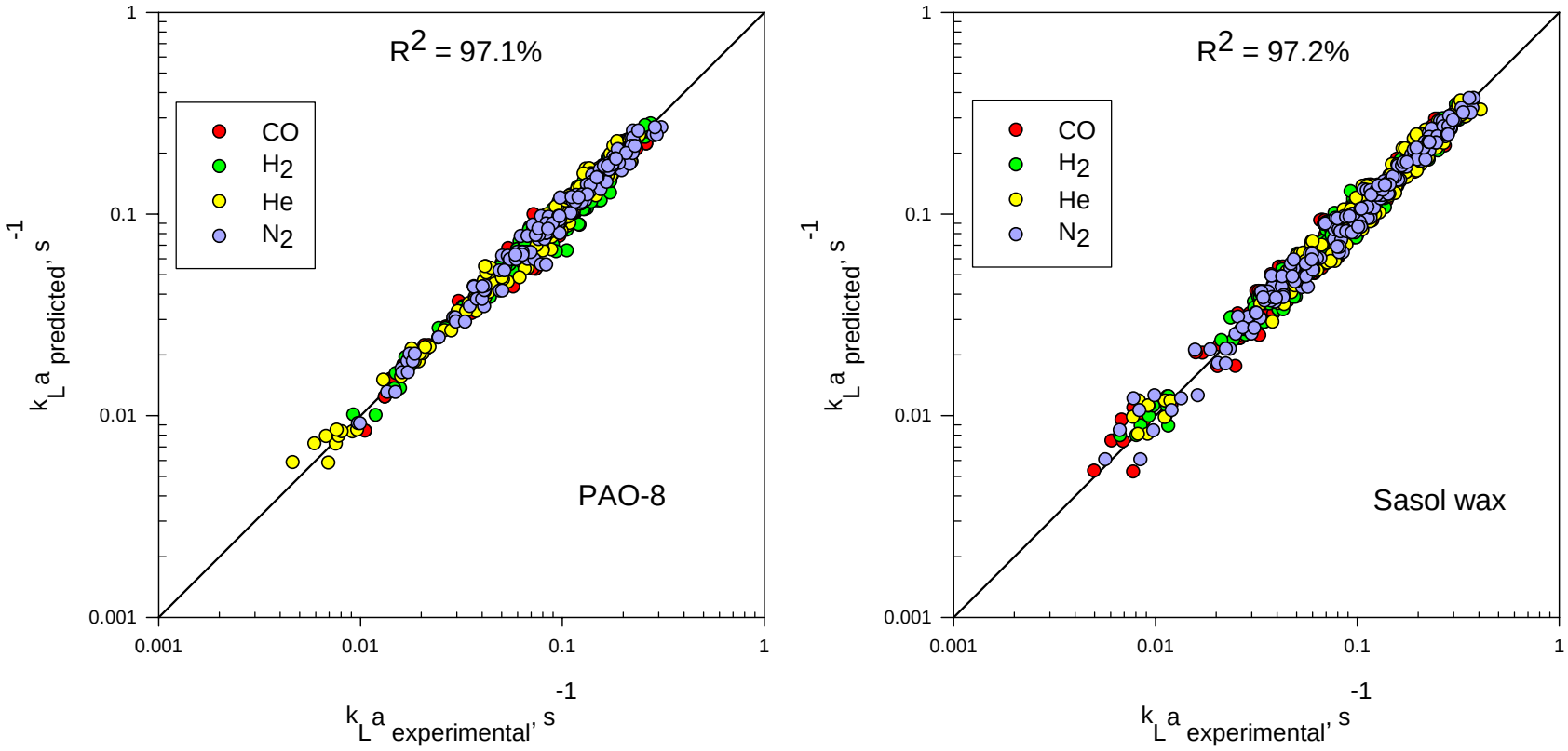

Figure 42: Comparison between Experimental and Predicted k_La Values Using the Statistical Correlation

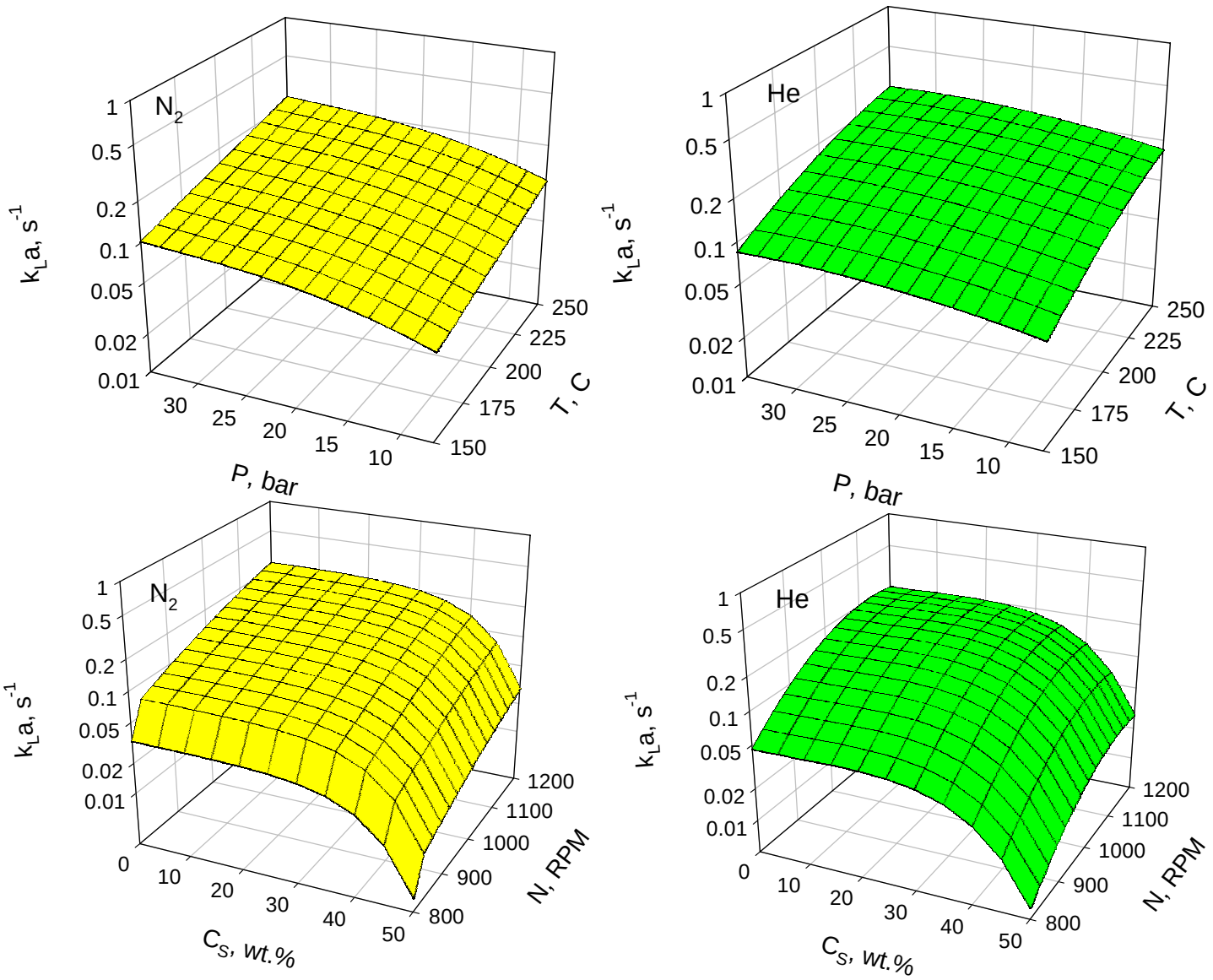

Figure 43: Effect of Operating Variables on Predicted k_La for N_2 and He in PAO-8

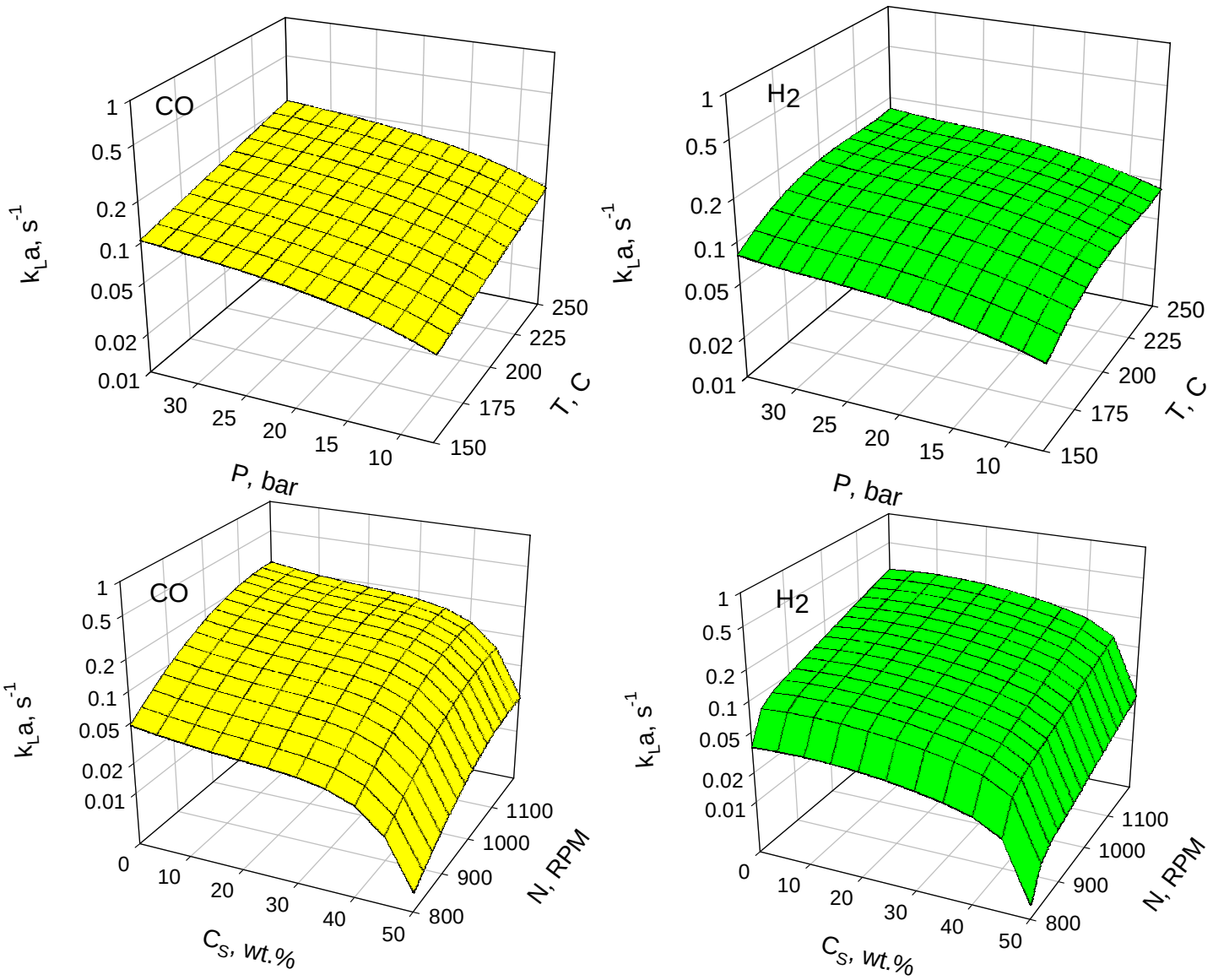

Figure 44: Effect of Operating Variables on Predicted k_La for CO and H_2 in PAO-8

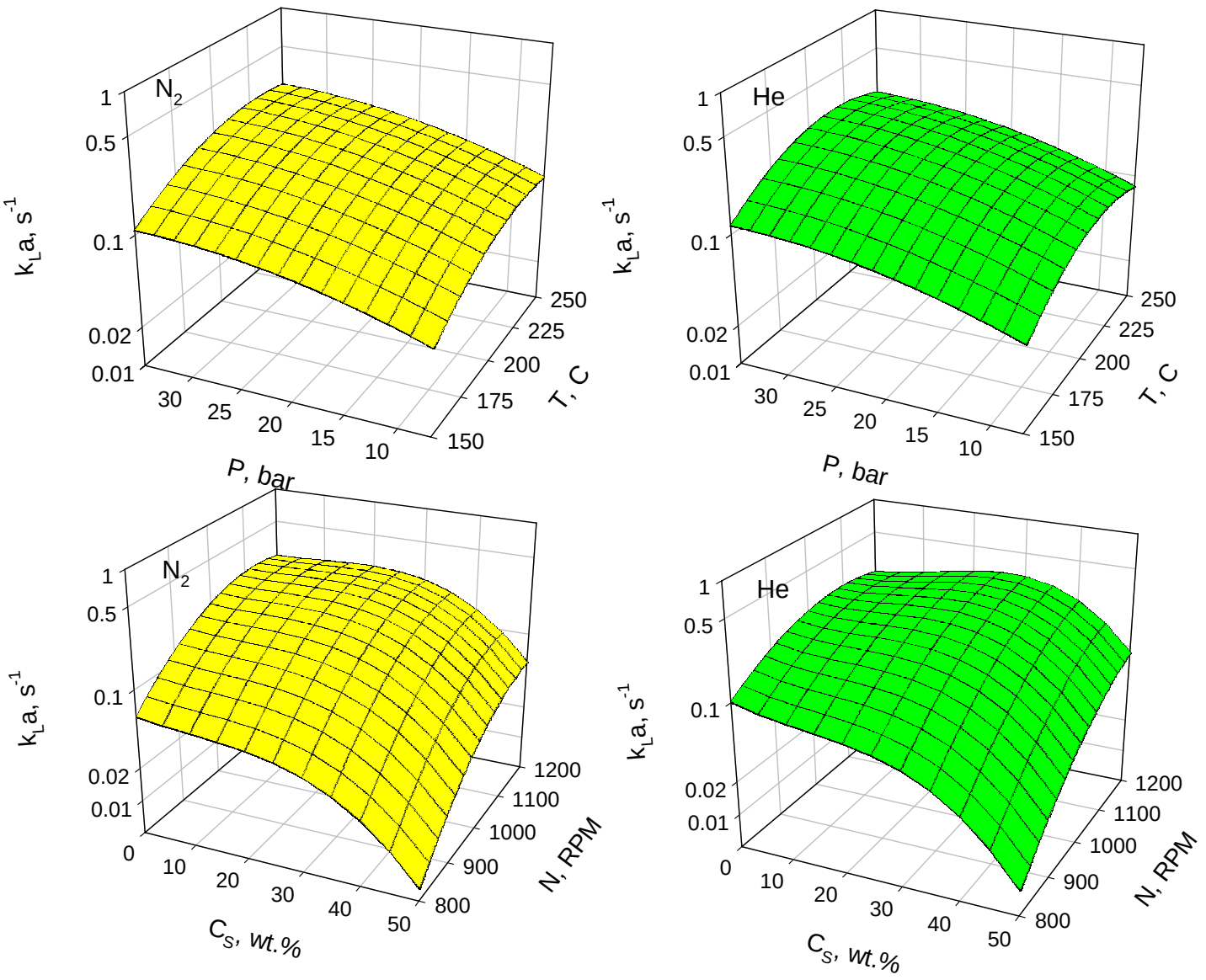

Figure 45: Effect of Operating Variables on Predicted k_La for N_2 and He in Sasol Wax

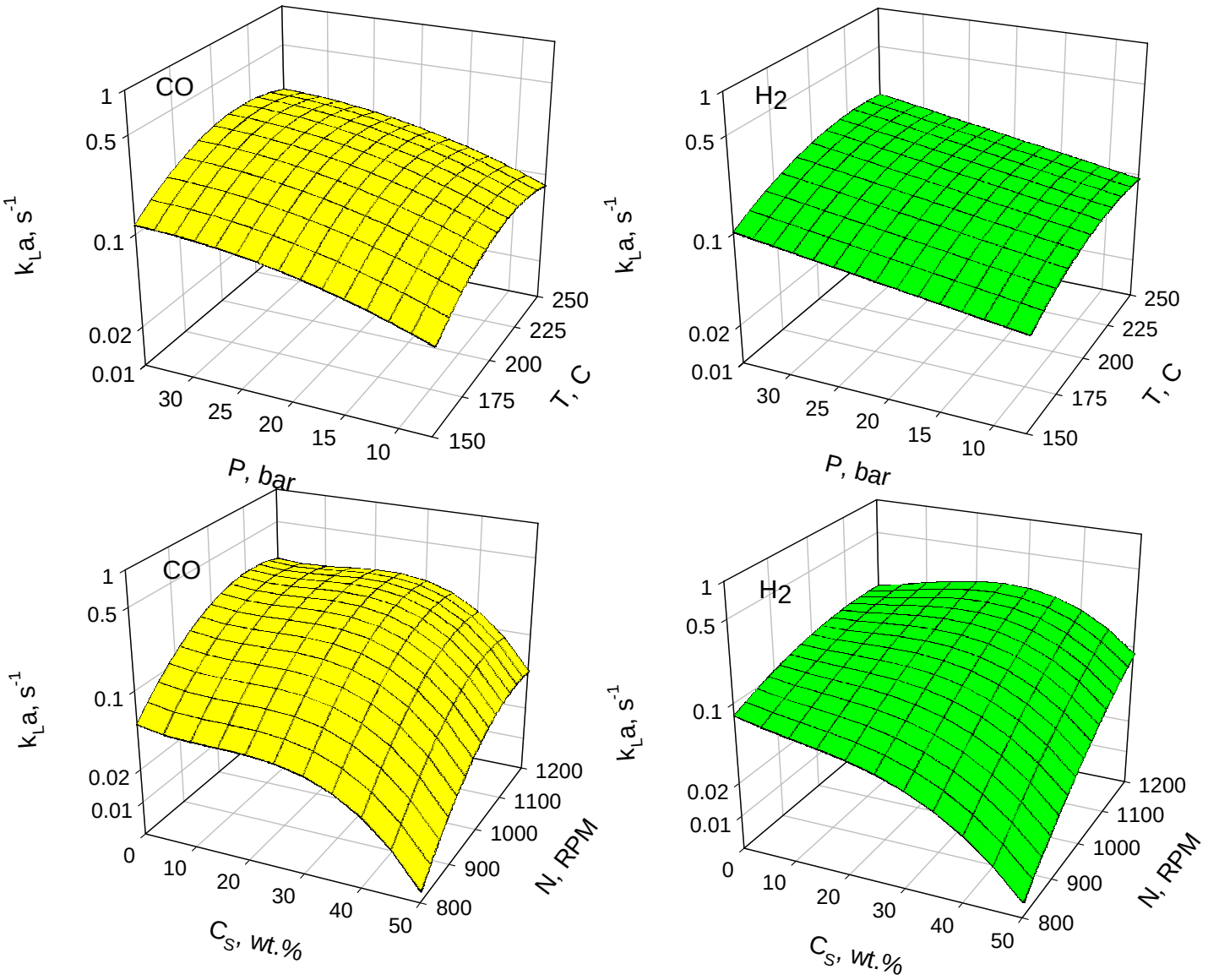

Figure 46: Effect of Operating Variables on Predicted k_La for CO and H_2 in Sasol Wax

6.4 EMPIRICAL CORRELATION OF k_La

The k_La values obtained in this study for H_2, N_2, He and CO in Sasol wax and PAO-8 along with those measured by Alghamdi[38] for the same gases in Isopar-M, all in a gas inducing reactor, were correlated using dimensionless numbers. The properties of Isopar-M are given in Appendix D. About 2000 experimental data points were used to develop the following empirical correlation:

$$Sh = 7.437 \times 10^{-6} Sc^{0.5} Eu^{0.527} We^{2.295} Re^{0.104} e^{(-28.26 C_V^{\,2} - 0.924 C_V)} \quad (6\text{-}9)$$

This correlation is capable of predicting the experimental Sherwood Number (*Sh*) with a regression coefficient, R^2 greater than 94% as can be seen in Figure 47. The above correlation is valid within the ranges of the dimensionless numbers given in Table 21.

Table 21: Lower and Upper Limits of the Dimensionless Numbers in Equation (6-9)

Variable	Minimum	Maximum
Sc	35	6111
Eu	2133	27049
We	195	480
Re	1935	21077
C_V	0 vol.%	19.60 vol.%

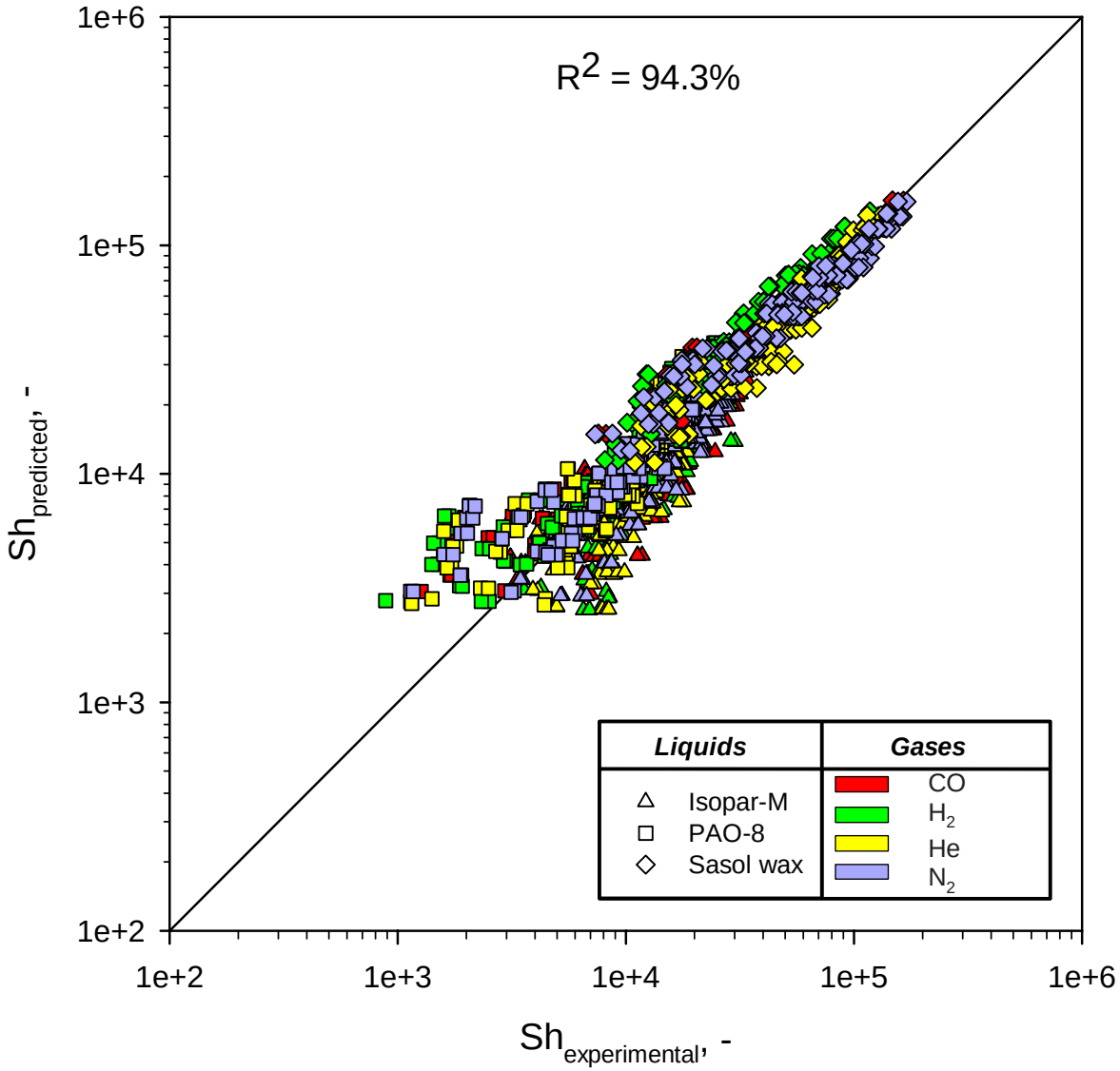

Figure 47: Comparison between Predicted and Experimental Sh Values

7.0 CONCLUSIONS

The Central Composite Statistical Design of experiment was used to measure the solubility, C^* and liquid-side volumetric mass transfer coefficient, k_La for four different gases (He, CO, N_2 and H_2) in two different liquids (PAO-8 and Sasol Wax) in a one-liter agitated reactor operating in a gas-inducing mode under typical conditions of the Fischer-Tropsch synthesis. The effect of operating variables, including pressure (0.7 – 3.5 MPa), temperature (423 – 523 K), mixing speed (13.3 – 20 Hz), and alumina powder (used as a support for cobalt catalyst) concentration (0 - 50 wt.%) on k_La and C^* values were investigated. At a given set of operating variables, the transient physical gas absorption technique was used to obtain k_La and C^* values were determined at the thermodynamic equilibrium conditions. From the experimental data obtained the following conclusions can be drawn:

- The C^* values for the four gases in the two liquids were found to linearly increase with the solute gas partial pressure at constant temperature and the data were modeled using Henry's Law. The effect of temperature on C^* was described using an Arrhenius-type equation, where the apparent activation energy of gas absorption was found to be dependant on temperature.
- The solubility values of the four gases in the two liquids followed the order: $C^*_{CO}>C^*_{N2}>C^*_{H2}>C^*_{He}$ which in agreement with the behavior of the solubility parameters for the components used. Also, under same pressure and temperature, the C^* values of the four gases in PAO-8 and Sasol wax were almost the same due to the closeness of the solubility parameters of both liquids.

- The k_La values of the four gases in the two liquids were found to increase with increasing mixing speed, temperature and pressure. The increase of k_La values with increasing mixing speed was greater from 800 rpm to 1050 rpm than from 1050 to 1200 rpm. Also, the increase of k_La values was greater from 7 to 21 bar than from 21 to 35 bar.
- The k_La values of the four gases in the two liquids appeared to slightly decrease (20%) with increasing solid concentration from 0 to 30 wt.% and dramatically decreased by about 80% when the solid concentrations was increased above this value.
- Under similar operating conditions, comparable k_La values were observed for N_2 and CO whereas the values for H_2 were different from those of He due to the difference between their diffusivities and solubilities in the two liquids. This difference between k_La values for H_2 and He was more noticeable in Sasol wax where k_La values for H_2 were comparable to those for N_2 and CO.
- Under similar operating conditions, k_La values for the four gases were found to be higher in Sasol wax than in PAO-8. This behavior was related to the greater gas-liquid interfacial area created in the Sasol wax due to its lower surface tension and foamability when compared with those of the PAO-8.
- Statistical correlations were developed to predict the k_La values for the four gases in the two liquids with a regression coefficient > 97%. Also, an empirical correlation using dimensionless numbers was proposed to correlate k_La values in gas induction slurry agitated reactors with a regression coefficient > 94%.

APPENDIX A

PLANNED AND EXISTING GTL PLANTS IN THE WORLD

Table A-1: Planned and Existing GTL Plants in the World[107]

Plant name	Country Location	Capacity (bbl/day)	Start date	Status	Type	FT Process
Shell (Argentina)	Argentina	75,000	2007	Potential	Commercial	SMDS
Australia GTL SasolChevron	Australia	30,000	2006	Potential	Commercial	Sasol
Shell (Australia)	Australia	75,000	2007	Potential	Commercial	SMDS
Sweetwater GTL	Australia Burrup peninsula	11,500	2005	Potential	Commercial	Syntroleum
GTL Bolivia	Bolivia	10,000	2006	Potential	Commercial	Rentech
Repsol/Syntoleum	Bolivia	103,500	N/A	Potential	Commercial	Syntroleum
Synergy/Stone Canyon Resources	Canada Calgary	4	2000	Existing	Pilot	SynGen
ENAP	Chile	10,000	2006	Potential	Commercial	Syntroleum
Shell/EGPC	Egypt	75,000	2005	Potential	Commercial	SMDS
Sicor	Ethiopia	20,000	N/A	Planned	Commercial	N/A
Pertamina	Indonesia	16,500	N/A	Potential	Commercial	Rentech
Shell (Indonesia)	Indonesia	75,000	2007	Potential	Commercial	SMDS
Nakangan	Iran	35,000	2006	Potential	Commercial	N/A
IFP/ENI	Italy	20	2001	Existing	Pilot	IFP/ENI
JNOC Tomakomai	Japan Hokkaido	7	2002	Existing	Pilot	JNOC-TRC
NKK Corp	Japan	0	1999	Existing	Pilot	NKK
Shell MDS	Malaysia Bintulu	12,500	1993	Existing	Commercial	SMDS
Shell (Malaysia)	Malaysia	75,000	2007	Potential	Commercial	SMDS
NZ Synfuels	New Zealand New Plymouth	12,000	1985	Closed	Commercial	N/A
Escravos GTL	Nigeria Escravos.	34,000	2005	Future	Commercial	Sasol
Syntroleum/BPZ	Peru Talara Basin	5,000	2003	Planned	Commercial	Syntroleum
ConocoPhillips/QP	Qatar	80,000	2009	Project	Commercial	ConocoPhillips
ExxonMobil/QP	Qatar	115,000	N/A	Planned	Commercial	Exxon AGC 21
Oryx GTL	Qatar Ras Laffan	100,000	2009	Future	Commercial	Sasol
QP/SasolChevron II	Qatar Ras Laffan	130,000	2010	Future	Commercial	Sasol
Shell (Qatar)	Qatar	140,000	2008	Future	Commercial	SMDS

Table A-1 (Cont'd)

Plant name	Country Location	Capacity (B/D)	Start date	Status	Type	FT Process
Yakutsk	Russia	0	N/A	Potential	Commercial	Syntroleum
Ivanhoe (Qatar)	Qatar	185,000	N/A	Potential	Commercial	Syntroleum
Forest Oil	South Africa	12,500	2006	Potential	Commercial	Non Av.
SASOL I	South Africa Sasolburg	5,600	1955	Existing	Commercial	Sasol
SASOL II/III	South Africa Secunda	124,000	1980	Existing	Commercial	Sasol
MossGass	South Africa Mossel Bay	24,000	1992	Existing	Commercial	Sasol
Orobos steel facility	Sweden	N/A	N/A	Potential	Commercial	Rentech
Petro SA	South Africa Mossel Bay	1,000	2003	Future	Pilot	Statoil
GTL Trinidad	Trinidad Point Lisas	10,000	2003	Future	Commercial	N/A (Based on DOE Research)
BP Nikiski	USA Alaska, Nikiski	300	2002	Existing	Pilot	BP/Kvaerner
Conoco (Ponca)	USA Ponca City	400	2002	Existing	Pilot	Conoco
Exxon Mobil (Baton Rouge)	USA Baton Rouge	300	1993	Existing	Pilot	Exxon AGC 21
DOE	USA LaPorte	35	1992	Existing	Pilot	N/A
Synfuels	USA Texas	12	2000	Existing	Pilot	N/A
Rentech Colorado	USA Colorado	1	1992	Existing	Pilot	Rentech
ANGTL	USA Alaska	50,000	2006	Potential	Commercial	Sasol
Syntroleum	USA Tulsa, OK	2	1990	Existing	Pilot	Syntroleum
ARCO/Syntroleum Cherry Point	USA Cherry Point	70	1999	Closed	Pilot	Syntroleum
Syntroleum/Marathon Tulsa	USA Tulsa, OK	70	2003	Future	Pilot	Syntroleum
Williams/EI	USA Pittsburgh	15	2003	Planned	Pilot	Williams GasCatSM
PDVSA	Venezuela	15,000	2007	Potential	Commercial	Intevep
PDVSA	Venezuela	100	2003	Planned	Pilot	N/A

APPENDIX B

ERROR ANALYSIS AND SAMPLE CALCULATIONS

Let x_i be the i-th independent variable to be considered and Δx_i is the error in x_i.

Let F be a function of those independent variables: $F=f(x_1, x_2,\ldots, x_i,\ldots, x_n)$

The differential of this function can be calculated as follows:

$$dF = \sum_{i=1}^{n} \left.\frac{\partial F}{\partial x_i}\right|_{x_{j\neq i}} dx_i \tag{B-1}$$

The error can then be estimated as:

$$\Delta F = \sum_{i=1}^{n} \left|\left.\frac{\partial F}{\partial x_i}\right|_{x_{j\neq i}}\right| \Delta x_i \tag{B-2}$$

Therefore, expressions of the errors for the different measured parameters can be derived in the following manner:

Solubility, C^*:

The solubility is calculated using the following equation:

$$C_i^* = \frac{N_{i,I} - N_{i,F}}{V_L} \tag{B-3}$$

$N_{i,I}$ and $N_{i,F}$ are calculated from:

$$N_{i,I} = \frac{P_{i,I} V_G}{R T_{r,I}} \tag{B-4}$$

$$N_{i,F} = \frac{P_{i,F} V_G}{R T_{r,F}} \tag{B-5}$$

The initial average ($Tr,_I$) and final average ($Tr,_F$) temperatures are calculated as:

$$T_{r,I} = \frac{T_{I,gas} + T_{I,liq.}}{2} \tag{B-6}$$

$$T_{r,F} = \frac{T_{F,gas} + T_{F,liq.}}{2} \tag{B-7}$$

The gas-phase volume is estimated from:

$$V_G = V_r - \left(\frac{m_L}{\rho_L} + \frac{m_{cat.}}{\rho_{cat.}} \right) = V_r - V_L - V_{cat.} \tag{B-8}$$

Thus, the independent variables in the solubility, C^* are:

$$C^* = f(V_r, V_L, V_{cat.} P_{r,I}, T_{r,I}, P_{r,F}, T_{r,F}) \tag{B-9}$$

The error in the experimental solubility value can be estimated as:

$$\Delta C^* = \left| \frac{\partial C^*}{\partial P_{r,I}} \right| \Delta P_{r,I} + \left| \frac{\partial C^*}{\partial T_{r,I}} \right| \Delta T_{r,I} + \left| \frac{\partial C^*}{\partial P_{r,F}} \right| \Delta P_{r,F} + \left| \frac{\partial C^*}{\partial T_{r,F}} \right| \Delta T_{r,F} + \left| \frac{\partial C^*}{\partial V_r} \right| \Delta V_r + \left| \frac{\partial C^*}{\partial V_L} \right| \Delta V_L + \left| \frac{\partial C^*}{\partial V_{cat.}} \right| \Delta V_{cat.} \tag{B-10}$$

The needed partial derivatives are:

$$\frac{\partial C^*}{\partial P_{r,I}} = \frac{(V_r - V_L - V_{cat.})}{R V_L T_{r,I}} \tag{B-11}$$

$$\frac{\partial C^*}{\partial T_{r,I}} = -\frac{(V_r - V_L - V_{cat.}) P_{r,I}}{R V_L T_{r,I}^{\,2}} \tag{B-12}$$

$$\frac{\partial C^*}{\partial P_{r,F}} = -\frac{(V_r - V_L - V_{cat.})}{RV_L T_{r,F}} \tag{B-13}$$

$$\frac{\partial C^*}{\partial T_{r,F}} = \frac{(V_r - V_L - V_{cat.})P_{r,F}}{RV_L {T_{r,F}}^2} \tag{B-14}$$

$$\frac{\partial C^*}{\partial V_r} = \frac{1}{RV_L} \cdot \left(\frac{P_{r,I}}{T_{r,I}} - \frac{P_{r,F}}{T_{r,F}} \right) \tag{B-15}$$

$$\frac{\partial C^*}{\partial V_L} = -\frac{V_r - V_{cat.}}{R{V_L}^2} \cdot \left(\frac{P_{r,I}}{T_{r,I}} - \frac{P_{r,F}}{T_{r,F}} \right) \tag{B-16}$$

$$\frac{\partial C^*}{\partial V_{cat.}} = -\frac{1}{RV_L} \cdot \left(\frac{P_{r,I}}{T_{r,I}} - \frac{P_{r,F}}{T_{r,F}} \right) \tag{B-17}$$

The volume of the liquid and catalyst phase in the reactor is given by:

$$V_L = \frac{m_L}{\rho_L} \tag{B-18}$$

$$V_{cat.} = \frac{m_{cat.}}{\rho_{cat.}} \tag{B-19}$$

The errors in the liquid and solid volumes are:

$$\Delta V_L = \left| \frac{\partial V_L}{\partial m_L} \right| \Delta m_L + \left| \frac{\partial V_L}{\partial \rho_L} \right| \Delta \rho_L \tag{B-20}$$

$$\Delta V_{cat.} = \left| \frac{\partial V_{cat.}}{\partial m_{cat.}} \right| \Delta m_{cat.} + \left| \frac{\partial V_{cat.}}{\partial \rho_{cat.}} \right| \Delta \rho_{cat.} \tag{B-21}$$

The required partial derivatives are:

$$\frac{\partial V_L}{\partial m_L} = \frac{1}{\rho_L}\Delta m_L \tag{B-22}$$

$$\frac{\partial V_L}{\partial \rho_L} = -\frac{m_L}{\rho_L{}^2}\Delta \rho_L \tag{B-23}$$

$$\frac{\partial V_{cat.}}{\partial m_{cat.}} = \frac{1}{\rho_{cat.}}\Delta m_{cat.} \tag{B-24}$$

$$\frac{\partial V_{cat.}}{\partial \rho_{cat.}} = -\frac{m_{cat.}}{\rho_{cat.}{}^2}\Delta \rho_{cat} \tag{B-25}$$

Volumetric Mass Transfer Coefficient, k_La

k_La values are calculated using equation (5-31):

$$\frac{P_{i,F}}{P_{i,I}}\ln\left[\frac{P_{i,I}-P_{i,F}}{P_{i,t}-P_{i,F}}\right] = k_L a.t \tag{B-26}$$

The independent variables used in this expression are:

$$k_L a = f(P_{r,F},\ P_{r,I},\ P_{r,t},\ t) \tag{B-27}$$

Therefore, the error for the volumetric mass transfer coefficient is calculated from equation (5-31) as follows:

$$\Delta k_L a = \left|\frac{\partial k_L a}{\partial t}\right|\Delta t + \left|\frac{\partial k_L a}{\partial P_{r,F}}\right|\Delta P_{r,F} + \left|\frac{\partial k_L a}{\partial P_{r,I}}\right|\Delta P_{r,I} + \left|\frac{\partial k_L a}{\partial P_{r,t}}\right|\Delta P_{r,t} \tag{B-28}$$

The needed partial derivatives are:

$$\frac{\partial k_L a}{\partial t} = \frac{-1}{t^2}\frac{P_{r,F}}{P_{r,I}}\ln\left(\frac{P_{r,I}-P_{r,F}}{P_{r,t}-P_{r,F}}\right) \tag{B-29}$$

$$\frac{\partial k_L a}{\partial P_{r,F}} = \frac{1}{tP_{r,I}}\left[\ln\left(\frac{P_{r,I}-P_{r,F}}{P_{r,t}-P_{r,F}}\right) + \frac{P_{r,F}\left(P_{r,I}-P_{r,t}\right)}{\left(P_{r,I}-P_{r,F}\right)\left(P_{r,t}-P_{r,F}\right)}\right] \tag{B-30}$$

$$\frac{\partial k_L a}{\partial P_{r,I}} = \frac{1}{t}\left[\frac{P_{r,F}}{P_{r,I}}\frac{1}{\left(P_{r,I}-P_{r,F}\right)} - \frac{P_{r,F}}{(P_{r,I})^2}\ln\left(\frac{P_{r,I}-P_{r,F}}{P_{r,t}-P_{r,F}}\right)\right] \tag{B-31}$$

$$\frac{\partial k_L a}{\partial P_{r,t}} = \frac{P_{r,F}}{tP_{r,I}}\frac{-1}{\left(P_{r,t}-P_{r,F}\right)} \tag{B-32}$$

An example of error calculation of C^* and k_La is provided in Table B-1.

Run #: CW220 Date: 05-04-2004

System: Gas: CO

Liquid: Sasol wax

Solid: alumina powder

Operating Conditions:

C_S = 0 wt%	V_L = 0.0005 m^3	$\rho_{cat.}$ = 3062 kg/m^3
N = 900 rpm	$V_{cat.}$ = 0 m^3	m_L = 0.3646 kg
V_r = 0.0010283 m^3	ρ_L = 729.18 kg/m^3	$m_{cat.}$ = 0 kg

Errors:

ΔV_r = 0 m^3	$\Delta P_{r,F}$ = 3972 Pa	Δm_L = 0.0001 kg
ΔV_L = 1.37x10^{-7} m^3	$\Delta T_{r,I}$ = 0.1 K	$\Delta m_{cat.}$ = 0.0001 kg
$\Delta V_{cat.}$ = 3.27x10^{-8} m^3	$\Delta T_{r,F}$ = 0.1 K	Δt = 0 s
$\Delta P_{r,I}$ = 3972 Pa	$\Delta \rho_L$ = 0 kg/m^3	
$\Delta P_{r,m}$ = 3972 Pa	$\Delta \rho_{cat.}$ = 0 kg/m^3	

Table B-1: Sample Error Calculation

$P_{r,I}$ bar	$T_{r,I}$ K	$P_{r,F}$ bar	$T_{r,F}$ K	$P_{r,m}$ bar	t s	C^* kmol/m^{-3}	$\Delta C^*/C^*$ %	k_La s^{-1}	$\Delta k_La/k_La$ %
7.09	448.4	6.157	448.4	6.58	13.2	0.0263	8.8%	0.04743	24.98%
14.05	448.5	13.001	448.5	13.47	9.0	0.0556	4.3%	0.07428	17.69%
21.035	449.0	19.969	449.0	20.47	6.9	0.0853	2.9%	0.08979	15.59%
27.992	449.2	26.931	449.2	27.4	6.4	0.1145	2.3%	0.10233	14.89%
35.017	449.0	33.947	449.0	34.43	5.7	0.1442	1.9%	0.12134	13.04%

APPENDIX C

EXAMPLE K_LA CALCULATION

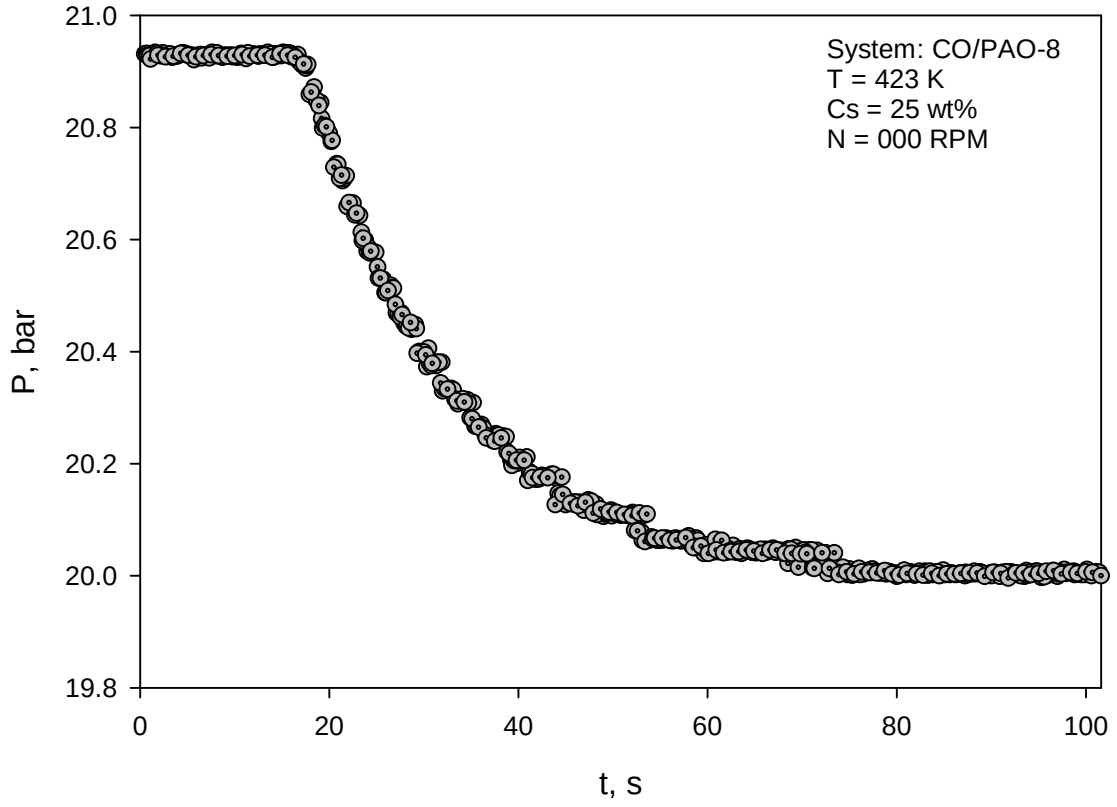

Figure C-1: Typical Experimental P(t) Curve Showing the Transient Gas-Absorption Behavior

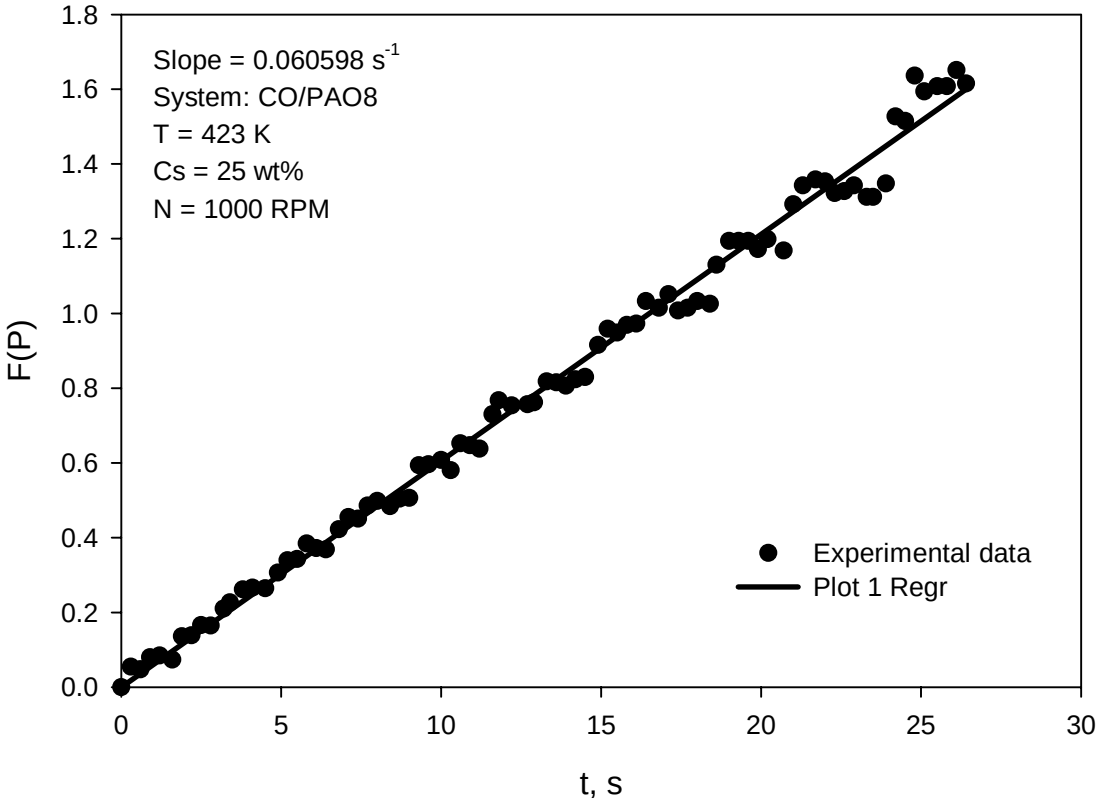

Figure C-2: A plot of F(P) vs Time from Equation (5-31)

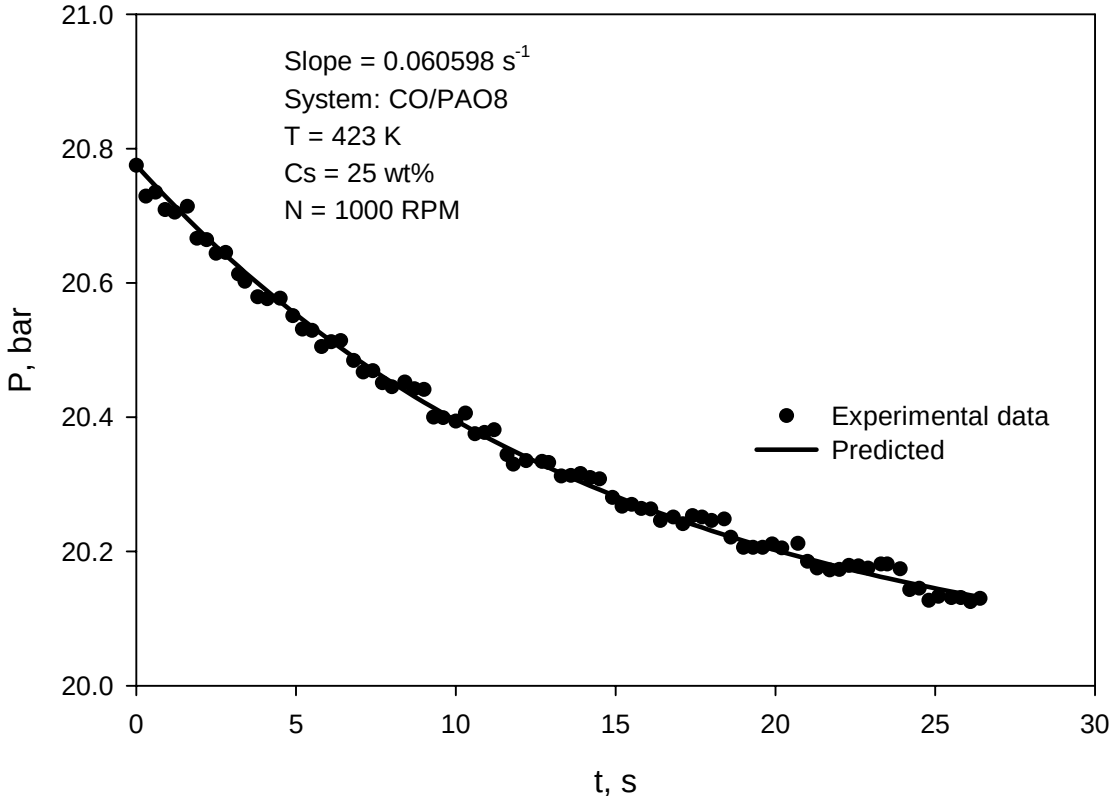

Figure C-3: Comparison between Calculated and Experimental P vs t Curves

APPENDIX D

CRITICAL MIXING SPEEDS FOR GAS INDUCTION AND SOLID SUSPENSION

The Critical mixing speeds for gas induction and for solid suspension were calculated using Equations (2-1) proposed by Lemoine et al.[14] and Equation (2-2) by Zwietering[15], respectively, as given in Section 2.2

$$\frac{N_{CRI}^2 d_{imp.}}{g} = 0.512 \times \left(\frac{\mu_L}{\mu_{Water}}\right)^{0.146} \left(\frac{\sigma_L}{\sigma_{Water}}\right)^{-0.180} \left(\frac{\rho_L}{\rho_{Water}}\right)^{-0.265} \left(\frac{H_L}{d_T}\right) \tag{2-1}$$

$$N_{suspension} = \frac{s\nu^{0.1} d_p^{0.2} \left(g\Delta\rho/\rho_L\right)^{0.45} C_V^{0.13}}{d_{imp.}^{0.85}} \tag{2-2}$$

It should be mentioned that Equation (2-1) was proposed for gas-liquid systems in gas-inducing reactors, whereas Equation (2-2) was proposed for gas-slurry systems in surface aeration not gas-inducing reactors.

Table D-1 shows a comparison between the calculated critical mixing speed for gas induction at Cs = 0 wt.% and the minimum mixing speeds used in the experiments at various temperatures and as can be seen in this table all the experiments with PAO-8 and all the runs, except at 473 K, with Sasol wax were conducted above the critical mixing speed for gas induction.

Table D-1: Critical Mixing Speed for Gas Induction

	PAO-8		*Sasol wax*	
T, K	N_{CRI}, ***RPM***	$N_{experiment}$ ***RPM***	N_{CRI}, ***RPM***	$N_{experiment}$ ***RPM***
423	827	1000	889	1000
448	812	900	887	900
473	797	800	886	800
498	781	900	886	900
523	766	1000	887	1000

Equation (2-2) was applied to predict the critical mixing speed for solid suspension at the worst case scenario in the statistical design of experiment (C_S = 50 wt.% and T = 473K) with a shape factor value (*s*) equals 5.4. The critical mixing speeds for solid suspension for PAO-8 and Sasol were 890 rpm and 1018 rpm, respectively whereas the minimum mixing speed used for PAO-8 and Sasol wax under this temperature was 1000 rpm. These predicted and actual mixing speeds indicate that the entire solid particles in PAO-8 should be suspended during the experiment, while it could be possible that few particles were not suspended in Sasol wax under these specific conditions. It should be mentioned, however, that Equation (2-2) does not account for the presence of induced gas bubbles which were reported by Murugesan[21] to have a positive impact on suspending the solids particles, and accordingly the solid particles were suspended under the experimental conditions employed as shown in Figure 17.

APPENDIX E

PROPERTIES OF ISOPAR-M

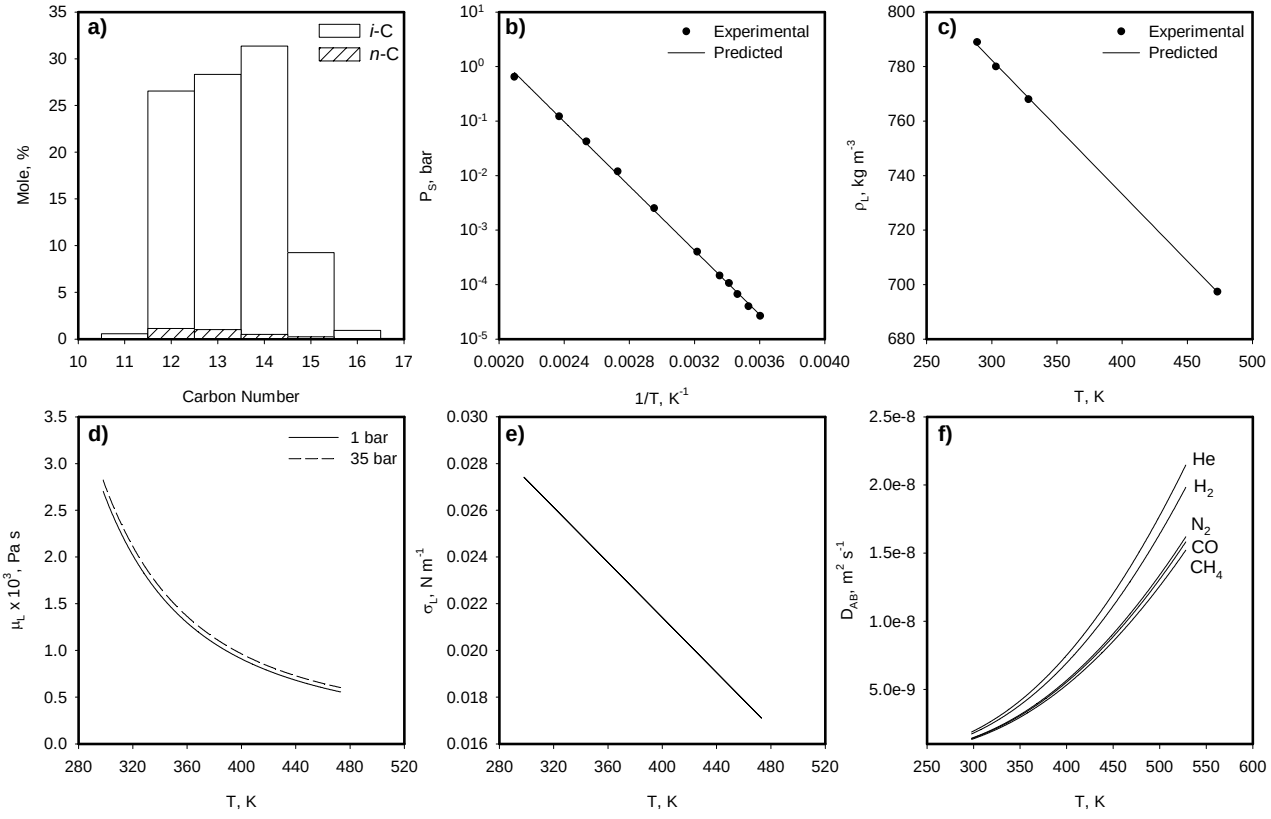

Figure E-1: Properties of Isopar-M[(74)]

(a) Composition, (b) Vapor Pressure, (c) Density, (d) Viscosity, (e) Surface Tension, (f) Diffusivity

BIBLIOGRAPHY

1. Hubbert, M. K., "Energy from Fossil Fuels," Science, Vol. 109 (2823), (1949), pp. 103-109.

2. Hubbert, M. K., "The Energy Resources of the Earth," Energy and Power, Vol. 3 (1971), pp. 31-40.

3. Hakes, J., "Long Term World Oil Supply," US DOE EIA (Energy Information Administration), Geologists, A. A. o. P., (New Orleans, LA, 2000).

4. Cavallo, A. J., "Predicting the Peak in World Oil Production," Natural Resources Research, Vol. 11 (3), (2002), pp. 187-195.

5. Laherrère, J. H., "Estimates of Oil Reserves," Workshop, I. I. E., (Luxembourg, 2001).

6. Rehaag, K., "Is the World Facing a 3rd Oil Shock?," IEA (International Energy Agency), Workshop, F. I., (Rio de Janeiro, 2004).

7. Sandrea, R., "Imbalances among oil demand, reserves, alternatives define energy dilemma today," The Oil and Gas Journal, Vol. 102 (26), (2004), pp. 34-38.

8. Chemlink Autralia, http://www.chemlink.com.au/gtl.htm, Gas to liquids technology worldwide.

9. Vosloo, A. C., "Fischer-Tropsch: a futuristic view," Fuel Processing Technology, Vol. 71 (1-3), (2001), pp. 149-155.

10. Dry, M. E., "Present and future applications of the Fischer-Tropsch process," Applied Catalysis A: General, Vol. 276 (1-2), (2004), pp. 1-3.

11. Wilhelm, D. J., Simbeck, D. R., Karp, A. D., Dickenson, R. L., "Syngas production for gas-to-liquids applications: technologies, issues and outlook," Fuel Processing Technology, Vol. 71 (1-3), (2001), pp. 139-148.

12. "World Energy Outlook," IEA (International Energy Agency), 2001

13. Inga, J. R., Morsi, B. I., "A Novel Approach for the Assessment of the Rate-Limiting Step in Fischer-Tropsch Slurry Process," Energy & Fuels, Vol. 10 (3), (1996), pp. 566-72.

14. Lemoine, R., Fillion, B., Morsi, B. I., "Hydrodynamic and mass transfer parameters in agitated reactors part I: critical mixing speed, induced gas flow rate, and wavy surface in SARs and GIRs," International Journal of Chemical Reactor Engineering, Vol. 2 (2004), p. No pp given.

15. Zwietering, T. N., "Suspension of solid particles in liquid by agitators," Chemical Engineering Science, Vol. 8 (1958), pp. 244-53.

16. Narayanan, S., Bhatia, V. K., Guha, D. K., Rao, M. N., "Suspension of solids by mechanical agitation," Chemical Engineering Science, Vol. 24 (2), (1969), pp. 223-30.

17. Sharma, R. N., Shaikh, A. A., "Solids suspension in stirred tanks with pitched blade turbines," Chemical Engineering Science, Vol. 58 (10), (2003), pp. 2123-2140.

18. Aravinth, S., Rao, P. G., Murugesan, T., "Critical impeller speeds for solid suspension in turbine agitated contactors," Bioprocess Engineering, Vol. 14 (2), (1996), pp. 97-9.

19. Armenante, P. M., Nagamine, E. U., "Effect of low off-bottom impeller clearance on the minimum agitation speed for complete suspension of solids in stirred tanks," Chemical Engineering Science, Vol. 53 (9), (1998), pp. 1757-1775.

20. Armenante, P. M., Nagamine, E. U., Susanto, J., "Determination of correlations to predict the minimum agitation speed for complete solid suspension in agitated vessels," Canadian Journal of Chemical Engineering, Vol. 76 (3), (1998), pp. 413-419.

21. Murugesan, T., "Critical impeller speed for solid suspension in mechanically agitated contactors," Journal of Chemical Engineering of Japan, Vol. 34 (3), (2001), pp. 423-429.

22. Lewis, W. K., Whitman, W. G., "Principles of gas absorption," Journal of Industrial and Engineering Chemistry (Washington, D. C.), Vol. 16 (1924), pp. 1215-20.

23. Chang, M. Y., Morsi, B. I., "Solubilities and mass transfer coefficients of carbon monoxide in a gas-inducing reactor operating with organic liquids under high pressures and temperatures," Chemical Engineering Science, Vol. 47 (13-14), (1992), pp. 3541-8.

24. Tsai, F. N., Huang, S. H., Lin, H. M., Chao, K. C., "Solubility of methane, ethane, and carbon dioxide in a Mobil Fischer-Tropsch wax and in n-paraffins," Chemical Engineering Journal (Amsterdam, Netherlands), Vol. 38 (1), (1988), pp. 41-6.

25. Ghosh, A., Chapman, W. G., French, R. N., "Gas solubility in hydrocarbons-a SAFT-based approach," Fluid Phase Equilibria, Vol. 209 (2), (2003), pp. 229-243.

26. Ronze, D., Fongarland, P., Pitault, I., Forissier, M., "Hydrogen solubility in straight run gas oil," Chemical Engineering Science, Vol. 57 (4), (2002), pp. 547-553.

27. Tong, J., Gao, W., Robinson, R. L., Jr., Gasem, K. A. M., "Solubilities of Nitrogen in Heavy Normal Paraffins from 323 to 423 K at Pressures to 18.0 MPa," Journal of Chemical and Engineering Data, Vol. 44 (4), (1999), pp. 784-787.

28. Park, J., Yi, X., Gasem, K. A. M., Robinson, R. L., Jr., "Solubilities of Carbon Monoxide in Aromatic Hydrocarbons at Temperatures from 323 to 433 K and Pressures to 23.3 MPa," Journal of Chemical and Engineering Data, Vol. 40 (1), (1995), pp. 245-7.

29. Park, J., Robinson, R. L., Jr., Gasem, K. A. M., "Solubilities of Hydrogen in Heavy Normal Paraffins at Temperatures from 323.2 to 423.2 K and Pressures to 17.4 MPa," Journal of Chemical and Engineering Data, Vol. 40 (1), (1995), pp. 241-4.

30. Chou, J. S., Chao, K. C., "Solubility of synthesis and product gases in a Fischer-Tropsch SASOL wax," Industrial & Engineering Chemistry Research, Vol. 31 (2), (1992), pp. 621-3.

31. Albal, R. S., Shah, Y. T., Carr, N. L., Bell, A. T., "Mass transfer coefficients and solubilities for hydrogen and carbon monoxide under Fischer-Tropsch conditions," Chemical Engineering Science, Vol. 39 (5), (1984), pp. 905-7.

32. Van Vuuren, D. S., Hunter, J. R., Heydenrych, M. D., "The solubility of various gases in Fischer-Tropsch reactor wax," Chemical Engineering Science, Vol. 43 (6), (1988), pp. 1291-6.

33. Huang, S. H., Lin, H. M., Tsai, F. N., Chao, K. C., "Solubility of synthesis gases in heavy n-paraffins and Fischer-Tropsch wax," Industrial & Engineering Chemistry Research, Vol. 27 (1), (1988), pp. 162-9.

34. Chou, J. S., Chao, K. C., "Correlation of synthesis gas solubility in n-paraffin solvents and Fischer-Tropsch waxes," Fluid Phase Equilibria, Vol. 46 (2-3), (1989), pp. 179-95.

35. Wang, Y. N., Li, Y. W., Bai, L., Zhao, Y. L., Zhang, B. J., "Correlation for gas-liquid equilibrium prediction in Fischer-Tropsch synthesis," Fuel, Vol. 78 (8), (1999), pp. 911-917.

36. Campanella, E. A., "Correlation and prediction of synthesis gas solubility in n-paraffin systems," Chemical Engineering & Technology, Vol. 20 (6), (1997), pp. 371-377.

37. Mandagaran, B. A., Campanella, E. A., "Correlation and prediction of gas solubility in heavy complex liquids," Chemical Engineering & Technology, Vol. 16 (6), (1993), pp. 399-404.

38. Alghamdi, A. K. A., "Mass transfer characteristics in a slurry agitated reactor with organic liquid mixtures under high pressures and temperatures," (Unpublished M.S. Thesis, Chemical and Petroleum Engineering Department, University of Pittsburgh, 2001).

39. Chang, M. Y., "Mass Transfer Characteristics of Gases in Aqueous and Organic Liquids at Elevated Pressures and Temperatures in Agitated Reactors," (Unpublished Ph.D Dissertation, Chemical and Petroleum Engineering Department, University of Pittsburgh, 1993).

40. Chang, M. Y., Morsi, B. I., "Mass transfer characteristics of gases in aqueous and organic liquids at elevated pressures and temperatures in agitated reactors," Chemical Engineering Science, Vol. 46 (10), (1991), pp. 2639-50.

41. Tekie, Z., Li, J., Morsi, B. I., "Mass Transfer Parameters of O2 and N2 in Cyclohexane under Elevated Pressures and Temperatures: A Statistical Approach," Industrial & Engineering Chemistry Research, Vol. 36 (9), (1997), pp. 3879-3888.

42. Inga, J. R., Morsi, B. I., "Effect of catalyst loading on gas/liquid mass transfer in a slurry reactor: a statistical experimental approach," Canadian Journal of Chemical Engineering, Vol. 75 (5), (1997), pp. 872-881.

43. Deimling, A., Karandikar, B. M., Shah, Y. T., Carr, N. L., "Solubility and mass transfer of carbon monoxide and hydrogen in Fischer-Tropsch liquids and slurries," Chemical Engineering Journal (Amsterdam, Netherlands), Vol. 29 (3), (1984), pp. 127-40.

44. Lekhal, A., Chaudhari, R. V., Wilhelm, A. M., Delmas, H., "Gas-liquid mass transfer in gas-liquid-liquid dispersions," Chemical Engineering Science, Vol. 52 (21/22), (1997), pp. 4069-4077.

45. Karandikar, B. M., Morsi, B. I., Shah, Y. T., Carr, N. L., "Effect of water on the solubilities and mass transfer coefficients of gases in a heavy fraction of Fischer-Tropsch products," Canadian Journal of Chemical Engineering, Vol. 65 (6), (1987), pp. 973-81.

46. Karandikar, B. M., Morsi, B. I., Shah, Y. T., Carr, N. L., "Effect of water on the solubility and mass transfer coefficients of CO and H2 in a Fischer-Tropsch liquid," Chemical Engineering Journal (Amsterdam, Netherlands), Vol. 33 (3), (1986), pp. 157-68.

47. Hichri, H., Accary, A., Puaux, J. P., Andrieu, J., "Gas-liquid mass-transfer coefficients in a slurry batch reactor equipped with a self-gas-inducing agitator," Industrial & Engineering Chemistry Research, Vol. 31 (8), (1992), pp. 1864-7.

48. Albal, R. S., Shah, Y. T., Schumpe, A., Carr, N. L., "Mass transfer in multiphase agitated contactors," Chemical Engineering Journal (Amsterdam, Netherlands), Vol. 27 (2), (1983), pp. 61-80.

49. Dietrich, E., Mathieu, C., Delmas, H., Jenck, J., "Raney-nickel catalyzed hydrogenations: gas-liquid mass transfer in gas-induced stirred slurry reactors," Chemical Engineering Science, Vol. 47 (13-14), (1992), pp. 3597-604.

50. Miller, S. A., Ekstrom, A., Foster, N. R., "Solubility and mass-transfer coefficients for hydrogen and carbon monoxide in n-octacosane," Journal of Chemical and Engineering Data, Vol. 35 (2), (1990), pp. 125-7.

51. Chen, J.-H., Hsu, Y.-C., Chen, Y. F., Lin, C.-C., "Application of gas-inducing reactor to obtain high oxygen dissolution in aeration process," Water Research, Vol. 37 (12), (2003), pp. 2919-2928.

52. Maalej, S., Benadda, B., Otterbein, M., "Influence of pressure on the hydrodynamics and mass transfer parameters of an agitated bubble reactor," Chemical Engineering & Technology, Vol. 24 (1), (2001), pp. 77-84.

53. Hsu, Y.-C., Chen, T.-Y., Chen, J.-H., Lay, C.-W., "Ozone Transfer into Water in a Gas-Inducing Reactor," Industrial & Engineering Chemistry Research, Vol. 41 (1), (2002), pp. 120-127.

54. Hsu, Y.-C., Peng, R. Y., Huang, C.-J., "Onset of gas induction, power consumption, gas holdup and mass transfer in a new gas-induced reactor," Chemical Engineering Science, Vol. 52 (21/22), (1997), pp. 3883-3891.

55. Sridhar, T., Potter, O. E., "Interfacial areas in gas-liquid stirred vessels," Chemical Engineering Science, Vol. 35 (3), (1980), pp. 683-95.

56. Ledakowicz, S., Nettelhoff, H., Deckwer, W. D., "Gas-liquid mass transfer data in a stirred autoclave reactor," Industrial & Engineering Chemistry Fundamentals, Vol. 23 (4), (1984), pp. 510-12.

57. Linek, V., Kordac, M., Fujasova, M., Moucha, T., "Gas-liquid mass transfer coefficient in stirred tanks interpreted through models of idealized eddy structure of turbulence in the bubble vicinity," Chemical Engineering and Processing, Vol. 43 (12), (2004), pp. 1511-1517.

58. Oguz, H., Brehm, A., Deckwer, W. D., "Gas/liquid mass transfer in sparged agitated slurries," Chemical Engineering Science, Vol. 42 (7), (1987), pp. 1815-22.

59. Joosten, G. E. H., Schilder, J. G. M., Janssen, J. J., "The influence of suspended solid material on the gas-liquid mass transfer in stirred gas-liquid contactors," Chemical Engineering Science, Vol. 32 (5), (1977), pp. 563-6.

60. Kluytmans, J. H. J., van Wachem, B. G. M., Kuster, B. F. M., Schouten, J. C., "Mass transfer in sparged and stirred reactors: influence of carbon particles and electrolyte," Chemical Engineering Science, Vol. 58 (20), (2003), pp. 4719-4728.

61. Ruthiya, K. C., van der Schaaf, J., Kuster, B. F. M., Schouten, J. C., "Mechanisms of physical and reaction enhancement of mass transfer in a gas inducing stirred slurry

reactor," Chemical Engineering Journal (Amsterdam, Netherlands), Vol. 96 (1-3), (2003), pp. 55-69.

62. Ruthiya, K. C., Kuster, B. F. M., Schouten, J. C., "Gas-liquid mass transfer enhancement in a surface aeration stirred slurry reactors," Canadian Journal of Chemical Engineering, Vol. 81 (3-4), (2003), pp. 632-639.

63. Inga, J. R., "Scaleup and scaledown of slurry reactors: a new methodology," (Unpublished Ph.D. Dissertation, Chemical and Petroleum Engineering Department, University of Pittsburgh, 1997).

64. Gao, W., Robinson, R. L., Jr., Gasem, K. A. M., "High-Pressure Solubilities of Hydrogen, Nitrogen, and Carbon Monoxide in Dodecane from 344 to 410 K at Pressures to 13.2 MPa," Journal of Chemical and Engineering Data, Vol. 44 (1), (1999), pp. 130-132.

65. Purwanto, P., Deshpande, R. M., Chaudhari, R. V., Delmas, H., "Solubility of Hydrogen, Carbon Monoxide, and 1-Octene in Various Solvents and Solvent Mixtures," Journal of Chemical and Engineering Data, Vol. 41 (6), (1996), pp. 1414-1417.

66. Twu, C. H., Coon, J. E., Harvey, A. H., Cunningham, J. R., "An Approach for the Application of a Cubic Equation of State to Hydrogen-Hydrocarbon Systems," Industrial & Engineering Chemistry Research, Vol. 35 (3), (1996), pp. 905-10.

67. Huang, S. H., Lin, H. M., Chao, K. C., "Experimental investigation of synthesis gas solubility in Fischer-Tropsch reactor slurry," Fluid Phase Equilibria, Vol. 36 (1987), pp. 141-8.

68. Breman, B. B., Beenackers, A. A. C. M., Rietjens, E. W. J., Stege, R. J. H., "Gas-Liquid Solubilities of Carbon Monoxide, Carbon Dioxide,Hydrogen, Water, 1-Alcohols ($1 < n < 6$), and n-Paraffins ($2 < n < 6$) in Hexadecane, Octacosane, 1-Hexadecanol, Phenanthrene, and Tetraethylene Glycol at Pressures up to 5.5 MPa and Temperatures from 293 to 553 K," Journal of Chemical and Engineering Data, Vol. 39 (4), (1994), pp. 647-66.

69. Darwish, N. A., Fathikalajahi, J., Gasem, K. A. M., Robinson, R. L., Jr., "Solubility of methane in heavy normal paraffins at temperatures from 323 to 423 K and pressures to 10.7 MPa," Journal of Chemical and Engineering Data, Vol. 38 (1), (1993), pp. 44-8.

70. Srivastan, S., Darwish, N. A., Gasem, K. A. M., Robinson, R. L., Jr., "Solubility of methane in hexane, decane, and dodecane at temperatures from 311 to 423 K and pressures to 10.4 MPa," Journal of Chemical and Engineering Data, Vol. 37 (4), (1992), pp. 516-20.

71. Campanella, E. A., "Correlation of solubilities of carbon monoxide, carbon dioxide, and hydrogen in paraffins," Journal of Chemical Engineering of Japan, Vol. 26 (1), (1993), pp. 48-51.

72. Peter, S., Weinert, M., "Solubility of hydrogen, carbon monoxide, carbon dioxide, and water vapor in liquid hydrocarbons," Zeitschrift fuer Physikalische Chemie (Muenchen, Germany), Vol. 5 (1955), pp. 114-21.

73. Matsumoto, D. K., Satterfield, C. N., "Solubility in hydrogen and carbon monoxide in selected nonaqueous liquids," Industrial & Engineering Chemistry Process Design and Development, Vol. 24 (4), (1985), pp. 1297-300.

74. Behkish, A., Men, Z., Inga, J. R., Morsi, B. I., "Mass transfer characteristics in a large-scale slurry bubble column reactor with organic liquid mixtures," Chemical Engineering Science, Vol. 57 (16), (2002), pp. 3307-3324.

75. Teramoto, M., Tai, S., Nishii, K., Teranishi, H., "Effects of pressure on liquid-phase mass transfer coefficients," Chemical Engineering Journal (Amsterdam, Netherlands), Vol. 8 (3), (1974), pp. 223-6.

76. Ozkan, O., Calimli, A., Berber, R., Oguz, H., "Effect of inert solid particles at low concentrations on gas-liquid mass transfer in mechanically agitated reactors," Chemical Engineering Science, Vol. 55 (14), (2000), pp. 2737-2740.

77. Reid, R. C., Prausnitz, J. M., Poling, B. E., "The Properties of Gases and Liquids," (New York: McGraw-Hill (5th Ed.), 2001).

78. Gao, W., Robinson, R. L., Gasem, K. A. M., "Improved correlations for heavy n-paraffin physical properties," Fluid Phase Equilibria, Vol. 179 (1-2), (2001), pp. 207-216.

79. Marano, J. J., Holder, G. D., "Prediction of bulk properties of Fischer-Tropsch derived liquids," Industrial & Engineering Chemistry Research, Vol. 36 (6), (1997), pp. 2409-2420.

80. Marano, J. J., Holder, G. D., "General Equation for Correlating the Thermophysical Properties of n-Paraffins, n-Olefins, and Other Homologous Series. 2. Asymptotic Behavior Correlations for PVT Properties," Industrial & Engineering Chemistry Research, Vol. 36 (5), (1997), pp. 1895-1907.

81. Marano, J. J., Holder, G. D., "General Equation for Correlating the Thermophysical Properties of n-Paraffins, n-Olefins, and Other Homologous Series. 1. Formalism for Developing Asymptotic Behavior Correlations," Industrial & Engineering Chemistry Research, Vol. 36 (5), (1997), pp. 1887-1894.

82. Marano, J. J., Holder, G. D., "Characterization of Fischer-Tropsch liquids for vapor-liquid equilibria calculations," Fluid Phase Equilibria, Vol. 138 (1-2), (1997), pp. 1-21.

83. Rogalski, M., Mato, F. A., Neau, E., "Estimation of hydrocarbon critical properties from vapor pressure and liquid densities," Chemical Engineering Science, Vol. 47 (8), (1992), pp. 1925-31.

84. Kudchadker, A. P., Zwolinski, B. J., "Vapor pressures and boiling points of normal alkanes, C21 to C100," Journal of Chemical and Engineering Data, Vol. 11 (2), (1966), pp. 253-5.

85. Liang, Y., Ma, P., Li, P., "Estimation of liquid viscosity of pure compounds at different temperatures by a corresponding-states group-contribution method," Fluid Phase Equilibria, Vol. 198 (1), (2002), pp. 123-130.

86. Marano, J. J., Holder, G. D., "A general equation for correlating the thermophysical properties of n-paraffins, n-olefins, and other homologous series, 3. Asymptotic behavior correlations for thermal and transport properties," Industrial & Engineering Chemistry Research, Vol. 36 (6), (1997), pp. 2399-2408.

87. Fanchi, J. R., "Calculation of parachors for compositional simulation: an update," SPE Reservoir Engineering, Vol. 5 (3), (1990), pp. 433-6.

88. Fanchi, J. R., "Calculation of parachors for compositional simulation," JPT, Journal of Petroleum Technology, Vol. 37 (12), (1985), pp. 2049-50.

89. Quayle, O. R., "The parachors of organic compounds. An interpretation and catalogue," Chemical Reviews (Washington, DC, United States), Vol. 53 (1953), pp. 439-589.

90. Wilke, C. R., Chang, P., "Correlation of diffusion coefficients in dilute solutions," Am. Inst. Chem. Eng. J., Vol. 1 (1955), pp. 264-70.

91. Barnea, E., Mizrahi, J., "Generalized approach to the fluid dynamics of particulate systems. 1. General correlation for fluidization and sedimentation in solid multiparticle systems," Chemical Engineering Journal (Amsterdam, Netherlands), Vol. 5 (2), (1973), pp. 171-89.

92. Thomas, D. G., "Transport characteristics of suspension. VIII. A note on the viscosity of Newtonian suspensions of uniform spherical particles," Journal of Colloid Science, Vol. 20 (3), (1965), pp. 267-77.

93. Saxena, S. C., Chen, Z. D., "Hydrodynamics and heat transfer of baffled and unbaffled slurry bubble columns," Reviews in Chemical Engineering, Vol. 10 (3-4), (1994), pp. 193-400.

94. Guth, E., Simha, R., "The viscosity of suspensions and solutions. III. The viscosity of sphere suspensions," Kolloid-Zeitschrift, Vol. 74 (1936), pp. 266-75.

95. Guth, E., "Experiments on the viscosity of suspensions and solutions. I. The viscosity of suspensions," Kolloid-Zeitschrift, Vol. 74 (1936), pp. 147-72.

96. Roscoe, R., "The viscosity of suspensions of rigid spheres," British Journal of Apllied Physics, Vol. 3 (8), (1952), pp. 267-269.

97. Einstein, A., "A new determination of molecular dimensions," Annalen der Physik (Weinheim, Germany), Vol. 19 (1906), pp. 289-306.

98. Vand, V., "Viscosity of solutions and suspensions. I. Theory," Journal of Physical and Colloid Chemistry, Vol. 52 (1948), pp. 277-99.

99. Chang, M. Y., Eiras, J. G., Morsi, B. I., "Mass transfer characteristics of gases in n-hexane at elevated pressures and temperatures in agitated reactors," Chemical Engineering and Processing, Vol. 29 (1), (1991), pp. 49-60.

100. Tekie, Z., Li, J., Morsi, B. I., Chang, M.-Y., "Gas-liquid mass transfer in cyclohexane oxidation process using gas-inducing and surface-aeration agitated reactors," Chemical Engineering Science, Vol. 52 (9), (1997), pp. 1541-1551.

101. Tekie, Z., "Mass Transfer and Modeling of Liquid-phase Cyclohexane Oxidation Process in Agitated Reactors," (Unpublished Ph.D. Dissertation, Chemical and Petroleum Engineering Department, University of Pittsburgh, 1997).

102. Fillion, B., " Modeling of soybean oil hydrogenation process," (Unpublished Ph.D. Dissertation, Chemical and Petroleum Engineering Department, University of Pittsburgh, 2001).

103. Martinez-Caamano Nieves, B., "Mass Transfer of H2 and N2 in a Slurry Agitated Reactor Operating Under Industrial Conditions with Organic Liquid Mixture," (Unpublished M.S. Thesis, Chemical and Petroleum Engineering Department, University of Pittsburgh, 2000).

104. Himmelblau, D. M., "Solubilities of inert gases in H2O: 0 Deg to near the critical point of H2O," Journal of Chemical and Engineering Data, Vol. 5 (No. 1), (1960), pp. 10-15.

105. Hildebrand, J. H., Scott, R. L., "The Solubility of Nonelectrolytes. 3rd ed," (1950).

106. Breman, B. B., Beenackers, A. A., "Thermodynamic Models To Predict Gas-Liquid Solubilities in the Methanol Synthesis, the Methanol-Higher Alcohol Synthesis, and the Fischer-Tropsch Synthesis via Gas-Slurry Processes," Industrial & Engineering Chemistry Research, Vol. 35 (10), (1996), pp. 3763-3775.

107. LNGCenter, http://gmaiso.free.fr/lng/index.php3?suj=gtl&page=gtlsearch, LNG Center, The LNG & GTL Portal.